Treatment of neonatal mouse hyperoxia-induced lung deficit with endothelial progenitor cells from bone marrow

Alexandra Firsova

Bachelor of Biology (Honours)
Master of Biomedical Science

Department of Biochemistry and Molecular Biology
Monash University

Supervisors: Dr Richard Mollard, A/Prof Tim Cole

Date of submission
10/22/2012

Copyright Notices

Notice 1

Notice 2

Table of Contents

Abstract

Premature birth-related lung deficit caused by high oxygen treatment (hyperoxia) can result in chronic lung disease. Previous studies demonstrated that disruption of alveolarisation (septation of the lung) and pulmonary vascularisation can be observed after hyperoxia. Injection of cultured cells isolated from bone marrow with mesenchymal or endothelial progenitor phenotype can return lung morphology to normal after neonatal hyperoxia in mice. However, long-term efficiency, as well as any potential side effects of such cell therapies, remains under investigation. In this study we hypothesised that endothelial progenitor cells and plate-adherent cells can be isolated from bone marrow, and can be used for treating the effects of hyperoxia in the lungs of neonatal mice by inducing or supporting alveolarisation via promotion of vascularisation. The aim of this project was to compare a number of endothelial progenitor cell types, first *in vitro*, and then *in vivo,* to determine how injection of various cell types from mouse bone marrow affects the hyperoxia-treated and healthy lung, which would result in the optimisation of a new treatment model. Newborn mice were treated with 90% oxygen or left in room air for four days. Samples of tissues were collected from hyperoxia-treated and normoxia mice at 5, 28 and 56 days *postpartum*. It was discovered that alveolarisation remains affected until 56 days of age, but vascularisation recovers by 28 days of age. Suitable cell types were then obtained in order to treat the effects of hyperoxia. Cell sorting of bone marrow, *in vitro* differentiation and analysis for the presence of vessel-like structures revealed that the freshly-isolated Kdr-enriched cell fraction is effective in forming blood-vessel-like structures *in vitro* and might have *in vivo* potential. EphA3-enriched cells from different passages were also selected based on relatively rapid vessel-like structure formation *in vitro*, and unsorted plate-adherent cells from passage 0 were used as a control. Hyperoxia-treated and normoxia mice were then injected intraperitoneally with $1x10^4$ cells (per 2 g of animal weight) of the different cell populations isolated from bone marrow at five days of age. Freshly-isolated cells sorted for Kdr, plate-adherent cells from bone marrow cultured for 7-10 days, and EphA3-enriched cells from passages 8, 12 and 13-15 were injected. PBS (saline) was injected as a control. After Kdr-enriched cells were

injected, partial recovery from hyperoxia was observed at 28 days, for example, alveolar size was significantly smaller than in PBS-injected hyperoxia-treated mice. This was followed by full recovery at 56 days. However, when cells were injected in normoxia mice, alveolar size was significantly increased compared to control. After injection of cultured plate-adherent cells some abnormalities were observed, i.e. increased number of mature blood vessels. These cells did not assist in alveolarisation recovery after hyperoxia. After the injection of EphA3-enriched cells at passage 8, partial alveolar recovery was observed with some increase in alveolar size in normoxia mice, at passage 12 – no recovery was observed with some increase in alveolar size in normoxia mice, and at passages 13-15 – animal death and aberrant growth formations were observed. These results indicate that fresh Kdr-enriched cells (and potentially EphA3^{+} cells from passage 8) have a higher corrective potential compared to plate-adherent and long-term cultured cells in this model. Although, when these cells are applied in the absence of deficit, potential harmful effects might be caused.

Project-related Publications

Firsova, A; Hyakumura, T; Cole, T J; Mollard, R (2010). Epithelial-mesenchymal interactions during lung development and their potential relevance to lung repair. Cell therapy for lung disease. J. Polak. London, UK, Imperial College Press: pp. 91-124.

Conference abstracts

Firsova, A; Cole, T J; Mollard, R (2011). Treatment of hyperoxia-induced lung deficit with endothelial progenitor cells from bone marrow. ComBio 2011, 25-29 September 2011, Cairns, QLD, Australia

Firsova, A; Cole, T J; Mollard, R (2010). Repairing high oxygen tension mediated respiratory deficit with endothelial progenitor cells. OzBio 2011, 21 September – 1 October 2010, Melbourne, VIC, Australia

Firsova A B, Cole T J, Mollard R (2010) Mouse endothelial progenitor cells for repair of respiratory deficit after high oxygen treatment. International Society for Stem Cell Research Congress, 16-19 June 2010 Moscone West, San Francisco, CA USA

Firsova A B, Cole T J, Mollard R (2010) Characterisation of a hyperoxia model of lung injury. Genome Conference, 14th -16th February 2010, Lorne, Australia

Thesis Declaration

This thesis, except with the Graduate Research Committees approval, contains no material which has been accepted for the award of any other degree or diploma in any university or other institution; and to the best of the candidates knowledge, this thesis contains no material previously published or written by another person, except where due reference or acknowledgement is made in the text of the thesis. This thesis is less than 100,000 words in length.

Alexandra Firsova_____22 October 2012

Acknowledgements

This project was supported by **NHMRC program grant 384100**. It took four-and-a-half years of hard work, but it would never have been possible without the following people. No titles are indicated in front of the names, as titles may change.

Richard Mollard – my supervisor and the author of most ideas in this project, who thoroughly worked on it together with me and guided me throughout all these years giving me moral support and advice on every important step I took

Tim Cole – my supervisor and the head of the laboratory, who kindly provided space for my work, my scholarship for three years, money for reagents and animal work, thesis proof-reading, and much more

Rosemary Clerehan – director of International Postgraduate Academic Support, who kindly provided thesis writing and editing course for students with English as a second language, and made comments on my writing style

Daniel Bird – postdoctoral fellow in our laboratory, who shared his expertise in methods and theories on lung research

Judy Ng – research assistant in our laboratory, who accompanied me in molecular experiments in which I haven't had much expertise, and gave me a hand every time I needed it, as well as a lot of guidance in other areas

Degu Abebe – postdoctoral fellow in Martin Lackmann laboratory, who provided cells for some experiments of my project and shared antibodies and some cell culture techniques

Megan O'Reilly – PhD student in Richard Harding laboratory, who shared her technique in pressure-fixing of mouse lungs, and gave me a hand during my first hyperoxia experiment and pressure-fixing trials

Natasha Blasch – animal technician in Richard Harding laboratory, who helped me to run the pilot experiments on mouse hyperoxia

Sharon Flecknoe – postdoctoral fellow in Stuart Hooper laboratory, shared her technique on histological method of visualising and measuring elastin and secondary septa in the lung

Nathanael Raschzok – research fellow in Germany, who kindly provided the protocol for fluorescent *in situ* hybridisation for mouse Y-chromosome

Irene Hatzinisiriou – head of the Imaging Facility, who assisted me in usage of numerous types of equipment, such as FACS machine, microscopes, cameras, image-analysis programs, plate readers etc.

Ian Boundy and Stefania Tombs – experts in histology and histochemistry, who gave me numerous advices during my project

Jeffrey Kerr – Associate Professor of anatomy, who gave me some advice on histology and measuring parameters of the lungs during my project

Lucy Gugasyan and Garey Dawson – our colleagues in the Department of Cytogenetics, who stained my trial mouse lung samples for Y chromosome

James Boon – research assistant in our laboratory, who shared some of his technique and advice in cell culture analysis methods

Paula Stoddart – representative of Miltenyi, who taught me MACS method and brought free antibody samples

Aidan Sudbury – Professor of Mathematics, who provided hours of advice in statistical analysis

Fenny Wiradjaja – postdoctoral fellow in Ian Smyth laboratory, who shared her western blotting methods

Andrew Fryga – Flowcore facility manager, who gave me a hand and advice in FACS analysis

Carli Esson – animal technician at Monash Animal Research Platform (MARP), who really cared for my animals

Gavin Langmaid – very kind animal technician at MARP

Emily Terry – animal technician at MARP, who made most hyperoxia experiments possible

Lilliana Jackanic – manager of Large Animal Facility, where all hyperoxia experiments were conducted, who helped to organise them

Katja Horvay – postdoctoral fellow in Helen Abud laboratory, shared a number of antibody aliquots for my trial immunohistochemistry runs

Jo Merriner – research assistant in Moira O'Brian laboratory, who shared the technique and gave me a hand in mouse Y-chromosome FISH

Florian Wiede – postdoctoral fellow in Tony Tiganis laboratory, who gave me advice in MACS usage and shared some antibody aliquots for cell sorting

Mary Vail - postdoctoral fellow in Martin Lackmann laboratory, who shared her expertise on cell lines that I used for my experiment

Ian Smyth – head of the laboratory in the Department of Anatomy and Developmental Biology, who shared antibodies from his lab and provided scientific advice

Foula Sozo and Richard Harding – heads of hyperoxia project, who shared hyperoxia experimental method with me

Martin Lackmann – head of the laboratory in the Department of Biochemistry and Molecular Biology, shared his expertise on EphA3, as well as lab antibody aliquots

Hong Wang – my office neighbour and research assistant in Gail Risbridger laboratory, who gave me advice on numerous occasions, samples of antibodies and friendly support

Lisa Kass – PhD student in Helen Abud laboratory, and the great moral support in most difficult situations

Mike Firsov – my beloved husband, my best friend and my constant moral, physical, technical and financial support

Evgenia Pereleshina – student from the Department of Anatomy and Developmental Biology, and my close friend, who was always supportive and ready to provide stress relief during a coffee break

Mei Ling Lim – postdoctoral fellow in Sweden, and my close friend, who always gave a hand when she was around, as well as scientific advice in the moments of confusion

Stephen Wong, Catherine To, Kirstyn Carey, Tomoko Hyakumura, Nisha Antony, Sally Ip, Alicia Corlette, Cecilia Naranjo Golborne, Tia Ditommaso, Lynelle Jones, Olga Plotnikova, Michelle Richards and **Shelley Hedwards** – my colleagues and neighbours from the office and laboratory, who were always or mostly around for a chat (or a long conversation), whether related or not related to this project, and shared their smiles, snacks and equipment

Jonathan Bensley – fellow-student, who was helpful in many situations, and discussed histology of tissues on my slides and statistical analysis with me

Boris Kozlov – my dad, who gave me a lot of encouragement, as well as data analysis and presentation advice

Nina Kozlova – my mum, who always cooked me dinners and gave me a roof above my head

John Baglin – my step-dad, who also cooked dinners, and proof-read this thesis

Anna and Satyam Riordan – my beloved family members, who loved me back and were always there to help when needed

Fr. Geoff and Janet Harvey – my spiritual parents, who constantly cared and prayed for me

Kristian Rotaru, Alexander Dokumenov, Ekaterina Chinarova, Maria and Sergei Kurov, Rachel Hughan, Karina Okotel, Andrey Svyatitskiy, Barbara Mattar, Svetlana Maslyuk and a lot of other friends, who were around

Most importantly, thanks be to God for revealing ideas to me at the right time and for answering my prayers.

Chapter 1. General Introduction

Preterm birth is a frequent event, occurring at an incidence of 10% of all pregnancies (Albertine 2004). It is mainly caused by an infection. During gestation, different organs develop at different rates, with one of the later organs to reach maturity being the lung. As a result, prematurely born children commonly suffer from lung disorders. Underdeveloped lungs are often forced to commence oxygen exchange by the administration of both glucocorticoids (i.e. betamethasone) and high oxygen concentrations (hyperoxia). Such treatment can, however, be suboptimal, with betamethasone having greater systemic effects and hyperoxia leading to chronic damage of the immature lung airway epithelium and vascular ultrastructure. To help provide more effective treatments for preterm infants, it is relevant to examine and understand the cellular and molecular mechanisms regulating early lung development and, as such, provide a clearer idea of the processes being affected by hyperoxia.

Hyperoxia is a higher than normal atmospheric oxygen supply to the organism, which is applied in medicine in cases when the lungs cannot provide enough oxygen to the body (for example, in preterm birth, when the lungs are under-developed, or in cases of lung disease due to injury or cancer). Hyperoxia triggers a number of changes in the organism, most of which can be harmful. Multiple studies have been performed in order to characterise the consequences of hyperoxia and find the treatment for such consequences. It has been shown that various organs are affected by hyperoxia, especially the lung itself. However, most of these treatments of hyperoxia-induced deficits are still under investigation. Therefore the problems associated with the use of hyperoxia in preterm birth remain a major issue in medical research.

The aim of this study was first to establish and characterise a robust neonatal mouse hyperoxia model to investigate whether specific temporal effects of hyperoxia on lung development are similar in the mouse and in the human. The second aim was to observe the recovery progress through to adulthood, and to document any chronic effects of neonatal high oxygen exposure. The third aim was to investigate the application of various

cell types that may be suitable for the treatment of morphological parameters of lung development that result from hyperoxia.

1.1. Preterm birth and lung development in gestation

Preterm birth is any delivery that occurs between 20 and 37 weeks (term) of human gestation. Children born before 20 weeks of gestation usually do not survive. Very premature children are born between 20 and 32 weeks of gestation with underdeveloped lungs, as this organ develops late in gestation and is not competent for exchange gas, a function that is performed by the placenta during gestation. The lungs undergo development in specific stages. These stages will be further described in the human and in the mouse in order to highlight the processes that might be disrupted by preterm birth.

1.1.1. Stages of lung development in gestation

The first overt morphological step of lung development occurs between four and six weeks of gestation in humans or on the 9^{th}-10^{th} embryonic day (E9-10) in mice, which is called the embryonic stage (Harding and Hooper 1996; Warburton, Gauldie et al. 2006). During this stage, the laryngotracheal groove forms in the foregut and starts budding. Between six weeks of human gestation (E10 in mice) and nearly eight years of age postnatally (at least three weeks of age in mice), lung development can be divided into four stages: pseudoglandular, canalicular, saccular and alveolar (Fig. 1.1).

The pseudoglandular stage starts at six weeks of human gestation and lasts approximately 10 weeks, when almost all pulmonary conducting airways and blood vessels are created and the lung proximal epithelium starts differentiating (McGowan 2004). In mice this stage lasts from E10 until E16.5 (Warburton, Gauldie et al. 2006).

The canalicular stage occurs during the next 10 weeks in human. It is characterised by the formation of respiratory bronchioles and alveolar ducts, the differentiation of alveolar type II cells and an increasing number of capillaries associated with the terminal ducts

(Albertine 2004; Warburton, Gauldie et al. 2006). Born at this stage, humans usually are not able to breathe, as the lungs are not mature enough to support proper gas exchange. In mice this stage occurs at E16.5-E17.4, when the terminal sacs and vascularisation start to develop (Warburton, Gauldie et al. 2006).

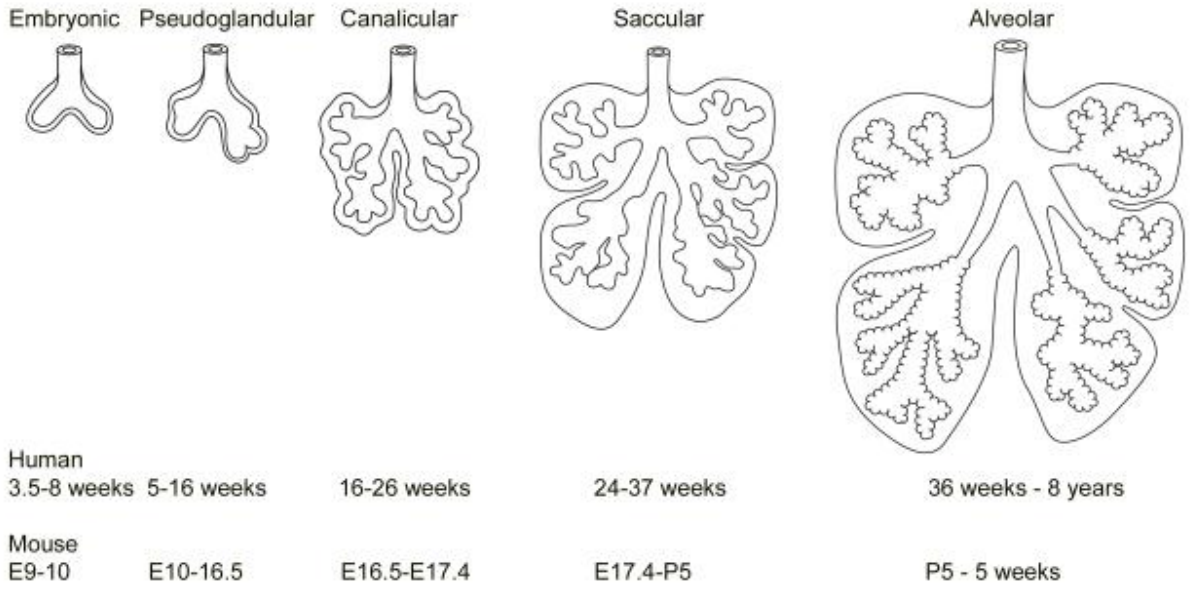

Figure 1.1. Stages of the lung development and their approximate timing in humans and mice: embryonic, pseudoglandular, canalicular, saccular and alveolar.

Starting from the 24th week of gestation and continuing until term, the human lung proceeds through the saccular stage of lung development, which is characterised by the formation of terminal sacs and ducts, and division of terminal tubules – a process that is also called primary septation (McGowan 1992; Burri 2006). The mouse gestation period only lasts for 18.5 days and the saccular stage of lung development occurs between E17.4 and P5, so mice are normally born during this stage (Yamamoto, Yun et al. 2007). This feature makes mice a suitable model for studying premature lung diseases without an increased animal mortality, as compared to other animals, such as sheep that would have the same lung physiology as humans if born at this stage (Alcorn, Adamson et al. 1981).

One of the more important events of the saccular stage is epithelial cell differentiation. It usually starts at approximately 24 weeks of gestation in the human. There are two main

types of cells present in the epithelium of the developed lung: the alveolar epithelial type I cells (AEC-I) that occupy 90-96% of the gas-exchange surface and the alveolar epithelial type II cells (AEC-II) that occupy less than 10% (McGowan 2004). AEC-II begin to differentiate at 24 weeks of gestation in humans (day E18 in mouse) and give rise to AEC-I (Burri 1997; Warburton, Gauldie et al. 2006). AECII are involved in respiratory immunity and produce alveolar surfactant. There are four surfactant associated proteins (Sftp) that have been identified: Sftpa, involved in innate host defense against pathogens and in an increase in surfactant surface tension lowering properties; Sftpb, facilitates the spreading of surfactant proteins on the alveolar surface; Sftpc, responsible for biophysical properties of other surfactant proteins; and Sftpd, involved in host defense and surfactant metabolism (McGowan 2004).

At the saccular stage the respiratory epithelium is immature, there are no alveoli and therefore there is a lack of gas-exchange surface area, as thinning of the epithelium has not yet occurred. There is a lack of smooth muscle in the airway walls and cell-cell adhesion is weak. The lungs of premature infants may not have an adequate number of AEC-II that only start to differentiate at the saccular stage, and as a consequence may not produce a sufficient amount of pulmonary surfactant and a sufficient number of differentiated AEC-I for efficient gas exchange. As a result, these premature infants can only survive with surfactant therapy (synthetic surfactant supplementation) and ventilation (Jobe and Bancalari 2001). In less severe cases high oxygen treatment (hyperoxia) is applied. Prenatal and antenatal administration of glucocorticoids, nutritional deficiencies, inflammation, hyperoxia and mechanical ventilation are all hypothesised to contribute to decreased alveolarisation and development of bronchopulmonary dysplasia, or BPD (McGowan 2004).

The alveolar stage is the last stage of human lung development. It starts during gestation, after the saccular stage, and ends during postnatal life (Burri 1997; Albertine 2004). In mice and rats it begins five days after birth and lasts for approximately three weeks (Warburton, Gauldie et al. 2006). It is essential that both epithelial and vascular structures of the lung undergo proper formation and growth during this stage. These two processes are closely linked, and therefore will be discussed in more detail.

The first event of alveolarisation in the mouse and in the human is secondary septation which is initiated by protrusion of secondary crests from the primary septal walls of the terminal sacs (McGowan 2004). The tension of the elastic fibers rearranges the collagen skeleton supporting the forming septum which has elastic fibers at the tip (Burri 2006). The second event is remodeling of the alveolar walls. Redistribution of tissue mass involving a proliferation of interstitial fibroblasts (IFs) stretches the septa (or crests), and this is followed by an increase in the number of AEC-II and endothelial cells, a decrease in the thickness of endothelial walls and an expansion of the lung space (Burri 1974; Kauffman, Burri et al. 1974). Proliferation of AEC-II is known to be triggered by fibroblast growth factors 1 and 7 (Fgf1, Fgf7), hepatocyte growth factor (Hgf) and by retinoic acid (RA, the active metabolite of vitamin A) (Massaro and Massaro 1997; Yen, Yang et al. 2006). RA is also known to regulate alveolar morphogenesis. Septation and gas-exchange surface may be increased with dexamethasone and RA treatment (Massaro and Massaro 1992; Massaro and Massaro 1996). At this stage the lungs are ready to support sufficient gas exchange, and children born at this stage are at a lower risk of bronchopulmonary dysplasia, or BPD.

1.1.2. The role of vascularisation in alveolar development

Vascularisation accompanies alveolarisation during lung development and repair (Schwarz, Lee et al. 1999; Warburton and Lee 1999; Fehrenbach, Voswinckel et al. 2008). These processes represent an intricate component of alveolar development, as blood vessels are involved in gas exchange directly and indirectly. The lung blood vessel system not only provides for exchange of oxygen and carbon dioxide from alveoli to all tissues and organs of the body, but also exchanges necessary molecules and metabolites for lung homeostasis.

Cooperation between alveolarisation and vascularisation exists at the molecular level. The process of vascularisation is stimulated by vascular endothelial growth factor A (Vegf-A) which is produced by alveolar epithelial cells (Ng, Rohan et al. 2001; Yamamoto, Yun et al. 2007). The establishment and remodeling of endothelial channels is controlled by the activity of transmembrane receptor tyrosine kinases; for example, the receptors of

angiopoietins 1 and 2 (Ang1/2) Tie2 or Tek, and VEGF receptors, such as FMS-like tyrosine kinase 1 (Flt1) and a kinase insert domain protein receptor (Kdr or Flk1) (Hanahan 1997; Patan 1998). Inhibition of VEGF receptors causes both alveolar and endothelial cell apoptosis and enlargement of lung airspaces (Kasahara, Tuder et al. 2000), which suggests that lung alveolar maintenance is highly dependent on the VEGF pathway. Tek is responsible for vessel structure and the interaction between the endothelial wall and the surrounding mural cells (i.e. pericytes and smooth muscle cells) including intussusceptive (non-sprouting, telescopic growth by inserting of new tissue pillars) vascular growth (Patan 1998; Burri and Djonov 2002). Flt1 activity is required for the formation of vascular tubes, and Kdr is essential for endothelial cell differentiation (Hanahan 1997). Once endothelial cells have differentiated, they form vessels and express platelet/endothelial cell adhesion molecule 1 (Pecam1) and von Willebrandt Factor (vWF) as well as other markers, depending on the specific type of vessel. Endothelial cells release paracrine factors (for example, Hgf) to coordinate epithelial growth during septation (Yamamoto, Yun et al. 2007). These findings confirm, that vascularisation and alveolarisation are closely linked and co-dependent. It is essential that the alveolar stage of lung development proceeds correctly, as it will determine the functional capability of the lungs in the future life.

Following preterm birth, therefore, there is a high chance that both vascularisation and alveolarisation of the lungs will be under-developed. Lung performance, therefore, would not be sufficient for proper gas exchange, which could cause changes in function as well as changes to the development of other essential organs through the lack of oxygen in the organism. To avoid hypoxic damage to the brain and other organs, high concentrations of oxygen are supplied via the lung in order to maintain normal levels of oxygen in the body. On the one hand, however, high oxygen concentrations will help to support a normal oxygen supply, but on the other, hyperoxia has been reported to slow down further lung development and damage vascularisation in the lungs and in the other organs. Therefore, these effects require further investigation in order to improve future clinical treatments.

1.2. Hyperoxia-induced lung deficit

There is a variety of methods (including different concentrations of oxygen and different oxygen flow pressure) that are used to supply oxygen to the organism via the premature lung. The high variability between various treatments and conditions in animal models makes it difficult to establish one injury model for studying a suitable universal repair therapy. Several experimental models and their physiological consequences in animals will, therefore, be further discussed below to justify a standard model of lung hyperoxia used in this thesis to study preterm lung deficit.

There are different methods for supplementing oxygen delivery to the lung, which include mechanical ventilation and high oxygen chamber treatment. Mechanical ventilation causes overinflation of the lungs, thus increasing microvascular permeability and leading to: (i) endothelial cell damage, (ii) alveolar flooding (edema), (iii) inactivation of surfactant synthesis and ultimately (iv) atelectasis, or collapse of the lungs (Tomashefski 2000; Albertine 2004). Extreme mechanical damage and injury of the lungs can be avoided by using chamber oxygen treatment instead of mechanical ventilation. The influence of high oxygen exposure during the saccular stage of lung development can then be investigated without mechanical lung damage. In this study, chamber oxygen treatment will therefore be the main method under discussion and investigation.

A variety of effects have been observed after different concentrations of oxygen have been applied in chamber oxygen treatment, and different results have been published in a number of studies on different species, such as the rat, rabbit and mouse (Dombrowsky, Tschernig et al. 2006; Mataloun, Rebello et al. 2006; Balasubramaniam, Mervis et al. 2007). Therefore it is rather difficult to isolate the effects of hyperoxia on lung development, as different species might react differently to high oxygen exposure, especially when different oxygen concentrations are used. Some of these studies described below refer to protein content in the lungs; others only describe pulmonary morphology or physiology, and therefore have to be considered as descriptions of the separate aspects of hyperoxia effects.

Studies on the rat have shown that hyperoxia exposure (85% oxygen) for 1 week after birth caused increased Sftpa and Sftpd content, which reduced lung surface tension (Dombrowsky, Tschernig et al. 2006). Hyperoxia exposure for longer periods of time (2-3 weeks) caused: (i) increased smooth muscle actin content, (ii) fibrosis, (iii) reduced *aquaporin 5* and *Hoxb5* expression, (iv) increased *Sftpb* expression, (v) decreased mean alveolar surface area and secondary crest number, and (vi) reduced microvessel formation (Ozer, Kumral et al. 2005; Fu, Xue et al. 2008). High surfactant-associated protein content and *Aqp5* and *Hoxb5* marker expression could indicate an increased number of AEC-II, as they can proliferate and repopulate the lung surface area. However, the mechanism of this increase has to be further investigated.

Exposure of premature rabbits to 95% oxygen for 11 days resulted in a reduced number of alveoli and an increased collagen deposition (which might indicate lung fibrosis), as well as increased septal thickness and mean linear intercept (Mataloun, Rebello et al. 2006). So a reduction in alveolarisation and an increase in fibrosis could be considered a common effect in adult rats and premature rabbits, after approximately one week of high oxygen treatment.

A number of hyperoxia studies have been performed on mice. When treated with 65% oxygen for the first month of life, mice had fewer and larger alveoli than control mice, and the weight of the treated animals was normal (Dauger, Ferkdadji et al. 2003). Eighty percent hyperoxia had a similar effect on neonatal mice (Balasubramaniam, Mervis et al. 2007). Also hyperoxia increased breath duration, respiratory system compliance and baseline tidal volume (Dauger, Ferkdadji et al. 2003). So alveolarisation is affected by hyperoxia in all examined species at ranges between 65%-95% of oxygen.

According to a number of reports, not only alveolarisation, but also vascularisation is affected in the lungs after hyperoxia treatment (Balasubramaniam, Mervis et al. 2007). Treatment with 80% oxygen has been shown to reduce the expression of *Vefg-A* mRNA and its product – vascular endothelial growth factor, or VEGF, as well as its receptor Kdr, endothelial nitric oxide synthase (eNOS) and erythropoietin receptor (EPO-R) protein levels in the mouse lungs (Balasubramaniam, Mervis et al. 2007; Zimova-Herknerova,

Myslivecek et al. 2008). It also reduces circulating $Prom1^{+}/Kdr^{+}$ endothelial progenitor cells (EPCs) in the blood, bone marrow and lungs (Balasubramaniam, Mervis et al. 2007). Treatment of hyperoxia-treated mice with either human recombinant VEGF or injection of Tek-positive EPCs increases alveolarisation (Kunig, Balasubramaniam et al. 2005; Balasubramaniam, Ryan et al. 2010), which suggests that vascular stimulation positively affects lung septation and development. Conversely, VEGFA expression (mRNA levels) is increased in AEC-II in adult rabbits three days after hyperoxia exposure, i.e. during recovery (Maniscalco, Watkins et al. 1995). It has also been reported that after hyperoxia VEGF mRNA splice variants change (Watkins, D'Angio et al. 1999). Also, human patients with acute lung injury display increased numbers of circulating EPCs in the blood following hyperoxia (Burnham and Moss 2006), which indicates that the organism responds to lowering oxygen conditions (returning back to normal oxygen) by stimulating vascularisation.

The difference in VEGF response in different experiments could be assigned to different reaction timing in different species, as in most studies only one time point has been tested. The number of EPCs is likely to be dependent on VEGF, the predominant endothelial mitogen (Ingbar 2000). VEGF remains one of the essential factors in lung growth and development, but has adverse effects. It can be concluded, that after hyperoxia exposure vascularisation is highly affected, and its stimulation increases in some animals during recovery process, which in turn increases the number of endothelial progenitor cells, which are reduced after high oxygen treatment. Alveolarisation and secondary crest formation are also disrupted. These data suggest, that hyperoxia is causing significant changes in lung structure and function.

In summary, the result of oxygen treatment seems to be rather dependent on the parameters of this treatment, such as the species treated and the time and concentration of oxygen applied, as well as the time after hyperoxia exposure when the analysis was performed. When the hyperoxia effects are analysed, it is essential to keep in mind that molecular responses might be rather dependent on these variable conditions, whereas physiological response could be easier to analyse. Interventive steps are taken to reinforce cell differentiation and repair lung tissue after ventilation or hyperoxia, but most

remain sub-optimal or under further investigation. To provide more effective treatments for preterm infants that have to stay in high oxygen conditions for a period of time, it is necessary to characterise the molecular and physiological reaction of the lungs to hyperoxia, as well as observe the long-term effects at different time points. By understanding temporal changes in the cellular and molecular mechanisms associated with lung development and recovery, novel and safer approaches that may supplement or replace glucocorticoid treatment following premature birth and hyperoxia can be developed.

1.3. Cell therapy for the treatment of lung deficiency or injury

Chronic lung disease that follows hyperoxia involves changes in various differentiation and developmental pathways in the lung. The key processes affected in chronic lung disease include pulmonary vascularisation, lung septation and the formation of alveoli (Thebaud and Abman 2007). Various potential treatments of this condition have been suggested, including cell therapy (Balasubramaniam, Ryan et al. 2010), growth factor and chemokine supplementation (Panos, Bak et al. 1995; Kunig, Balasubramaniam et al. 2005; Zimova-Herknerova, Myslivecek et al. 2008) and blockage (Deng, NicholasMason et al. 2000; Kim, Chow et al. 2012), as well as conditioned media treatment (Aslam, Baveja et al. 2009; van Haaften, Byrne et al. 2009; Ionescu, Alphonse et al. 2012). Growth factors and conditioned media supplementation might have a short-term effect *in vivo*; and the repeated injections would be required. It is hypothesised therefore that cell therapy may be more effective due to the ability of cells to multiply *in vivo* and adjust to the environment, i.e. differentiate into the required type of cell at the injury site (Kajstura, Rota et al. 2011).

A number of cell types might be required to restore lung structure, because both alveolarisation and vascularisation are affected as a result of hyperoxia. The lung is anatomically a complex organ with a vast number of morphologically differentiated cell lineages (Engelhardt 2001). Multiple cell types represented in the lung might be damaged,

which makes it difficult to determine the right stem cell population for treatment. Apart from ciliated columnar cells, mucus secreting cells, Goblet cells, Clara cells, AEC-I and –II, and other epithelial cells, there are also IFs, vascular, lymphatic and neuronal cells that may be damaged. There are endogenous (bronchoalveolar) and exogenous (mesenchymal) sources of stem cells for the lung (Warburton, Perin et al. 2008). Among endogenous cells there are basal epithelial cells, variant-Clara cells, bronchoalveolar stem cells and AEC-II, that are hypothesised to be precursors of most lung epithelial cells (Olsson, Denham et al. 2007). These cells carry great potential, but are not suitable for cell therapy; as their isolation from donors is rather complicated because these cells are not easily accessible. One source of exogenous stem cells that is easily accessible is the vascular and mesenchymal progenitor containing bone marrow (Warburton, Perin et al. 2008). The potency of these cells and the mechanism of their reported trans-differentiation into cell types that may contribute to lung homeostasis, however, remain unclear.

1.3.1. Cell populations of the bone marrow and their potency

Several researchers hypothesise that bone marrow cells can differentiate into epithelial cells (Wang, Bunnell et al. 2005; Chun-mao, Su-yi et al. 2007). However, this hypothesis can theoretically be proven false by considering the limited potency of bone marrow cells (Beck, Voswinckel et al. 2003). The three germ layers (ectoderm, endoderm and mesoderm) are represented in various organs throughout the body. Lung epithelial cells, for example, are known to be of endodermal origin, and lung interstitial cells – of mesodermal origin, assisting lung development via mesenchymal-epithelial interactions (Spooner and Wessells 1970; Wessells 1970; Firsova, Hyakumura et al. 2010). Bone marrow is located within trabecular bone, surrounded by cortical bone or cartilage, and is of mesodermal origin (Wilkins 1992). There have been no reports that endoderm derivatives are present in the bone marrow. All cell types in the population of bone marrow cells isolated by flushing the bones are considered to be either mesoderm or ectoderm derivatives.

Human bone marrow contains three kinds of stem cells: hematopoietic stem cells (HSCs), endothelial progenitor cells (EPCs) and mesenchymal stromal cells (MSCs), as well as several types of differentiated cells: lymphocytes, plasma cells, mast cells, adipocytes, nerves, fibroblasts and macrophages (Reimann and Christensen 1977; Wilkins 1992; Chun-mao, Su-yi et al. 2007). HSCs differentiate into lymphoid progenitors (T cells and B cells) and myeloid progenitors (monocytes and macrophages, neutrophils, eosinophils, mast cells, erythrocytes, megakaryocytes), but not into epithelial cells (Orkin 2000). EPCs give rise to endothelial cells, and MSCs (also known as marrow stromal cells) that possess the potential to differentiate into bone, cartilage and fat (Aguilar, Nye et al. 2007). All mentioned types of stem cells have been reported to migrate from the bone marrow to wound sites via the blood stream, where they are suggested to engraft and repair the tissues. However, all stem cell types of the bone marrow originate from the embryonic mesoderm, while the lung epithelium is vastly an endoderm-derived tissue. In one recent study it was reported that MSCs (i.e. plate-adherent cells) express stage-specific embryonic antigen 4 (SSEA-4), a marker of pluripotency, thus raising questions regarding the pluripotency of bone marrow stem cells (Gang, Bosnakovski et al. 2007). Furthermore, the question of limited trans-differentiation has been raised a number of times in studies on bone marrow cells, especially MSCs (Chun-mao, Su-yi et al. 2007). It has also been suggested that EPCs can become MSCs via an endothelial-mesenchymal transformation, which could lead to the hypothesis, that these cell types share the same precursor (Bernanke and Markwald 1982; Medici, Shore et al. 2010). Whether these cells are truly pluripotent and capable of giving rise to lung endoderm, however, still remains unknown.

As mesodermal derivatives, MSCs and EPCs may improve the vascular structure of the lung by differentiating into mural and endothelial cells depending on the type of injury. MSCs could carry potential in the lung, contributing to fibrocytes and supporting mesenchyme, and by promoting alveolarisation via mesenchyme-epithelial interactions (Spooner and Wessells 1970; Wessells 1970; Firsova, Hyakumura et al. 2010). Compared to MSCs, EPC engraftment in lung tissue after the injury has not been a popular area of research, although this cell type is more specific and is likely to be more valuable in lung injury due to vascularisation damage (Balasubramaniam, Mervis et al.

2007). EPCs have not been described and characterised as thoroughly as HSCs and MSCs, and there is no common technique for their isolation. However, a number of researchers have published their perspective on EPCs (such as definition, representative types and common surface markers) and optimised their own methods for their isolation and culture. These methods are described below.

1.3.1.1. Endothelial progenitor cell characteristics

Endothelial progenitor cells are essential for vasculogenesis, especially in the case of vessel damage and leakage, which can happen after lung injury. Human EPCs share similar features with both MSCs (i.e. plate-adherence) and HSCs, i.e. some surface markers, for example: Prominin (PROM1 or CD133), Cd34 molecule (CD34), kinase insert domain protein receptor (KDR or FLK1), platelet/endothelial cell adhesion molecule (PECAM1 or CD31) and alanyl-aminopeptidase (ANPEP or CD13) (Bertolini, Shaked et al. 2006; Yoder, Mead et al. 2007). EPCs circulate in the blood stream and engraft the endothelial wall of wound sites. *In vitro* EPCs are able to (i) differentiate into mature endotheliocytes, immunoreactive to the Von Willebrandt factor (VWF) and PECAM1, (ii) uptake acetylated low-density lipoprotein (LDL) and (iii) bind to lectins (Khakoo and Finkel 2004). Various types of injuries have different effects on the number of EPCs in circulation. Hyperoxia of the neonatal lungs reduces the number of EPCs in the circulation, bone marrow and lungs, whereas patients with acute lung injury have an increased number of circulating EPCs (Burnham and Moss 2006; Balasubramaniam, Mervis et al. 2007). Transplanted EPCs have been observed in various injured tissues, not only engrafting in existing vessels, but also creating new capillaries via angiogenesis (Asahara, Masuda et al. 1999; Yoder, Mead et al. 2007). All these results suggest direct or indirect involvement of EPCs in a mechanism of injury repair and suggest that EPC administration may represent a suitable cell therapeutic tool.

1.3.1.2. Types of endothelial progenitor cells

There have been a number of studies reporting at least two types of EPCs; however, there is still no uniform definition for an EPC as such. Various studies demonstrate the early and late EPC populations, isolated from peripheral blood (Yoon, Hur et al. 2005; Deschaseaux, Selmani et al. 2007), indicating that late EPCs have a higher capacity to produce blood vessel-like tube structures. However, late EPC isolation involves a period of time in culture which increases the chance of mutations and reduces further cell survival *in vivo*. This makes these cells less suitable for transplantation and cell therapy use, compared to freshly-isolated cells.

1.3.1.3. Endothelial progenitor cell markers

Human EPCs are reported to possess the following surface markers: PROM1, CD34, Endoglin (ENG or CD105), melanoma cell adhesion molecule (MCAM or CD146), Cadherin 5 (CDH5 or CD144), PECAM1, ANPEP, v-kit Hardy-Zuckerman 4 feline sarcoma viral oncogene homolog (KIT or CD117), KDR, fms-related tyrosine kinase 4 (FLT4) and, in some fractions, protein tyrosine phosphatase receptor C (PTPRC or CD45) (Khakoo and Finkel 2004; Bertolini, Shaked et al. 2006). Most of these markers are shared with HSCs and some with lymphocytes and macrophages (Khakoo and Finkel 2004; Bertolini, Shaked et al. 2006; Yoder, Mead et al. 2007). However, they are currently used for EPC isolation, and will be discussed and tested in this study.

Tyrosine kinase receptor KDR is also called vascular endothelial growth factor receptor 2 (VEGFR2). It is known to be expressed not only in EPCs, but also in fractions of HSCs and mature myeloid cells at a lower level (Asahara, Masuda et al. 1999; Bertolini, Shaked et al. 2006). It has also been observed in alveolar epithelial type II cells during antenatal and postnatal lung development (Ahlbrecht, Schmitz et al. 2008). This receptor is essential for the formation of blood islands and blood vessels in mouse embryos, and for the proliferation and differentiation of endothelial precursors (Shalaby, Rossant et al.

1995). Vascular endothelial growth factor A (VEGF-A) phosphorylates KDR (or Kdr in mice) and activates Nck (MAP kinase), PLCɣ (PKC), as well as Shb (FAK and PI3K) and VRAP (Src), promoting proliferation, migration, permeability and survival of EPCs (Shibuya 2006; Holmes, Roberts et al. 2007).

Melanoma cell adhesion molecule CD146 (MCAM) is widely expressed in various bone marrow cells, including EPCs, MSCs and subsets of lymphocytes (Elshal, Khan et al. 2005; Kang, Wang et al. 2006; Covas, Panepucci et al. 2008). The molecular mechanism of MCAM in different cell types in still unclear, although it is known to promote tumor-induced angiogenesis by activating p38/IKK/NFκB signalling and therefore promoting endothelial motility (Zheng, Qiu et al. 2009).

Prominin (CD133 or Prom1) is a cell surface-associated protein, which is present in various progenitor populations, including HSCs and EPCs, and also cancer stem cells (Yin, Miraglia et al. 1997; Mizrak, Brittan et al. 2008). It contains a functional polypeptide AC133 with five transmembrane domains, but its exact mechanism of maintenance of 'stemness' remains unknown (Miraglia, Godfrey et al. 1997).

TEK (or TIE2) is a receptor tyrosine kinase, with immunoglobulin and epidermal growth factor homology domains-2 and is critical for vascular development, especially vessel structure (angiogenesis) and endothelial cell proliferation (Sato, Qin et al. 1993; Dumont, Gradwohl et al. 1994). In bone marrow, TEK is expressed in populations of EPCs and HSCs, and is responsible for the interaction between the endothelial wall and the surrounding mural cells including intussusceptive vascular growth and for endocardial/myocardial interaction during development (Sato, Qin et al. 1993; Dumont, Gradwohl et al. 1994; Davis, Aldrich et al. 1996; Sato, Iwama et al. 1998). TEK is activated by Ang1 and becomes phosphorylated, activating cell motility, anti-inflammatory response, and promoting cell survival via different pathways (Davis, Aldrich et al. 1996).

CD34 is a highly glycosylated transmembrane protein, which is expressed in HSCs and some, but not all, endothelial cells of the blood vessels (Delia, Lampugnani et al. 1993; Baumhueter, Dybdal et al. 1994). It is hypothesised to play an inhibitory role in endothelial adhesion functions (Delia, Lampugnani et al. 1993). CD34 is an essential marker of progenitor cells for the bone marrow repopulation of irradiated animals, and could be used for hemopoietic and vascular therapies (Berenson, Andrews et al. 1988; Krause, Ito et al. 1994). It has also been hypothesised to be essential for bone marrow cell homing (Krause, Theise et al. 2001).

1.3.1.4. Other novel endothelial and mesenchymal progenitor cell markers

Ephrin type-A receptor 3 (EphA3 or HEK) is a receptor tyrosine kinase with a single-pass transmembrane domain and several extracellular domains (Lackmann, Oates et al. 1998). It binds several ephrins, having stronger affinity with ephrins-A, especially ephrin-A5, and weaker affinity with ephrins-B (Lackmann, Mann et al. 1997). Applied with ephrin-A5, it inhibits a number of critical events in early zebrafish embryogenesis, especially cell migration (Oates, Lackmann et al. 1999). *EphA3*$^{-/-}$ knockout mice demonstrate defective formation of the endocardial cushion, atrial septa and mesenchymal cup as well as a reduced mesenchymal cell number in atroventricular canal explants (Stephen, Fawkes et al. 2007). These data indicate an involvement of EphA3 in an endothelial-mesenchymal transition during heart development. EphA3 is not known as an endothelial or mesenchymal progenitor marker, however, EphA3^{+} cells from bone marrow have been demonstrated to differentiate into osteocytes, as well as to locate in close association with Pecam1-positive blood vessel formation (Vail, Tan et al. 2012). EphA3 is highly expressed in malignant cells and is hypothesised to be essential for their metastases: anti-EphA3 antibody is being investigated for use in cancer therapy (Vearing, Lee et al. 2005; Vail, Tan et al. 2012). Together, these data suggest that EphA3 may be a promising endothelial and mesenchymal progenitor marker that could support formation of blood vessels and their surrounding layers. Therefore, EphA3^{+} cells might also have a contribution to the repair of the lung after hyperoxia, either via contributing to

mesenchymal layers associated with blood vessels, or by promoting vascular development via signalling molecules.

1.3.1.5. Mature endothelial markers

Mature endothelial cells can be characterised by *in vitro* vessel structure formation and immunoreactivity to a number of functional markers, including: PECAM-1 (CD31) and von Willebrandt Factor (vWF). Platelet endothelial cell adhesion molecule-1 (PECAM-1) is a member of the immunoglobulin superfamily. It is located on the surface of endothelial progenitors as well as on mature endothelial cells, circulating platelets, monocytes, mature myeloid cells neutrophils, and selected T cell subsets, as well as on HSCs (Newman 1997; Bertolini, Shaked et al. 2006). It can be observed in significant amounts on the sites of endothelial and platelet cell interaction junctions, and is characterised as an important molecule for cell adhesion, it is also likely to be involved in leukocyte migration, integrin activation and angiogenesis (Albelda, Oliver et al. 1990; Newman 1997). Von Willebrandt Factor (vWF) is a large glycoprotein that mediates the adhesion of platelets to subendothelial connective tissue in hemostasis, and it binds blood clotting factor VIII (Sadler 1998). VWF is synthesised in endothelial cells and megakaryocytes and therefore can be used as an intracellular marker for mature endothelial cells (Jaffe, Hoyer et al. 1974; Nachman, Levine et al. 1977). These two markers are used in this study to demonstrate the presence of endothelial cells after the stimulation of EPC differentiation.

1.3.1.6. Hematopoietic cell markers to determine non-endothelial lineage

PTPRC (CD45) is a protein tyrosine phosphatase receptor type C, a transmembrane glycoprotein with multiple ligands, that participates in the immune response of T cells (Altin and Sloan 1997). It is expressed in different isoforms on enucleated HSCs and lymphocytes, but not (or at very low levels) on EPCs (Altin and Sloan 1997; Bertolini, Shaked et al. 2006). This marker is used in this study to demonstrate the number of cells that are positive for EPC markers, mentioned above, but that also represent hematopoietic cells.

1.3.1.7. Isolation of endothelial progenitor cells

Endothelial progenitor cells (EPCs) can be conveniently isolated from bone marrow. However, there is currently no common or standardised method for their isolation. It is therefore essential to define EPCs using cell surface markers as well as optimise a consistent method of isolating them for cell therapeutic purposes. As described earlier, EPCs share various surface markers with other cell types, yet can be separated based on plate adherence. It can, therefore, be hypothesised that the optimal method of isolating EPCs is to enrich the bone marrow for endothelial cell surface markers and then culture these cells *in vitro* for further analysis of blood vessel formation. The cell fraction displaying the most effective vessel forming ability is then suggested to be the one optimal for use in cell therapies.

1.3.1.8. Endothelial progenitor cell culture and differentiation methods

To date there is no common method of culture and differentiation of mouse EPCs into mature endothelial cells. Most methods are optimised for human EPCs or ECs, and culture conditions for mouse EPCs are still to be developed. Methods used in different laboratories vary both in human (Table 1.1) and in mouse (Table 1.2) culture systems. Common factors used for growth and differentiation of EPCs are VEGF, FGF2 (or bFGF), heparin, L-glutamine and ascorbic acid, and the more common attachment factors are gelatin and fibronectin (Visner, Staples et al. 1994; Asahara, Takahashi et al. 1999; Gehling, Ergün et al. 2000; Kalka, Tehrani et al. 2000; Quirici, Soligo et al. 2001; May, Mueller et al. 2005; Kahler, Wechselberger et al. 2007; Schniedermann, Rennecke et al. 2010; Sekiguchi, Ii et al. 2011; Yang, Ii et al. 2011). As for basal medium, EBM-2 or EGM-2 (manufactured by Lonza Group Ltd.) is commonly used for endothelial cell growth (Asahara, Takahashi et al. 1999; Kahler, Wechselberger et al. 2007; Sekiguchi, Ii et al. 2011). However, Lonza Group Ltd. does not provide a list of media and supplement components, which makes it difficult to dissect conditions optimal for cell growth and differentiation. In the current project various media bases were tested in order to observe salt balance effects on EPC growth and morphology. Furthermore, media supplements

and growth factors were applied according to common concentrations described in the literature (General Materials and Methods). Standard medium was used for control to culture cells without differentiation (Rochefort, Vaudin et al. 2005).

Media component	Visner et al, 1994	Gehling et al., 2000	Kalka et al., 2000	Kahler et al, 2007	Quirici et al., 2001
Cultured cells source	Human pulmonary artery	Human peripheral blood	Human blood	Human lung	Human bone marrow
Media	M199	IMDM	EGM-2	EBM-2	M199
FCS	20%	10% +10% Horse serum	5%	10%	10%
Hydrocortisone		10^{-6} M/L		present	
Growth factors	Retinal-derived GF	SCGF, VEGF	hEGF, VEGF, hFGF, IGF	VEGF, FGF2, IGF, hEGF, SCGF	VEGF, FGF2, IGF
Additional factors	L-glutamine, ITS, Heparin	L-glutamine	Ascorbic acid	Ascorbic acid	
Dish coating	Gelatin	Fibronectin	Fibronectin	Matrigel	

Table 1.1. Cell culture conditions used for *in vitro* culture of human EPCs and ECs.

Media component	Asahara et al., 1999	Yang et al., 2011	May et al., 2005; Schniedermann et al., 2010	Sekiguchi et al., 2011
Cultured cells source	Mouse blood	Mouse bone marrow	Mouse embryos, mouse lung	Mouse bone marrow
Media	EBM-2	M3236	DMEM	EBM-2
FCS	5%	10%	20%	10%
Growth factors	Unknown	VEGF, SCF, EGF, IL-3, IGF-1, FGF2	ECGF for growth, VEGF and FGF2 for differentiation	Supplement contains FGF2 (Lonza)
Additional factors	Gelatin	Heparin	L-glutamine, NEAA, heparin, β-mercaptoethanol	
Dish coating	Vitronectin		Gelatin	Pronectin or vitronectin

Table 1.2. Cell culture conditions used for *in vitro* culture of mouse EPCs and ECs.

1.3.2. Engraftment of transplanted stem/progenitor cells into lung tissue

The contribution of various stem cells to the damaged lung, especially cells derived from bone marrow has been under investigation during the last decade (Kotton, Ma et al. 2001; Ishizawa, Kubo et al. 2004; Chang, Summer et al. 2005; Wang, Bunnell et al. 2005; Zander, Baz et al. 2005; Kahler, Wechselberger et al. 2007; Aslam, Baveja et al. 2009). Bone marrow is known to contain various cell types, and is accessible from donors (Albera, Polak et al. 2005). There is some evidence that bone marrow cells are able to repair the damaged lung and other organs (Yamada, Kubo et al. 2004; Spees, Whitney et al. 2008; Balasubramaniam, Ryan et al. 2010). In these studies, various lung injury models have been used in order to demonstrate engraftment and structural or functional improvement of the lung after cell injection, and various endothelial progenitor cell types have been selected for treatment.

Several studies have demonstrated engraftment of plate-adherent cells from bone marrow in the lung following bleomycin administration (a bacterial protein that induces inflammation): injected plastic adherent bone marrow cells were present in the alveoli wall and were immunoreactive to antibodies for: a donor-specific marker, the AEC-I marker Podoplanin (T1-alpha) and epithelial pan-cytokeratin, thus indicating a close relationship of injected cells with lung epithelial cells (Kotton, Ma et al. 2001; Anjos-Afonso, Siapati et al. 2004). After injection of $CD34^-/Ptprc^-$ plastic adherent bone marrow cells into the lung injured with bleomycin, inflammation and collagen depositions were reduced (Ortiz, Gambelli et al. 2003).

Apart from plastic-adherent cells, other cell types from the bone marrow have been analysed for engraftment and lung injury repair. Green fluorescent protein (GFP) positive bone marrow mononuclear cells transplanted into irradiated mice were observed in lung sections at an incidence of 1-7% of all cells expressing cytokeratin (Grove, Lutzko et al. 2002; Abe, Lauby et al. 2003). Similar results have been obtained following injury of mouse lungs with porcine pancreatic elastase (Abe, Boyer et al. 2004; Ishizawa, Kubo et al. 2004). Another group has also shown engraftment of GFP-positive fetal liver transplanted cells (that replaced original irradiated bone marrow) in the lung after

lipopolysaccharide- (LPS-) induced lung injury (Yamada, Kubo et al. 2004). Cells that were positive for cytokeratin and GFP, but negative for Ptprc, were observed in the alveolar wall. No GFP positive cells were observed in the lungs of untreated animals (Yamada, Kubo et al. 2004).

As a result of such studies, it was hypothesised by several groups that some form of lung injury is required for engraftment of donor cells (Aliotta, Passero et al. 2005). However, bone marrow plastic-adherent cells transplanted into non-irradiated mice have been observed in both control and hypoxia-injured lung (Rochefort, Vaudin et al. 2005). Also, donor cells have been reported to engraft at a frequency of 0.83% of all cells within the bronchial epithelium after bone marrow irradiation with no lung injury (MacPherson, Keir et al. 2005). Irradiation would increase the chance of donor-derived cells repairing the damages tissues, but when no irradiation is involved, the host cells are likely to still play a major role in repopulating the lung. Therefore, in experiments with no irradiation it is possible to see very few or even no cell engraftment at the injury site.

This does not, however, contradict the involvement of injected cells in the injury repair. Injected cells might fulfill other functions that are not yet discovered. Human patients have been reported to have bone marrow derivatives in lung tissue after sex-mismatched bone marrow transplantation; however, the function of these cells is not clear (Suratt, Cool et al. 2003; Mattsson, Jansson et al. 2004; Albera, Polak et al. 2005; Zander, Baz et al. 2005). In a recent study on mice with induced pulmonary hypertension, donor bone marrow cells were observed to stain positively for the markers of IFs, myofibroblasts, hematopoietic cells, Clara cells, vascular endothelial cells and smooth muscle cells in the recipient lung (Spees, Whitney et al. 2008). However, in some cases transplanted bone marrow cells damaged the lung, and contributed to lung fibrosis (Anjos-Afonso, Siapati et al. 2004). So, the functions of donor-derived cells in the repair of the lung injury are not always straightforward or clear.

In cases of various lung injuries, bone marrow cells have behaved differently (Abe, Lauby et al. 2003; Anjos-Afonso, Siapati et al. 2004; Yamada, Kubo et al. 2004). After some lung injuries cytokines could induce bone marrow cell differentiation into cells that contribute to

the lung; however, bone marrow cells are mostly believed to have limited potency, as was discussed at the beginning of the General Introduction, Section 1.3.1. Also, according to Chang, Summer et al. (2005) lung sections might have been thicker than a single cell, and might therefore have contained two or three overlaid cells, thus causing overlapping signals and making data difficult to clearly interpret. The detection methods for engraftment in the above-mentioned experiments involved therefore a simple visualisation of staining morphology and as such could have led to false conclusions due to overlapping fluorescent signals (Chang, Summer et al. 2005). To avoid confusion with interpreting visual data, deconvolution microscopy or three-dimensional micro-imaging could be used in future studies.

1.3.3. Other sources of adult stem cells apart from the bone marrow

HSCs, EPCs and MSCs could also be obtained from peripheral blood after they enter the circulation, and from umbilical cord blood (UCB) (Kumar, Yoo et al. 2007; Wu, Lensch et al. 2007). Peripheral blood is, however, low in progenitor cell numbers, which enter the bloodstream mainly after induction, such as after injury. It has been demonstrated, that circulating endothelial progenitor cells did not participate in compensatory alveolarisation and vascularisation after lung injury (Voswinckel, Ziegelhoeffer et al. 2003). UCB is said to be a valuable source of cells for research as compared to the bone marrow, it is easier to isolate and is associated with a lower incidence of immune reaction following transplantation (Rogers and Casper 2004; Tse and Laughlin 2005). UCB cells can also be isolated from children at birth, and then later transplanted into the same child's bloodstream with no risk of immune rejection.

1.3.4. Challenges of cell therapy

Stem cell transplantation is still not used to its full potential today. There are many issues that are still to be overcome. Freezing-thawing, culture and cytokine induction of isolated cells are likely to be followed by changes in mitochondria, methylation profiles or other

epigenetic changes, some of which might result in the loss of tumour suppressor activity or activation of an oncogene (Ahrlund-Richter, De Luca et al. 2009). This could be avoided in some cases, when the cells are isolated freshly from the donor, and injected immediately into the recipient. However, sometimes donors are not available, and stem cell banking is required. Banking involves freezing of the cells and sometimes long-term storage, which damages some cell types. Some cells need cytokine induction to proliferate or differentiate, and this procedure is very easy to perform in culture. Epigenetic changes can be monitored by multiple karyotyping or methylated DNA PCR. Detailed testing should be considered for any type of cell therapy, especially pathogen screening in cases where the cells are transplanted from another patient.

In some cases not the whole population of isolated cells is suitable for transplantation. Sorting and selecting cells based on antibodies could damage the cells, activate or block biochemical pathways, as well as leave fragments of unnecessary molecules (beads, fluorescent markers) within the cell population. In some cases (MSC isolation) negative selection can be used, i.e. the antibody used does not react with the cells to be transplanted, but with all other cell types. This method improves the quality of the selected cells, but does not guarantee the purity of the cell population, which might be contaminated with other cell types. These and other issues are being considered during the preparation of clinical trials for most stem cell therapies. In this study stem/progenitor cells will be used for the treatment of lung injury and strategies to minimise the risk of rejection, contamination or epigenetic changes will be considered.

Summary

Respiratory alveolarisation and vascularisation are two physiological processes that are disrupted by premature birth and decreased due to the injury caused by mechanical ventilation or hyperoxia, as well as lung inflammation, nutritional deficiencies and prenatal and antenatal administration of glucocorticoids (Hitka, Cerny et al. 2004; McGowan 2004). Alveolarisation involves septation of the lung as well as proliferation and differentiation of AECs. Vascularisation can be induced by vascular endothelial growth factor (VEGF) and involves proliferation and differentiation of endothelial progenitor cells, which may

potentially be obtained from a number of sources, including the circulation, umbilical cord blood and bone marrow. Both alveolarisation and vascularisation are critical for gas exchange. In case of disruption of these processes chronic lung disease is most likely to occur.

Stem cell therapeutic approaches may provide methods to repair and replace damaged tissue and might be a suitable addition to glucocorticoid treatment after premature birth. In many recent studies on rodents and rabbits with induced lung injury, donor bone marrow cells were reported to be positive for some markers of AEC-I, IFs, myofibroblasts, hematopoietic cells, Clara cells, vascular endothelial cells and smooth muscle cells in the recipient lung (Kotton, Ma et al. 2001; Chang, Summer et al. 2005; Spees, Whitney et al. 2008). Whether this represents non-linear differentiation of bone marrow cells remains contentious as in some cases lung sections are thicker than a single cell, and might therefore contain two or three overlaid cells, thus causing overlapping signals and making data difficult to clearly interpret (Chang, Summer et al. 2005). However, bone marrow is known to contain EPCs and it is possible that some of these cells may engraft at the site of injury to affect neo-vasculogenesis. This area of research has not been widely studied to date.

Though rodents are born with underdeveloped lungs, during post-natal life they do not require high oxygen or other treatments for lung development. These animals remain popular models for studying human lung diseases. In order to find the best treatment for hyperoxic injury of the lung, it is necessary to optimise the treatment conditions (i.e. determine the cell type for transplantation and efficiency of its differentiation) in preclinical models and to develop strategies that address issues of immune rejection, epigenetic changes and contamination.

In this study we hypothesise that endothelial progenitor cells and plate-adherent cells can be isolated from bone marrow, and can be used for treating the effects of hyperoxia in the

lungs of neonatal mice by inducing or supporting alveolarisation by promoting vascularisation. The aim of this project is to compare a number of bone marrow derived cell types, first *in vitro*, and then *in vivo*, for their ability to efficiently form blood vessels and their ability to effect repair of the lung following hyperoxia injury, respectively.

Chapter 2. General Materials and Methods

2.1. Animal care and oxygen treatment

Pregnant C57Bl/6J females housed in the specific pathogen free (SPF) conditions were brought into SPF procedure room of the animal house at E14. They were left to adjust to the room conditions for the following three days. At E17.5 (the night before mice gave birth at E18.5), five pregnant females were placed in clear plastic chambers 405x205x185mm (LxWxH); floor area 501cm^2 (Techniplast), in which a continuous oxygen (Coregas, #202-50) flow was introduced under pressure to maintain a uniform oxygen concentration of ~90% for four days. The concentration of oxygen was measured by a portable gas analyser (Servomex 5200 Multi-Purpose) and automatically recorded in the attached computer every 15 minutes in order to observe oxygen concentration 24 hours per day. Animal monitoring once a day resulted in oxygen levels returning to room air conditions in the cage for five minutes (21% oxygen). It took approximately 30 minutes each time to reach the concentration of 90% of oxygen each time after the cage lid was opened for animal check-up. Slight oxygen concentration variations (±5%) were observed throughout the treatment time. The pups were born in high oxygen conditions (one litter per chamber) and were housed with their mothers. The number of pups was equalised in hyperoxia and normoxia (room air) groups by culling extra pups in order to eliminate effects of amount of milk available per pup. Every 24 hours hyperoxic mothers were swapped with normoxic mothers (housed in normal room air, 20% oxygen) to avoid oxygen toxicity and to make sure pups were receiving the same quality and amount of milk, that might have been affected by high oxygen together with mother's general wellbeing. Pups stayed in the same cages all the time until weaning at 3 weeks of age. Pups were weighed once a week from day 7 to day 56. Both males and females were culled for analysis on postnatal day 5, 28 and 56. The lungs, bone marrow and blood were isolated at each time point from culled mice.

2.2. Morphological and morphometric analysis of the lungs

Lungs were pressure-fixed *in situ* with 4% paraformaldehyde (PFA) at 20 cm (H_2O) via a cannula inserted into the trachea. The lungs filled with PFA were separated from the rest of the body embedded in the rib cage and were left in 4% PFA at 4^{o}C overnight. The next day the lungs were removed from the rib cage and placed into Zamboni's fixative for 24 hours at room temperature. The lungs were then embedded in paraffin and sectioned as 5-6 µm serial coronal sections in the ventral to dorsal plane. Preliminary analyses to determine optimal sites for morphometry were undertaken. Serial sections from the first sign of tissue were counted.

Staining method	Hematoxylin and eosin	Masson's trichrome stain	Periodic acid and Schiff's reagent (PAS)	Weighert's elastin stain
Reagents used	Hematoxylin – 5 min	Celestin Blue – 5 min	Periodic acid 1% - 5 min	Potassium permanganate 0.25% - 5 min
	Water – 1 min	Water – rinsed	Distilled water – 1 min	Distilled water – 30 sec
	Acid alcohol – 3 sec	Mayer's hematoxylin – 3 min	Schiff's reagent – 5 min	Oxalic acid 5% - 3 sec
	Water – 1 min	Water – rinse	Water – 5 min	Water – 1 min
	Scott's tap water – 10 sec	Acid alcohol – 3 sec	Hematoxylin – 5 min	Distilled water – 1 min
	Water – 1 min	Water – 1 min	Water – 1 min	Resorcin-fuchin - overnight
	Eosin – 3 min	Biebrich Scarlet / Acid Fuchsin – 5 min	Acid alcohol – 3 sec	Water – 5 min
	Ethanol 100% – 30 sec	Distilled water – 1 min	Water – 1 min	Tartrazine in saturated picric acid 0.25% - 3 min
		Phosphomolybdic acid 1% – 5-7 min	Scott's tap water – 10 sec	Ethanol 70% - 30 sec
		Water – 2-3 min	Water – 1 min	
		Aniline blue – 5 min		
		Water – 5 min		

Table 2.1. Histochemical staining methods, min – minutes.

The first 30 sections of lung tissue were assessed for the contribution of alveolar tissue, blood vessels and major bronchial structures in the area of whole tissue on a slide. Sections on glass slides were deparaffinised in xylene and rehydrated in 100% ethanol (three serial incubations in each of the solutions for five minutes each), then rinsed in water for one minute. Lung sections were stained using four methods: hematoxylin and eosin stain, Masson's trichrome stain, periodic acid and Schiff's (PAS) stain and Weighert's elastin stain. All stains were prepared according to standard protocols of the Monash University Histology laboratory. Staining was performed as described in Table 2.1. After staining, slides were dehydrated in 100% ethanol and xylene (three serial incubations in each of the solutions for five minutes each) and mounted in DPX mounting medium (BDH Laboratory Supplies, # 360294H). Five photographs were taken per section to assess the whole alveolar area. Photographs of lung sections were analysed under the microscope for the following characteristics: diameter of alveoli, tissue area, the number of alveoli per area, the number of blood vessels surrounded by elastin per area, the number of secondary septa (crests) per tissue area, the amount of elastin per tissue area, the presence of mucus and mucin-secreting cells, the presence of collagen depositions and fibrosis. To evaluate the number and diameter of alveoli, three vertical and two horizontal lines were drawn across the lung section image. The total length of vertical and horizontal lines was equal. Approximate summary length of all lines per image was 3.63 mm. The average number of alveoli was calculated from a number of airspaces appearing on those lines (the blue line going across or touching a white area or airspace on Fig. 2.1-A was counted as 1 alveolus), per 3.63mm of lung alveolar tissue. Average alveolar size was calculated from measurements of the lengths (Fig. 2.1-B) of airspaces (white areas on Fig. 2.1) falling on top of the blue lines (black lines are the distances measured on Fig. 2.1-B). The number of vertical measurements was equal to the number of horizontal measurements. Secondary septa and blood vessels were detected by the presence of elastin that was stained black by resorcin-fuchsin (Fig. 2.1-C). The number of secondary septa and the amount of elastin were calculated in relation to the area of tissue per total area. The number of blood vessels was calculated both per total area and per tissue area. The tissue area was calculated using the Image-Pro Plus software (Media Cybernetics) by selecting all coloured pixels on a lung picture (Fig. 2.1-D, in black) and then transferring them into microns according to a scale bar. The amount of elastin was calculated from the

percentage of elastin-positive tissue (Figures 2.1-A to 2.1-C – black staining, Fig. 2.1-D – coloured pixels) from selected total tissue pixels (total tissue area) (Fig. 2.1-D).

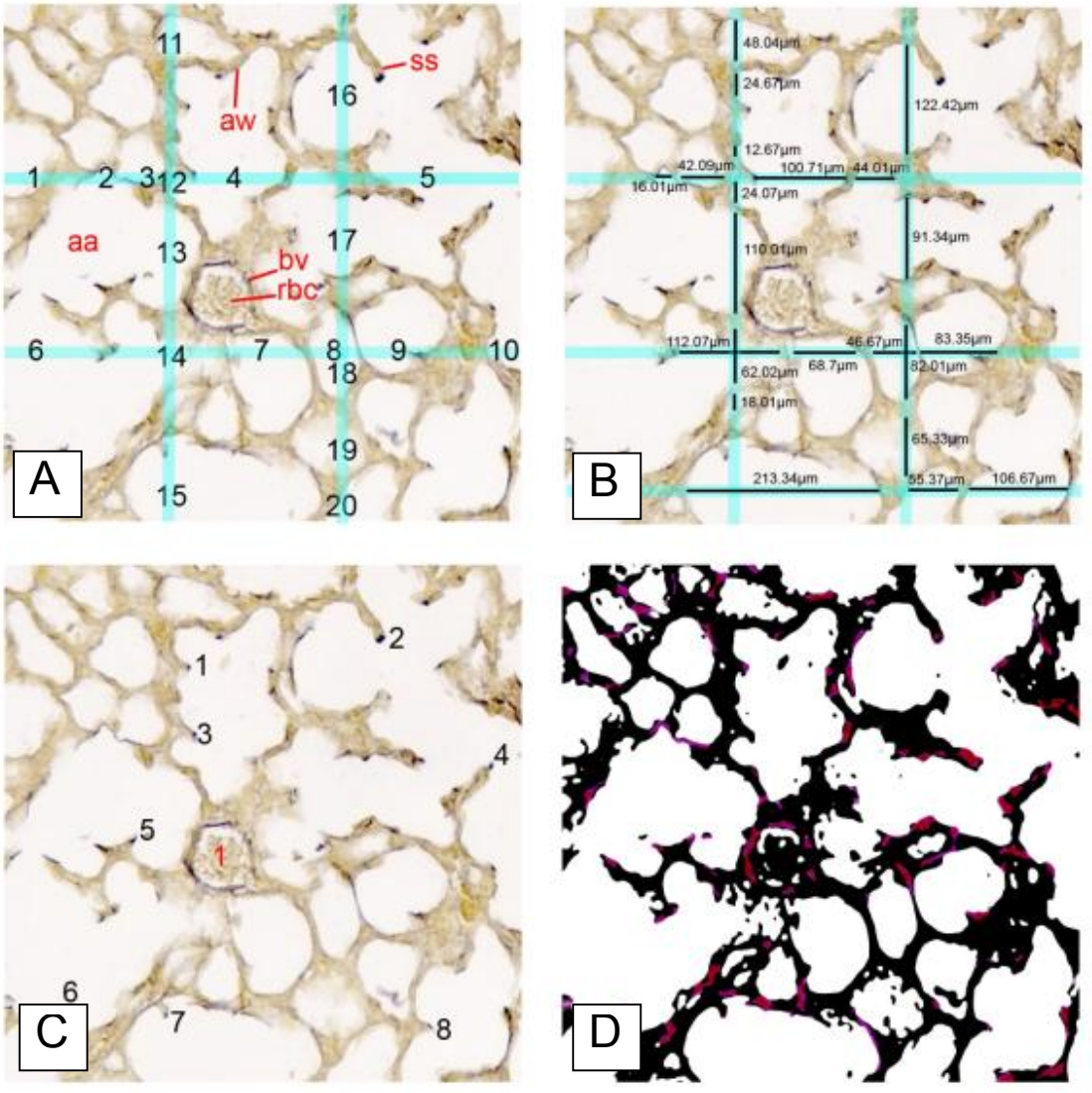

Figure 2.1. Image of lung sections stained with Weighert's elastin stain and morphometric measurements. A. Measurement of the number of alveoli by counting airspaces falling on lines; B. Measurement of the alveolar size on a lung section; C. Counting the number of secondary septa with elastin "dot" on top of the septum (marked with black digits) and blood vessels surrounded by elastin (stained black; marked with red digit); D. Counting the amount of total tissue in pixels (area in black) and percentage of elastin-positive tissue (area in red/pink). aa – alveolar airspace, aw – alveolar wall, bv – blood vessel, rbc – red blood cells, ss – secondary septum.

2.3. Immunohistochemistry on lung paraffin sections

Lung paraffin sections were analysed for: the vascular marker Pecam1, vascular endothelial growth factor A (Vegfa) and green fluorescent protein (GFP). Lung sections were deparaffinised and rehydrated as described above, boiled in 0.01M sodium citrate solution (with additional 0.07% Tween-20 for GFP antibody) for 20 minutes, left to cool at room temperature for 30 minutes and then rinsed in distilled water. Slides were then incubated in 3% H_2O_2 for ten minutes, rinsed in water and blocked with 5% goat serum at 4^{o}C overnight. Primary and secondary antibodies were applied to the lung sections and incubated for one hour at room temperature in a wet chamber. Primary antibodies were used at the following concentrations: Pecam1 (Abcam, #ab28364) at 1:100, Vegfa (Santa Cruz, #sc-152) at 1:750 and GFP (Abcam, #ab290) at 1:1000. Secondary goat anti-rabbit IgG antibodies were both used at 1:1000: biotinilated antibody (Invitrogen, #B2770) or AlexaFluor-568-conjugated antibody (Invitrogen, #A11036). Streptavidin-HRP (DAKO, #P0397) complex solution was applied in cases when secondary antibody was biotinilated, and incubated for 30 minutes at room temperature. Sections were washed with PBS (Appendices, Section III) with 1% of Tween-20 (PBST) for 15 minutes (three changes for five minutes each) after each incubation. DAB-chromogen drop in 1 ml of DAB-substrate buffer complex (DAKO, K3468) was applied for five minutes for Pecam1 antibody and for 5-15 minutes (depending on the age of mouse) for Vegfa antibody developing. Sections were counter-stained with Mayer's hematoxylin as described above, dehydrated with ethanol and xylene and mounted in DPX mounting medium. For fluorescent secondary antibody Hoechst-33342 (Sigma) counterstain was applied for five minutes, and slides were mounted in fluorescent mounting medium (DAKO, #S3023).

2.4. Immunohistochemistry on frozen sections - tyramide signal enhancement

Right lobes from lungs were frozen mounted in Tissue-Tek OCT Compound 4583 (ProSciTech, #IA018) placed in a container with isopropanol and dry ice. The lobes were cut at 10 μm sections in the same plane as paraffin-embedded lungs. Slides were dried at room temperature for 30 minutes, and fixed with 4% ice-cold PFA for ten minutes. Slides

were rinsed in PBST twice, boiled in 0.01M sodium citrate solution for 15 minutes, left to cool at room temperature for one hour, and then rinsed in distilled water and PBST. Slides were then incubated in 3% H_2O_2 for 15 minutes, rinsed in water and PBST and blocked with 5% goat serum for 1 hour at room temperature on a shaker. Primary antibody was applied overnight at 4^{o}C (rabbit anti-GFP from Abcam, #ab290 was applied at 1:1000). Slides were washed three times for ten minutes in PBST after each of the following steps, which were all performed at room temperature. Secondary biotinilated antibody (goat anti-rabbit IgG, Invitrogen, #B2770, at 1:1000) was applied for one hour on a shaker. Streptavidin-HRP (Perkin Elmer, #SAT700001EA) was applied at 1:1000 for 30 minutes. Biotin-Tyramide (Perkin Elmer, #SAT700001EA) was applied at 1:50 for seven minutes. Streptavidin-488 (Invitrogen, #S-11223) was applied at 1µg/ml for 30 minutes. Hoechst-33342 was applied for two minutes, then slides were coverslipped using fluorescent mounting medium (as in General Materials and Methods, Section 2.3) and analysed under fluorescent microscope (Olympus IX70).

2.5. Western blot analysis

Lung samples were snap-frozen in dry ice without fixation and stored at -80^{o}C until analysis. Frozen samples were thawed in 1 ml of RIPA buffer in 1.5 ml microtubes (Axygen, #MCT-175-C) for 30 minutes, homogenised and centrifuged at 14000 rpm for 20 minutes at 4^{o}C. Protein concentration was measured in the supernatant using protein assay solution (BioRad) at 1:5 diluted in distilled water. Samples (the supernatant) were diluted 2x in reducing sample buffer (Appendices, Section III) and boiled for five minutes at 100^{o}C, and then either stored at -20^{o}C, or loaded into 7% (for Pecam1) or 12% (for Vegfa and Sftpc) polyacrylamide gels prepared using stacking and resolving gel buffers (Appendices, Section III). Proteins were separated by electrophoresis at 95V for 2-3 hours and transferred onto PVDF membranes at 35V, 4^{o}C overnight in transfer buffer 1x (Appendices, Section III). Membranes were blocked with 10% filtered skim milk in PBS. Primary rabbit anti-mouse antibodies were used at the following dilutions: Pecam1 (Abcam, #ab28364) at 1:100, Vegfa (Santa Cruz, #sc-152) at 1:200, β-actin (Actb, Sigma, #A-2066) at 1:500, β-tubulin (Tubb, Thermo Scientific, #RB-9249-PO) at 1:1000 and Pro-Sftpc (Millipore, #AB3786) at 1:2000. Membranes were incubated in primary antibody for

1 hour at room temperature, washed with PBS with 1% Tween-20 (PBST) for 30 minutes, and incubated in secondary HRP-conjugated goat anti-rabbit IgG antibody (GE Healthcare, #NA934V) at 1:15000 for 1 hour at room temperature. Developing reagent (Amersham ECL Plus, GE Healthcare, #RPN2132) was applied for five minutes. Membranes were manually exposed to X-ray film (Fujifilm); the films were developed and scanned (Canon Image Scanner), and the bands were analysed using ImageQuant TL, gel analysis software.

2.6. Collection of bone marrow (BM) and blood for FACS analysis

Hyperoxia-treated and normoxia mice were culled by cervical dislocation. In adult mice (28 and 56 days of age) blood was collected from the heart using a 3 ml syringe and 29 gauge (29G) needle. For newborn mice (five days of age) blood was collected by decapitation and drops were collected from the bleeding site. BM was flushed from femurs with 0.2 ml sterile phosphate buffered saline (PBS) using an 18-21G (depending on bone size) beveled needle. Both blood and bone marrow were fixed immediately with 1% paraformaldehyde in 20 mg/ml glucose. Red blood cell lysis buffer 1 ml (Sigma, #R7757) was applied for one minute, followed by 10 ml PBS. The resulting cell suspension was centrifuged at 1500 rpm for one minute and the supernatant was discarded, the cell suspension was then used for FACS analysis.

2.7. Fluorescence-Activated Cell Sorting (FACS) analysis

The cell pellet was resuspended in 1 ml blocking solution (5% FCS in PBS). Cell clumps were immediately separated by filtering cell suspensions through 100 µm mesh and discarded. Remaining cells were stained for cell surface markers for analysis. Filtered cell preparations were centrifuged and resuspended in a low volume (approximately 1 ml), collected in 1.5 ml microtubes (Axygen, #MCT-175-C) and blocked for 30 minutes at 4ºC. Fluorophore-conjugated antibodies were added for one hour at 4^{o}C according to the manufacturers' recommended concentrations. Antibodies were grouped in such a way that fluorophore colors did not overlap: PE-Cy5.5-conjugated anti-mouse CD45 (Ptprc, eBioscience, #35-0451), PE-conjugated anti-mouse Kdr (eBioscience, #12-5821), APC-

conjugated anti-mouse Kdr (BD Pharmigen, #560070), FITC-conjugated anti-mouse Prominin-1 (Prom1, eBioscience, #11-1331), PE-conjugated anti-mouse Prom1 (eBioscience, #12-1331), Rabbit polyclonal anti-Pecam1 (Abcam, #ab28364), PE-conjugated anti-mouse Tek (eBioscience, #12-5987), FITC-conjugated anti-mouse Mcam (Miltenyi, #130-092-026), Rabbit polyclonal Prom1 (Abcam, #ab19898), APC-conjugated Prom1 (eBioscience, #17-1331), FITC-conjugated anti-mouse Cd34 (eBioscience, #11-0341) and FITC-conjugated anti-mouse Pecam1 (eBioscience, #11-0311). AlexaFluor647-conjugated anti-mouse ChIIIA4 (EphA3) antibody (home-made) was used for characterising EphA3-enriched cells. Cell suspensions were washed three times in PBS. For the anti-Pecam1 and anti-Prom1 primary antibodies, AF568-conjugated goat anti-rabbit IgG (Invitrogen, #A11036) was applied for 30 minutes and washed three times in PBS. Cells were sorted using FACS-Calibur, Influx LSRIIb or FACS-Diva equipment. Analysis was performed with FlowJo and CellQuest software.

2.8. Bone marrow cell isolation for cell culture

C57Bl6/J adult male and female mice were culled by cervical dislocation. BM was flushed from femurs with 0.2 ml sterile phosphate buffered saline (PBS) using an 18-21G (depending on bone size) beveled needle and added to 10% fetal calf serum (FCS) in a 15 ml tube (BD Falcon, #352097). Red blood cell lysis buffer 1 ml (Sigma, #R7757) was applied for one minute, followed by 10 ml PBS. The resulting cell suspension was centrifuged at 1500 rpm for one minute and the supernatant was discarded. The cell pellet was resuspended in 1 ml blocking solution (5% FCS in PBS). Cell clumps were immediately separated by filtering cell suspensions through a 100 µm mesh and discarded. An aliquot of cells was plated in culture without any sorting. Remaining cells were used for FACS analysis or for magnetic sorting (MACS) as described in General Materials and Methods, Sections 2.7 and 2.9.

2.9. Magnetic-Activated Cell Sorting (MACS)

All antibodies were diluted in PBS with 5% FCS as recommended by respective commercial companies. Cell suspensions were blocked for 30 minutes in FCS as

described in General Materials and Methods, Section 2.7, divided into five fractions and incubated for one hour with the following respective antibodies: PE-conjugated anti-mouse Kdr (eBioscience, #12-5821), FITC-conjugated anti-mouse Prom1 (eBioscience, #11-1331), PE-conjugated anti-mouse Tek (eBioscience, #12-5987), FITC-conjugated anti-mouse Mcam (Miltenyi, #130-092-026), FITC-conjugated anti-mouse Cd34 (eBioscience, #11-0341), FITC-conjugated anti-mouse Pecam1 (eBioscience, #11-0311) and no antibody (unsorted fraction was set aside to be further plated in the same conditions as the other fractions). Cell suspensions were washed three times in PBS. For FITC-conjugated primary antibodies, anti-FITC Microbeads (Miltenyi, #130-048-701) were applied for ten minutes and for PE-conjugated primary antibodies, anti-PE Microbeads (Miltenyi, #120-000-743) were applied for ten minutes and washed three times in PBS. Cells were magnetically sorted using an AutoMACS Separator (Miltenyi) in positive selection-sensitive mode in PBS with Ethylenediaminetetraacetic acid (PBS-EDTA, Appendices, Section III) containing 0.5% FCS.

2.10. Endothelial differentiation of cells *in vitro*

Cells from both positive and negative fractions, as well as unsorted cells, were counted and then plated on 0.1% Attachment Factor (Cascade Biologics, #S-006-100)-coated 24-well plates (Costar, #3524) at 2.0-3.0x 10^5 cells per cm^2 containing 500ul of Endothelial differentiation culture medium (EDCM, Table 2.2). EDCM was optimised using unsorted BM. It contained one of the following commercial media bases: Iscove's Modified Dulbecco's Medium (IMDM, Gibco #12440-046), Dulbecco's Modified Eagle Medium (DMEM, Gibco, #11965-092) or Medium 199 Medium (Sigma, #M4530) and supplementary factors: 20% FCS (HyClone, Thermo Scientific), 2mM L-glutamine, 1% insulin-transferrin-selenite solution (Gibco, #41400-45), 1% non-essential amino acid solution (Gibco; #11140-050), 0.5% penicillin-streptomycin solution (Gibco, #15070-063), 0.1% *β*-mercaptoethanol solution (Gibco, #21985-023), 15 IU/ml heparin (Fisons Pharmaceuticals), 50 ng/ml vascular endothelial growth factor (VEGF; Sigma, #V4512), 75μM ascorbic acid (Sigma, #A4544), 1μM hydrocortisone (Sigma, #H0888), and 5 ng/ml basic fibroblast growth factor (FGF2; Sigma, #F0291). Cell culture medium was changed every two days. On day six of culture, the serum concentration was reduced to 2%. After

two weeks of culture, cells were fixed *in situ* with 1% paraformaldehyde (PFA) for 30 minutes, and processed for immunohistochemistry.

2.11. Immunohistochemistry on fixed cell cultures

Fixed cells were rinsed with PBS, incubated in 0.01% Triton (for Pecam1 antibody only) for five minutes and blocked with 5% goat serum (for all antibodies). Primary rabbit anti-mouse Pecam1 (Abcam, #ab28364), Tek (Santa Cruz, #sc-324) and von Willebrandt Factor (vWF; Santa Cruz, #sc-14014) antibodies were used at dilutions of 1:50 in 5% goat serum. Cells were incubated in primary antibody for one hour at room temperature, washed with PBS with Tween-20 (1%) for 30 minutes, and incubated in secondary antibody (AF568-conjugated goat anti-rabbit IgG used at 1:1000) for one hour at room temperature. Immunoreactivity to Pecam1 and vWF and hence the presence of vessel-like structures were analysed using a fluorescent microscope (Olympus, #IX70). The number of branches of vessel-like structures was counted in each fraction.

2.12. EphA3$^+$ cell isolation and culture

BM was isolated as described above from GFP heterozygote C57Bl/6J adult male mouse. No red blood cell lysis or sorting was performed. Cells were plated on uncoated plastic dishes in growth medium (Table 2.2) optimised by our collaborator Dr. Degu Abebe (DMEM, 10% FCS, 1000 U/ml LIF, 10 ng/ml EGF and 10 ng/ml PDGF). Cells were cultured at 37ºC in 10% CO_2 for two weeks, and then trypsinised and re-passaged every week until senescence. Cells were analysed for the presence of EphA3 (using AlexaFluor647-conjugated anti-mouse ChIIIA4; generously supplied by Prof. Martin Lackmann) and GFP (no staining required), as described in General Materials and Methods, Section 2.7, at passages 8, 10 and 13. Cells were then expanded and frozen for storage for further analysis and injections at passages 11 and 13. Preliminary analysis was performed to determine the most suitable passage number for cell injection. Cells were plated in 0.1% Attachment Factor (Cascade Biologics, #S-006-100)-coated wells at 2.0 – 3.0 x 10^5 cells per cm^2 with EDCM. No coating and DMEM with pen/strep, NEAA, FCS and L-glutamine was used as control medium (no differentiation factors, Table 2.2).

After cells formed vessel-like structures, they were fixed *in situ* with 1% PFA for 30 minutes and immunohistochemistry for Pecam1 was performed for further characterisation and analysis.

Components	Growth medium	Control medium	EDCM
FCS (%)	10%	20-2%	20-2%
LIF (U/ml)	1000	0	0
EGF (ng/ml)	10	0	0
PDGF (ng/ml)	10	0	0
VEGF (ng/ml)	0	0	10
Hydrocortisone (μM)	0	0	1
Heparin (IU/ml)	0	0	15
Ascorbic acid (μM)	0	0	75
Pen/strep	0	1x	1x
NEAA	0	1x	1x
L-glutamine (mM)	0	2	2
B-mercaptoethanol	0	0	0.1%

Table 2.3. Different medium components for EphA3$^+$ cell culture.

2.13. Deriving unsorted plate-adherent cells (PAC)

Cells isolated from BM as described above were plated on 0.1% Attachment Factor-coated wells at 2.0-3.0x10^5 cells per cm^2. Dulbecco's Modified Eagle Medium and supplementary factors: 20% FCS, 2mM L-glutamine, 1% insulin-transferrin-selenite solution, 1% NEAA solution and 0.5% penicillin-streptomycin solution were used for

culture conditions. Medium was changed every two days. This method was chosen according to a standard MSC isolation procedure (Rochefort, Vaudin et al. 2005; Rojas, Xu et al. 2005). After 7-10 days of culture without re-passaging, cells were trypsinised, and counted, and then analysed by FACS or injected into mice ($1x10^4$ cells per 20 µl per 2 g of mouse weight).

2.14. Analysis of green fluorescence protein (GFP) in cells

Cell suspensions were analysed for the presence of GFP by FACS as described in General Materials and Methods, Section 2.7. Cells were filtered through 100 µm mesh and resuspended in PBS without calcium and magnesium (Gibco, # 14190-235), with added 5% FCS. Then the FACS Calibur was used to analyse the number of GFP^+ cells. The same method was used to prepare cell types from wildtype mice for negative controls. Cultured cells were analysed for the presence of GFP using visualisation under a fluorescent microscope (Olympus IX70). Cells from a wildtype mouse in culture were used as a negative control.

2.15. Intraperitoneal cell and PBS injection

At postnatal day five, mouse pups were injected with either PBS (sterile, Life Technologies, #10010-023) or PBS containing $1x10^4$ cells per 20 µl. Cells were either plate-adherent (PAC), cells enriched for the respective and selected EPC marker (uncultured, freshly-isolated on the same day from bone marrow) or EphA3-enriched cells (at passages 8-15). Injection was performed intraperitoneally above the right hip. Twenty microliters per 2 g of body weight were injected.

2.16. Blood, lung and liver isolation for GFP analysis by FACS

Cells were isolated from blood, liver and lungs of mice culled at day 14 and day 21 of age (9 and 16 days after cells were injected). Blood was collected into a 15 ml tube filled with KCl (hypotonic solution to reduce red blood cell number) using a 19G needle inserted in

the heart *post mortem*. Cells were incubated at 37°C for 20 minutes, and then washed with PBS-EDTA by centrifuging and adding fresh solution. Liver and lung cells were isolated by placing a lobe of each organ into a tube with pre-warmed (37°C) collagenase solution (4 mg of collagenase I, 9 mg of collagenase IV in 45 ml of PBS without calcium and magnesium; Gibco, # 17100-017, # 17104-19 and # 14190-235, respectively). The lobes were chopped into smaller pieces (1-2 mm^3 each) using a scalpel blade and incubated on a shaker at 37°C for 20 minutes. Then the separated cells were filtered through a 70 µm mesh and washed with PBS-EDTA by centrifuging and adding 1 ml of fresh PBS-EDTA. All cell types were then analysed for the presence of GFP using a FACS machine (FACS Calibur) as described in General Materials and Methods, Section 2.14.

2.17. FISH for Y-chromosome

The method used for Y-chromosome staining was adapted from Dr. Nathanael Raschzok (Campus Virchow, Universitätsmedizin, Berlin)**.** In this method four samples of lung tissue were placed on the end of the glass slide, deparaffinised in xylene for ten minutes (three changes) and rehydrated in a series of ethanol washes as described in General Materials and Methods, Section 2.2. Slides were rinsed in distilled water and pre-treated with citrate buffer for 30 minutes at 80°C. After cooling to room temperature, slides were washed in two changes of SSC 2x (five minutes each at room temperature) and then incubated in 0.5% pepsin in 0.01M HCl at 37°C for 20 minutes. Slides were then washed in two changes of SSC 2x (five minutes each at room temperature) and incubated in 1% formalin for ten minutes, rinsed in water and washed again in two changes of SSC 2x (five minutes each at room temperature). Slides were then dehydrated with a series of ethanol washes (as in General Materials and Methods, Section 2.2) and air-dried for ten minutes. Mouse IDetect Y chromosome paint probe (IDLabs, #IDMR1056) was applied on each tissue section, including a positive control (male lung tissue), coverslipped and sealed with rubber cement (SuperGlueCorp). The probe and chromosomal DNA were denatured on a hot plate for 15 minutes at 80°C. Hybridisation was performed overnight at 37°C in a humidified chamber. The next day coverslips were removed using 2xSSC, and then slides were incubated in 0.3% Igepal (Sigma, # I3021) in SSC 0.4x for one and a half minutes at

73^{o}C. Slides were then washed for two minutes in 0.1% Igepal in SSC 2x at room temperature, rinsed in water, stained with DAPI (Life Technologies, #D21490), dehydrated in a series of ethanol and coverslipped in fluorescent mounting medium (DAKO, #S3023). Y chromosomes within the nuclei were visualised and photographed using a confocal microscope (Olympus FluoView FV500).

Chapter 3. Characterisation of a mouse model of hyperoxia and associated long-term respiratory deficit

3.1. Introduction

During the late stages of gestation the lungs still develop actively; therefore very preterm children are born with underdeveloped lungs. The structural abnormalities of the premature lungs do not permit appropriate gas exchange, and therefore this can cause a lack of oxygen in the bloodstream. Prescribed mechanical ventilation and hyperoxia can disrupt alveolarisation and vascularisation and, as a result, lead to respiratory deficit. Both alveolarisation and vascularisation are critical, as the large surface area of contact between air and gas-exchanging tissue and the density of small vessels to support oxygen transport from the lung to the other organs and tissues are required for proper gas exchange. In the case of disruption to either of these processes, chronic lung disease may occur. Therefore, an animal model of lung deficit is essential for studying disease progression and the development of effective treatments. A number of animal models have been established to mimic the hyperoxia treatment of the premature lung in humans, for example using mouse models. However, the numerous differences between human and mouse development of lung structures during gestation and after birth require consideration.

The aim of this study was to establish a hyperoxia model of lung deficit in the mouse in order to better characterise such disease progress and hence provide information that may assist in developing an alternative treatment base. The effect of 90% oxygen treatment on alveolarisation and vascularisation of the newborn mouse lung was investigated by morphometric, histochemical, immunohistochemical and protein analysis at different stages (up to mouse adulthood or eight weeks to observe not only any direct effect of excess oxygen on the mouse lung, but also any long-term recovery progress. This could further lead to offering a treatment option, taking into account natural recovery

processes. Although present therapeutic advances have increased survival rates among very prematurely born infants, the long-term effects of these diseases are still untreatable. This mouse model will be used for future research into the therapy of newborn lung disease but specifically relating to hyperoxia injury.

3.2. Materials and methods

3.2.1. Experimental design

Pregnant females were separated into two groups. The first group was placed in 90% oxygen conditions the night before giving birth and the second group was left at room air. The hyperoxia experiments were performed as described in General Materials and Methods, Section 2.1. After four days in 90% oxygen, pups recovered in room air, and tissues were collected on postnatal days 5, 28 and 56 (D5, D28, D56) as described on Figure 3.1. The lungs were pressure-fixed as described in General Materials and Methods, Section 2.2, or snap-frozen for protein analysis. Morphometric (Mayer's hematoxyllin-eosin and Weighert's elastin stains), histochemical (Weighert's elastin for elastin, Masson's trichrome for collagen and fibrosis and periodic acid-Schiff's stain for mucin) and immunohistochemical (Pecam1 and Vegfa) analyses were performed on pressure-fixed paraffin-embedded lung tissue as described in General Materials and Methods, Sections 2.2 and 2.3. Western blotting (WB) was used to analyse the quantity of Pecam1 and Vegfa as described in General Materials and Methods, Section 2.5. Blood and bone marrow were collected as described in General Materials and Methods (Section 2.6), and analysed for the presence of Kdr, Ptprc, Prom1 and Pecam1 by FACS (Section 2.7).

3.2.2. Pilot experiment

A pilot study was conducted, as recommended by the Institutional Animal Ethics Committee, to verify that the oxygen treatment level caused no unpredicted effects on animal health (method of oxygen treatment is described in the Section 2.1 in General Materials and Methods).

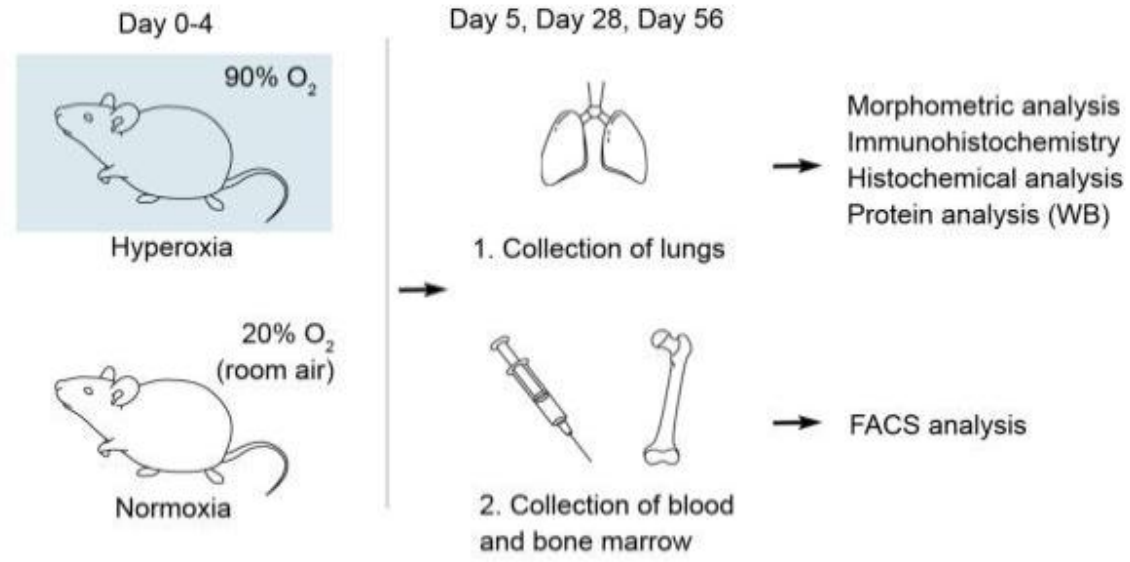

Figure 3.1. Experimental design for characterisation of the mouse hyperoxia model. At D0-4 mice were divided into two groups and treated with either 90% oxygen or left at room air. At D5, D28 and D56 samples were collected for analysis from both groups.

Seven mice were assigned to each normoxia and hyperoxia group, two to three animals of each were analysed at postnatal day 5 (D5), day 28 (D28) and day 56 (D56). The highest oxygen concentration produced by equipment used was 90-95%. To avoid death of animals caused by oxygen toxicity, a maximum number of four days for oxygen treatment was selected for newborn mice as has been previously reported for adult mice (Johnston, Mango et al. 1997; Johnston, Wright et al. 1997). Mouse health and wellbeing were monitored throughout the whole experimental time, i.e. the ability to run around the cage, sniff, defecate and urinate, as well as any signs of weight loss (by weighing mice once a week) or pain, as described by Langford and colleagues (Langford, Bailey et al. 2010). The lung samples were collected for the pilot study to optimise conditions for morphometric analysis. Critical observation determined that at the 10^{th} section cut from the frontal side of the lung there was insufficient tissue for analysis but after 30 sections the contribution of blood vessels and bronchioles to the total tissue was increased. Therefore for each mouse one section from the 20^{th} to 26^{th} section was taken to represent the total alveolar area. At each time point five areas of lung section were analysed per mouse. Analysis was performed on tissue area and alveolar diameter. Power analysis,

which is used to calculate the minimum sample size required to see the significance in the effect of a given size, was then performed to determine how many mice per group may be sufficient to observe significant differences in various parameters of the lung tissue following hyperoxia. Three experiments were performed after the pilot study. The lungs, bone marrow and blood were isolated at each time point from culled mice. Lung section photographs were analysed by light microscopy for the following characteristics: diameter of alveoli, tissue area, the number of alveoli per area, the number of blood vessels surrounded by elastin per area, the number of secondary septa per tissue area, the amount of elastin per tissue area, the presence of mucus and mucin-secreting cells, the presence of collagen depositions and fibrosis. All of the above evaluations were performed as described in Chapter 2, General Materials and Methods.

3.2.3. Statistical analysis

A univariate general linear model, where “group” was allocated as the main factor and “animal”, the random factor (five measurements per animal were taken), was applied for analysis of variance to determine significant differences in morphometric characteristics between hyperoxia-exposed and control lungs at different stages. The “litter” was not included as a random variation factor since only one to two mice per litter were used at each time point. The interaction between hyperoxia and normoxia data at different time points was calculated using the univariate general linear model followed by Student Newman-Keuls posthoc test, using the SPSS statistical package (PASW, IBM), and indicated whether normoxia and hyperoxia charts were parallel. Data charts were drawn in Microsoft Excel. Error bars indicate standard error (SEM), calculated from average values per mouse, without taking into account variations within each animal.

One-way analysis of variance (ANOVA) was used to determine significant differences in mouse body weight, the protein levels and the number of certain cell types between hyperoxia-exposed and control lungs at different stages.

3.3. Results

3.3.1. Results of the pilot study

The pilot study confirmed that 90-95% oxygen exposure for four consecutive days following birth produced no unpredicted effects on mouse well-being, i.e. mouse cage activity and behaviour (sniffing, defecating and urinating) appeared normal and no weight loss or overt sign of pain were observed. For the pilot study, it was assumed that male and female mice would have similar lung morphometric parameters so they were grouped together. This assumption was later tested in the larger general study. Using power analysis, it was determined that four mice per group would be sufficient to observe significant differences in the alveolar size and of the lung tissue area after hyperoxia treatment. Due to ethical standards for mouse number reduction in experiments, these data are included in the larger study described below.

3.3.2. Animal general health

A total of 55 mice (29 males and 26 females) were used for the large scale investigation of 90% oxygen lung injury. Twenty-seven pups were treated with 90% oxygen and 28 pups were used as controls (normoxic mice). A total number of 19 mice (nine males and ten females) were culled at five days of age (12 lungs from six males and six females were pressure-fixed for morphometric analysis and 7 lungs from three males and four females were frozen for protein analysis), 15 mice (nine males and six females) were culled at 28 days of age (eight lungs from five males and three females for morphometric and seven lungs from four males and three females for protein analysis) and 21 mice (11 males and ten females) were culled at 56 days of age (13 lungs from six males and seven females for morphometric and eight lungs from five males and three females for protein analysis). The 55 mice were treated and analysed over a period of ten months in three experimental pools.

During the eight weeks following treatment both normoxia and hyperoxia-treated mice did not demonstrate any signs of pain, they moved around the cage actively and they gained weight. An exception was that during the first two postnatal weeks, all hyperoxia-treated mice demonstrated an abnormal breathing pattern when placed under stress, e.g. when the bedding was being changed or when mice were being weighed, they started to breathe heavily with a 'clicking' noise. This sound was not heard from normoxia mice under the same stress conditions.

There was no persistent significant difference in mouse body weight between normoxia and hyperoxia-treated mice throughout the whole experiment (Fig. 3.2). Males and females were compared separately, as males generally gained weight faster than females after 28 days.

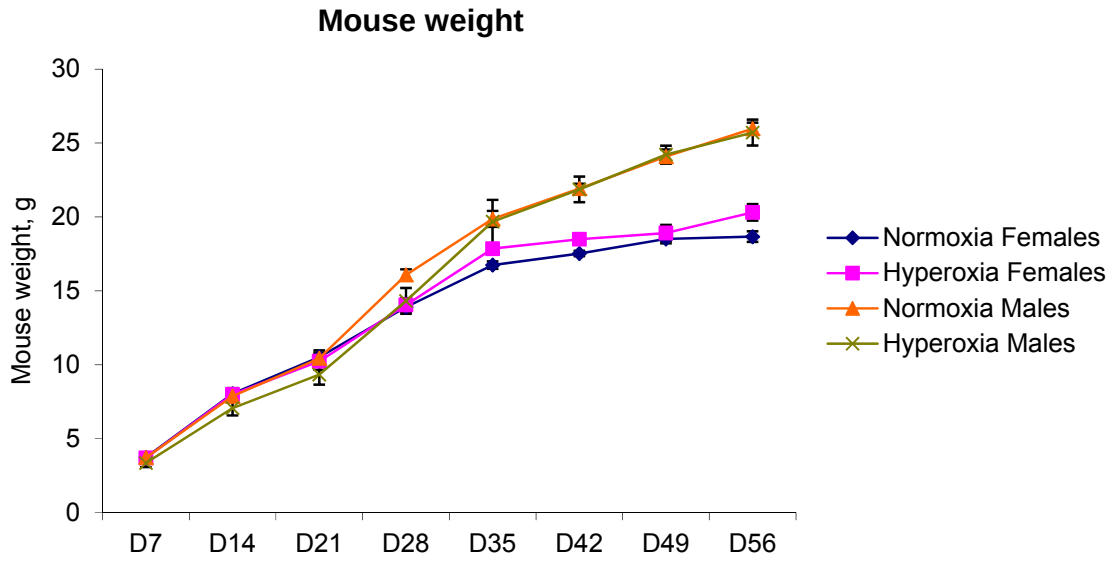

Figure 3.2. Body weight of male and female mice with (Hyperoxia) or without (Normoxia) high oxygen treatment. Error bars represent SEM, from D7 to D28 n=6; from D35 to D56 n=4.

3.3.3. Morphometric analysis of the lungs after hyperoxia treatment

Persistent and reversible significant differences in lung morphometric parameters were observed in respect to normoxia versus hyperoxia treatment and are described below. These significant differences were not dependent on gender, with males and females reacting in the same way.

3.3.3.1. Persistent changes in lung septation (irreversible before 56 days of age)

Hyperoxia treatment induced a significant decrease in alveolar number, measured as airspaces per linear 3.63 mm (General Materials and Methods, Section 2.2), and this decrease was observed at all time points examined: Day 5 (D5), 50.09 (hyperoxia, n=6) versus 58.75 (normoxia, n=6), $P<0.01$; D28, 75.35 (hyperoxia, n=4) versus 84.10 (normoxia, n=4), $P< 0.01$; and D56, 72.52 (hyperoxia, n=6) versus 82.35 (normoxia, n=6), $P<0.05$; (Fig. 3.3, 3.4-A). Conversely, hyperoxia treatment induced a significant increase in alveolar size at all time points examined: D5, 57.13 µm (hyperoxia, n=6) versus 45.02 µm (normoxia, n=6), $P<0.01$; D28, 35.15 µm (hyperoxia, n=4) versus 31.64 µm (normoxia, n=4), $P<0.01$; and D56, 38.91 µm (hyperoxia, n=6) versus 33.61 µm (normoxia, n=6) , $P<0.01$; 160 measurements per animal per group (Fig. 3.3, 3.4-A). These measurements of alveolar number and alveolar size, therefore, demonstrate that hyperoxia treatment of pups causes an immediate deficit in septation and that this decrease is not reversed with time.

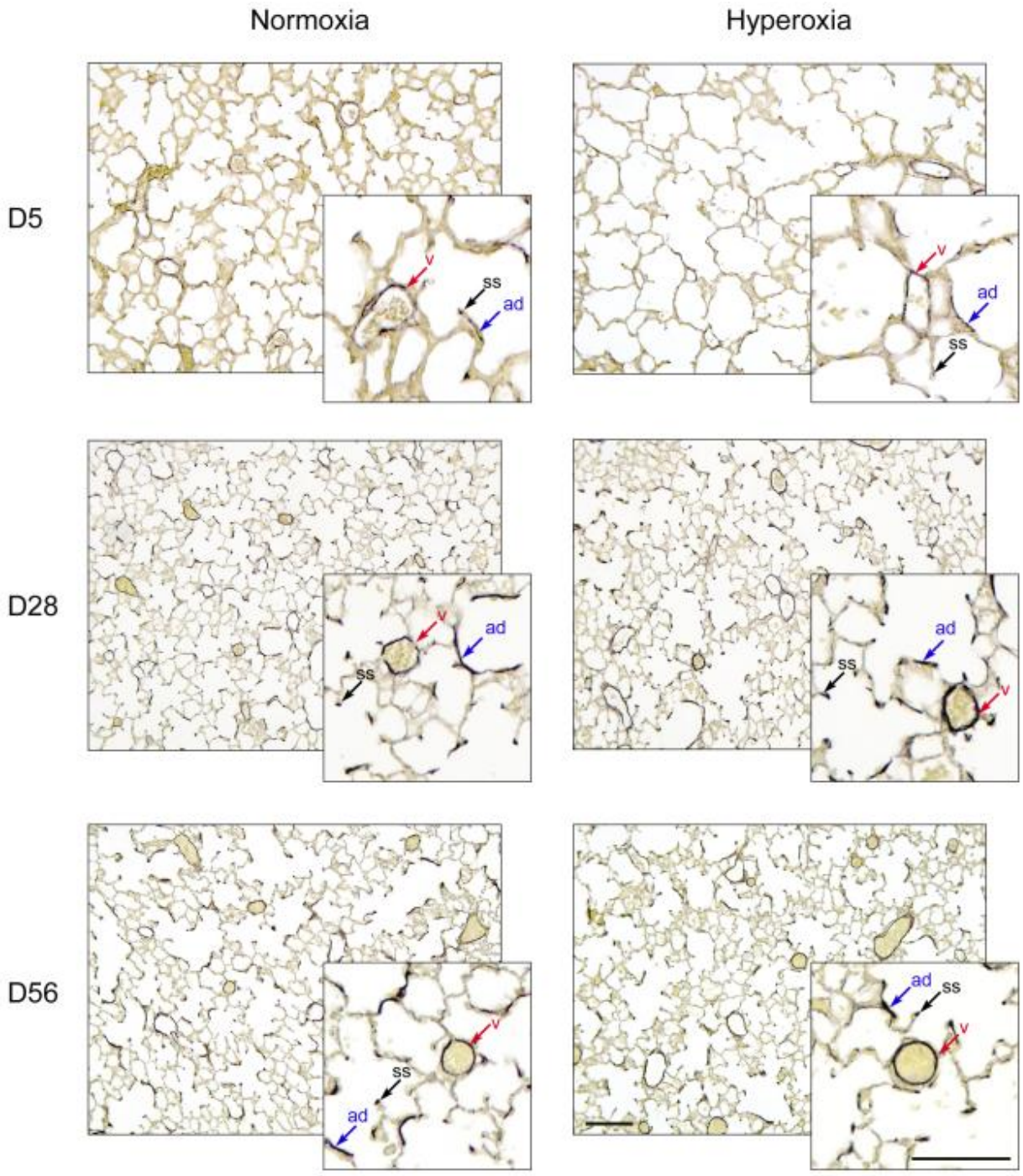

Fig. 3.3. Weighert's elastin staining of control and hyperoxia-treated lungs at D5, D28 and D56. Elastin is stained black. Sections were counterstained with tartrazine, all cells are stained yellow. Secondary septa (ss) are shown with black arrows, blood vessels (v) are shown with red arrows, elastin depositions in the alveolar walls (ad) are shown with blue arrows. Scale bar = 100µm.

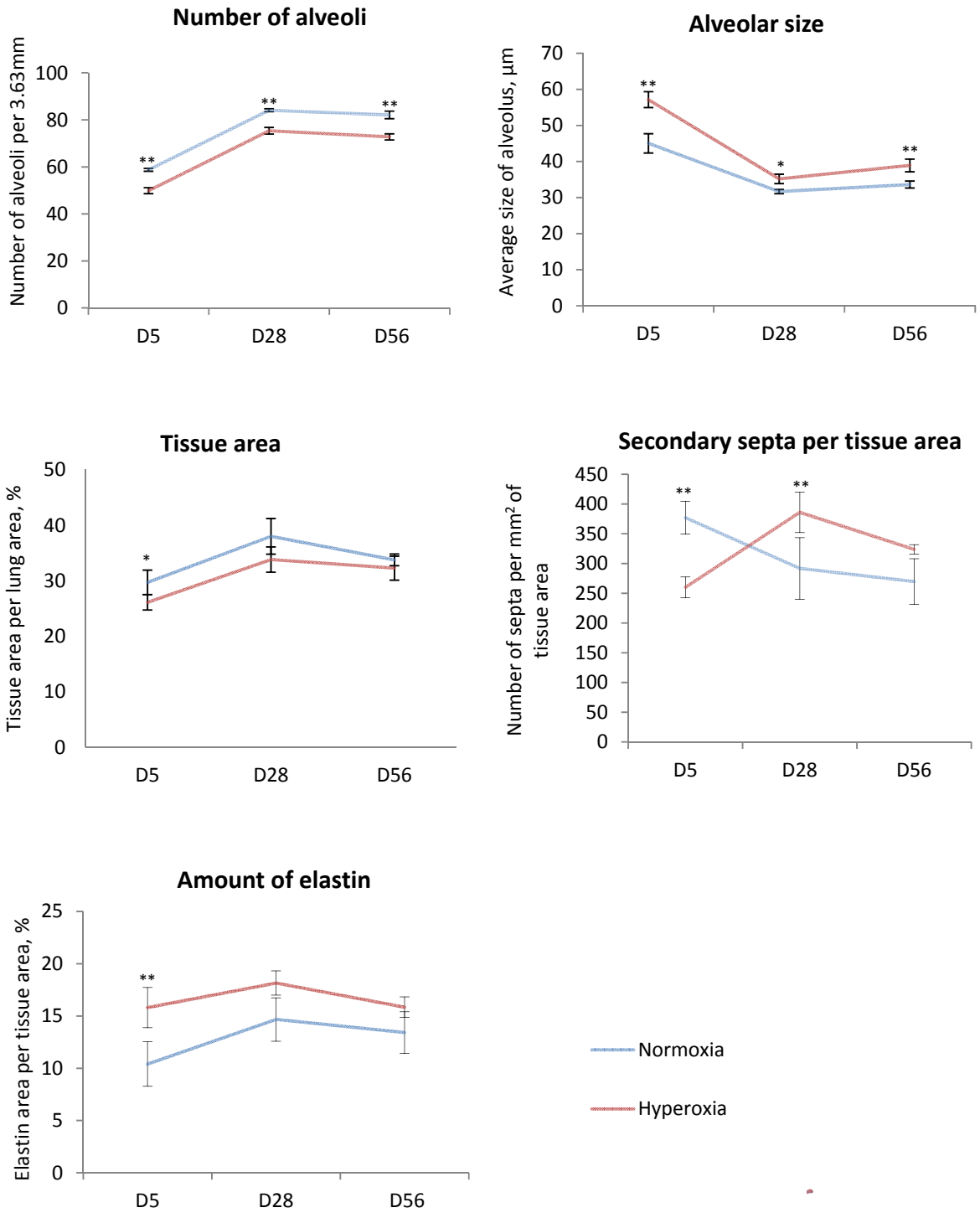

Figure 3.4-A. Statistical data for morphometric analysis of lungs after hyperoxia. Control (normoxic lungs) – blue line, hyperoxia-treated lungs – red line. The differences between normoxia and hyperoxia values were calculated using a general linear model (SPSS). $P<0.05$ is indicated as one asterisk, and $P<0.01$ is indicated as two asterisks. Error bars indicate SEM, n=4-6. Plot interactions are described in the text.

3.3.3.2. Temporary (reversible) changes in the lung tissue area, in the number of secondary septa and in the elastin content per tissue area

Converse to persistent changes in alveolar number and alveolar size, other parameters measuring postnatal lung development demonstrated transient changes that were normalised to control levels with time. For example, lung tissue area of hyperoxia-treated mice was significantly decreased compared to normoxia mice at D5, but was not significantly different at D28 and D56: D5, 26.12% (hyperoxia, n=6) versus 29.71% (normoxia, n=6), $P<0.05$; D28, 33.84% (hyperoxia, n=4) versus 38.01% (normoxia, n=4), $P=0.05$; and D56 32.28% (hyperoxia, n=6) versus 33.77% (normoxia, n=6), $P>0.05$; (Fig. 3.3, 3.4-A). The number of secondary septa per tissue area in hyperoxia-treated lungs was significantly reduced compared to normoxia mice at D5, significantly increased at D28 and was not significantly different at D56 (measurements are given as septum number per mm^2 of tissue): D5, 259.94 (hyperoxia, n=6) versus 377.12 (normoxia, n=6), $P<0.01$; D28, 385.98 (hyperoxia, n=4) versus 291.83 (normoxia, n=4), $P<0.01$; and 323.74 (hyperoxia, n=6) vs 269.73 (normoxia, n=6), $P\geq0.05$; (Fig. 3.3 and 3.4-A). Finally, elastin deposits were found on the tips of secondary septa, around blood vessels and within alveolar walls (Fig. 3.3). The amount of elastin (measured by Image-Pro Plus per lung tissue area per section area 0.564 mm^2, General Materials and Methods, Section 2.2) was significantly increased in hyperoxia-treated lungs compared to normoxia lungs at D5; however, no significant differences were observed at D28 and D56: D5, 15.85% (hyperoxia, n=6) versus 10.40% (normoxia, n=6), $P<0.01$ (Fig. 3.4-A).

These results indicate that processes affecting lung tissue area, secondary septa formation per tissue area and elastin deposition during post-natal lung development, are significantly affected during hyperoxia treatment, but subsequent compensatory mechanisms return these parameters to control levels.

3.3.4. Timeline of morphometric parameters of the lung

Timeline analysis was executed to examine more specifically how morphometric parameters affected during hyperoxia treatment were maintained or altered with time

compared to normal developmental events. To do this, changes in normoxia mouse development from D5 to D28 to D56 were analysed and then compared to those of hyperoxia treated mouse development using time-line plot interaction analysis.

With respect to the number of alveoli (per 3.63 mm), both normoxia and hyperoxia charts were parallel ($P<0.05$), with the number of alveoli increasing from D5 to D28 and then showing no change from D28 to D56 (Fig. 3.4-A). Alveolar size decreased from D5 to D28 in both normoxia and hyperoxia-treated mice and then increased from D28 to D56 ($P<0.05$, Fig. 3.4-A). The charts for the lung tissue area were parallel, i.e. there was no interaction between the plots and time had similar effects on the lung tissue area in both normoxia and hyperoxia-treated groups. The charts for the number of secondary septa per tissue area and the amount of elastin per tissue area were not parallel ($P<0.05$). Although lung tissue area of both normoxia and hyperoxia-treated mice both increased from D5 to D28, it did not change from D28 to 56 in the normoxia and hyperoxia-treated mice (Fig 3.4-A). The number of secondary septa per tissue area decreased from D5 to D28 in normoxia mice, but increased during this time in hyperoxia-treated mice (Fig 3.4-A). Between D28 and D56 the number of secondary septa decreased in hyperoxia-treated mice and stayed at the same level in normoxia mice. Lastly, the amount of elastin per tissue area increased from D5 to D28 in normoxia mice, but not in hyperoxia-treated mice, and persistently remained high in hyperoxia mice (Fig. 3.4-A). These data demonstrate that some morphometric changes elicited by hyperoxia treatment are subject to subsequent secondary compensatory mechanisms while others are not.

3.3.5. Analysis of the lung vascularisation after hyperoxia treatment

In addition to studying morphometric changes of the lung parenchyma following hyperoxia treatment, changes to the accompanying lung vasculature were also examined. Significant differences were observed in respect to blood vessel number per lung section area (i.e. including airspaces) and blood vessel number per total tissue area (i.e. excluding airspaces), and differences were not dependent on mouse gender. For example, the number of blood vessels surrounded by an observable elastin layer (per

0.564mm^2 of lung section area) was significantly decreased at D5 yet no differences were observed at D28 or D56: D5, 12.41 (hyperoxia, n=6) versus 14.6 (normoxia, n=6); P<0.05; (Fig. 3.4-B). With respect to blood vessel number per total tissue area (per mm^2), no significant difference was observed at D5 and D56, yet at D28 hyperoxia treated vessel numbers per total tissue area were significantly increased compared to normoxia lungs: D28, 87.42 (hyperoxia, n=4) versus 92.04 (normoxia, n=4); P<0.05.

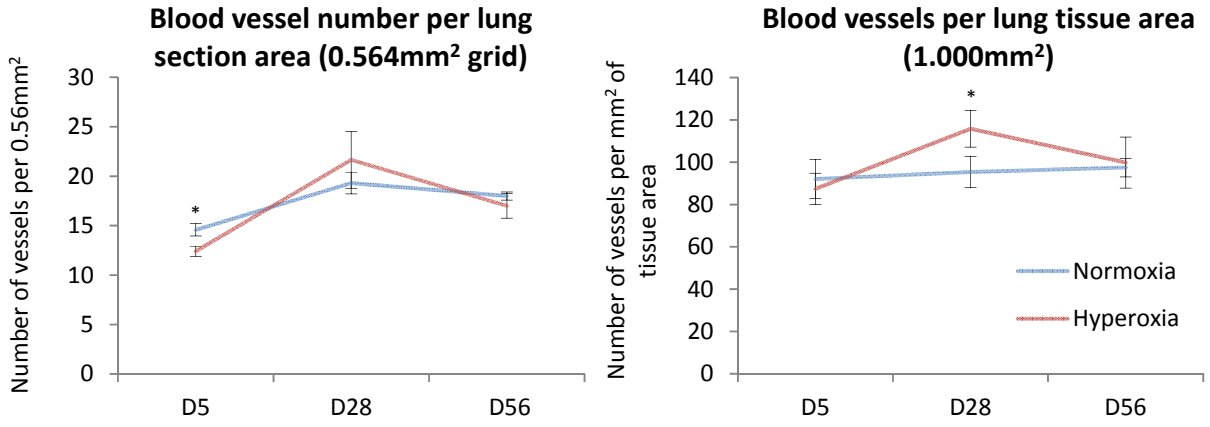

Figure 3.4-B. Statistical data for vascular analysis of lungs after hyperoxia. Control (normoxia lungs) – blue line, hyperoxia-treated lungs – red line. The differences between normoxia and hyperoxia values were calculated using a general linear model (SPSS). P<0.05 is indicated as one asterisk, and P<0.01 is indicated as two asterisks. Error bars indicate SEM, n=4-6. Plot interactions are described in the text.

Timeline analysis was similarly executed as above to examine more specifically how blood vessel morphometric parameters affected during hyperoxia treatment were maintained or altered with time compared to normal developmental events. With respect to the number of blood vessels per lung section area (including airspaces), there was a significant increase in blood vessel number in both normoxia and hyperoxia groups from D5 to D28 (P<0.05 for both groups). Subsequently, from D28 to D56, there was a significant reduction in blood vessel number in the hyperoxia group (P<0.05), yet no reduction in the normoxia group. Despite these differences between D28 to D56, overall, according to interaction analysis, charts were parallel, i.e. time had a similar effect on the number of blood vessels in both treatments (Fig. 3.4-B). With respect to the number of blood vessels per lung tissue area, no significant differences were seen in the normoxia group from D5 to D56. However, the hyperoxia group demonstrated a significant increase

from D5 to D28 ($P<0.05$) and a significant decrease from D28 to D56 ($P<0.05$; Fig 3.4-B). Normoxia and hyperoxia charts were not parallel ($P<0.05$). Together, these data indicate that hyperoxia treatment exerts either or both direct or indirect latent stimulatory effects upon vascular development (observable at D28) and that these effects are subsequently interpreted and normalised in respect to surrounding tissue area by D56.

With respect to mechanisms effecting changes to vascular development, Pecam1 immunoreactivity as an indicator of endothelial differentiation status and Vegfa immunoreactivity as an indicator of AECII cell ability to affect adjacent vascular behaviour, were investigated by both Western blot analysis and immunohistochemistry. Pecam1 protein levels standardised to the loading control β-actin (Actb) were significantly lower in hyperoxia-treated lungs compared to normoxia lungs at D5, while no significant differences were observed at D28 and D56: D5, 12.22% (hyperoxia, n=3) versus 79.92% (normoxia, n=4); $P<0.01$ (Fig. 3.5-B, C). No significant difference in Vegfa protein levels were observed at any time point examined (Fig. 3.6-B). Immunohistochemical analysis of Pecam1 demonstrated localisation to blood vessel walls (i.e. endothelial cells, Fig. 3.5-A), while immunohistochemical analysis of Vegfa demonstrated localisation to lung epithelial cells (Fig 3.6-A), which is consistent with the expression of Vegfa by AECII (Ng, Rohan et al. 2001). Some Vegfa-immunoreactive epithelial cells were associated with blood vessels.

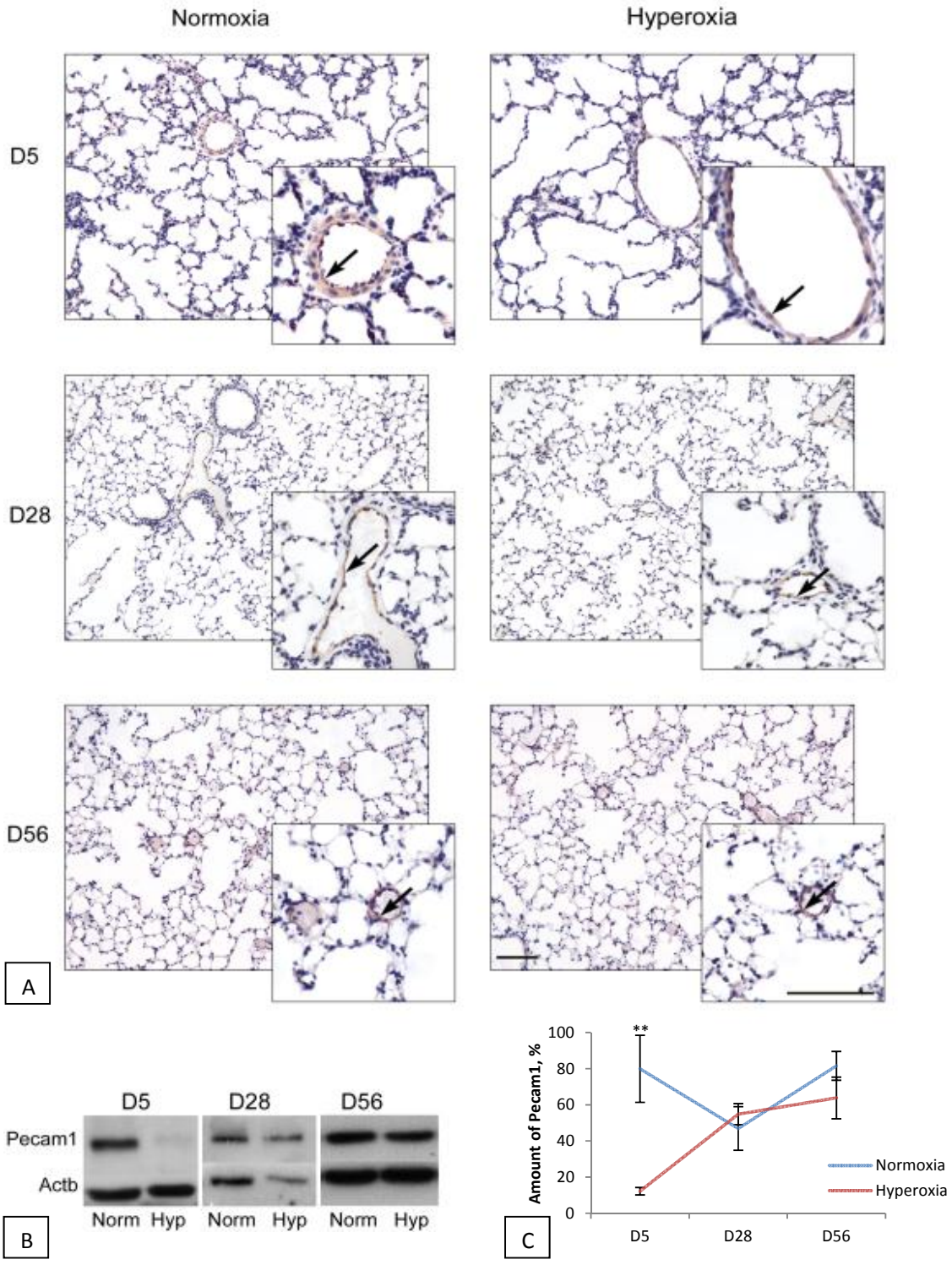

Figure 3.5. A. Immunohistochemistry for Pecam1. Brown staining indicates localisation of Pecam1 in the lung at three time points (D5, D28 and D56). Mayer's hematoxyllin staining (dark blue) indicates nuclei. Blood vessels are marked with arrows. Scale bar = 100μm. B. Western blot for Pecam1 (140kDa) in the lung at three time points (D5, D28 and D56). Actb is used as loading control (42kDa). Norm – Normoxia, Hyp – Hyperoxia. C. Levels of Pecam1 per total protein (relative to stained Actb) according to the western blot. Error bars represent SEM, n=3-4. Significant difference is marked with two asterisks (P<0.01, n=3-4).

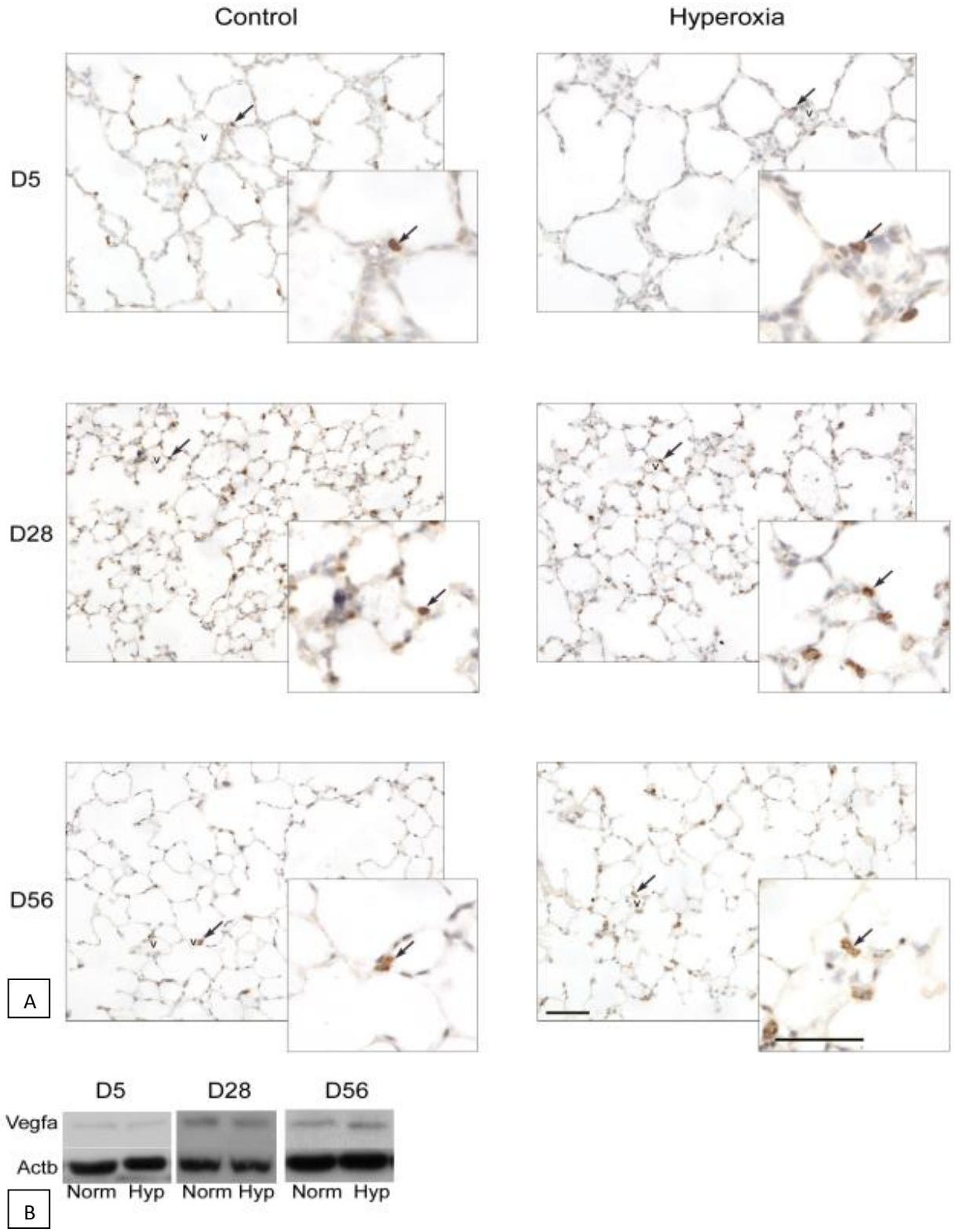

Figure 3.6. A. Immunohistochemistry for Vegfa on lung sections of control and hyperoxia-treated mice. Brown staining indicates Vegfa (marked with arrows) and blue staining indicates nuclei. Blood vessels are marked with "v". Scale bar = 50 μm. B. Western blot for Vegfa (21kDa). Actb is used as loading control (42kDa). Norm – Normoxia, Hyp – Hyperoxia.

3.3.6. Analyses of respiratory damage and pathological changes following hyperoxia treatment

As described above and following hyperoxia treatment, an increase in lung tissue elastin was observed at D5, but levels returned to control values by D28 (Fig. 3.3, 3.4-A). Further, morphological analyses of lung tissue revealed no visible respiratory damage or pathological changes in the lung after hyperoxia treatment, i.e. no airway mucus and no obvious fibrosis or abnormal collagen deposits were observed at any time point examined (Fig. 3.7, 3.8).

3.3.7. Analysis of the cell composition of bone marrow and blood

It has been previously demonstrated that the number of endothelial progenitor cells is significantly reduced in the bone marrow and in circulation after neonatal hyperoxia (Balasubramaniam, Mervis et al. 2007). FACS analysis was therefore performed on normoxia and hyperoxia-treated mouse blood and bone marrow at D5, D28 and D56 in a preliminary exercise to determine whether changes observed locally within the lung vasculature may relate to changes in the level of endothelial progenitor markers in the bone marrow and blood. The number of mice examined in this preliminary study was low (between two and four per group) and no significant differences between normoxia and hyperoxia-treated mice were observed in the number of Kdr^{+}, $Prom1^{+}$ and $Pecam1^{+}$ cells in both the bone marrow and blood at any time point examined. In the case of Ptprc, however, although no significant differences in immunoreactive cell number in the blood of hyperoxia-treated and normoxia mice was observed at any time point, a significant increase in Ptprc immunoreactivity was observed in the bone marrow of hyperoxia-treated mice compared to normoxia mice at D28 ($n=4$, $P<0.05$; data not shown).

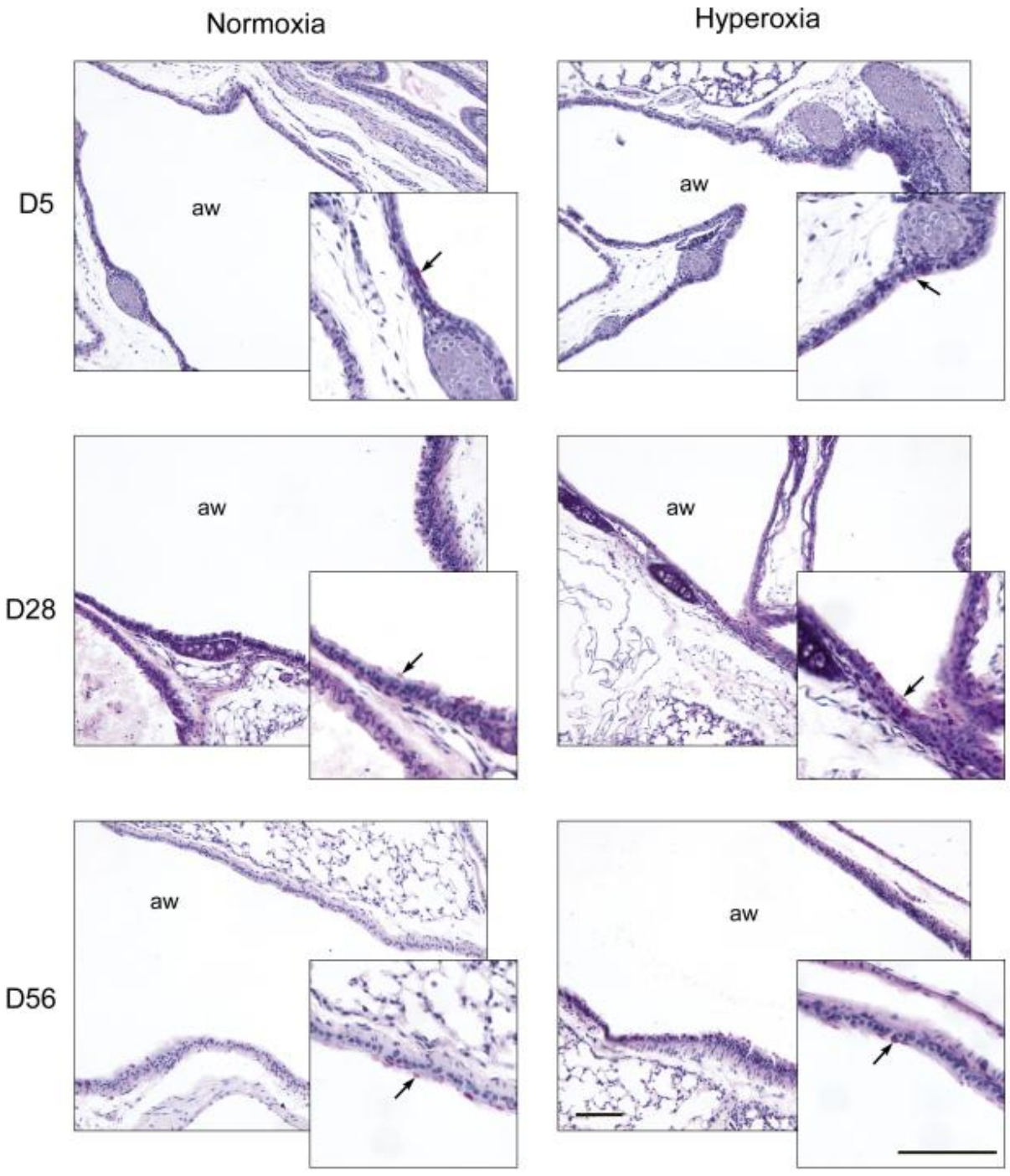

Figure 3.7. Representative periodic acid-Schiff's reagent staining of lung airways, counterstained with Mayer's hematoxyllin. Mucin-secreting cells are stained purple and are marked with arrows. No mucus deposits are present in the airways (aw) of either normoxia or hyperoxia-treated mice. Scale bar = 100 μm.

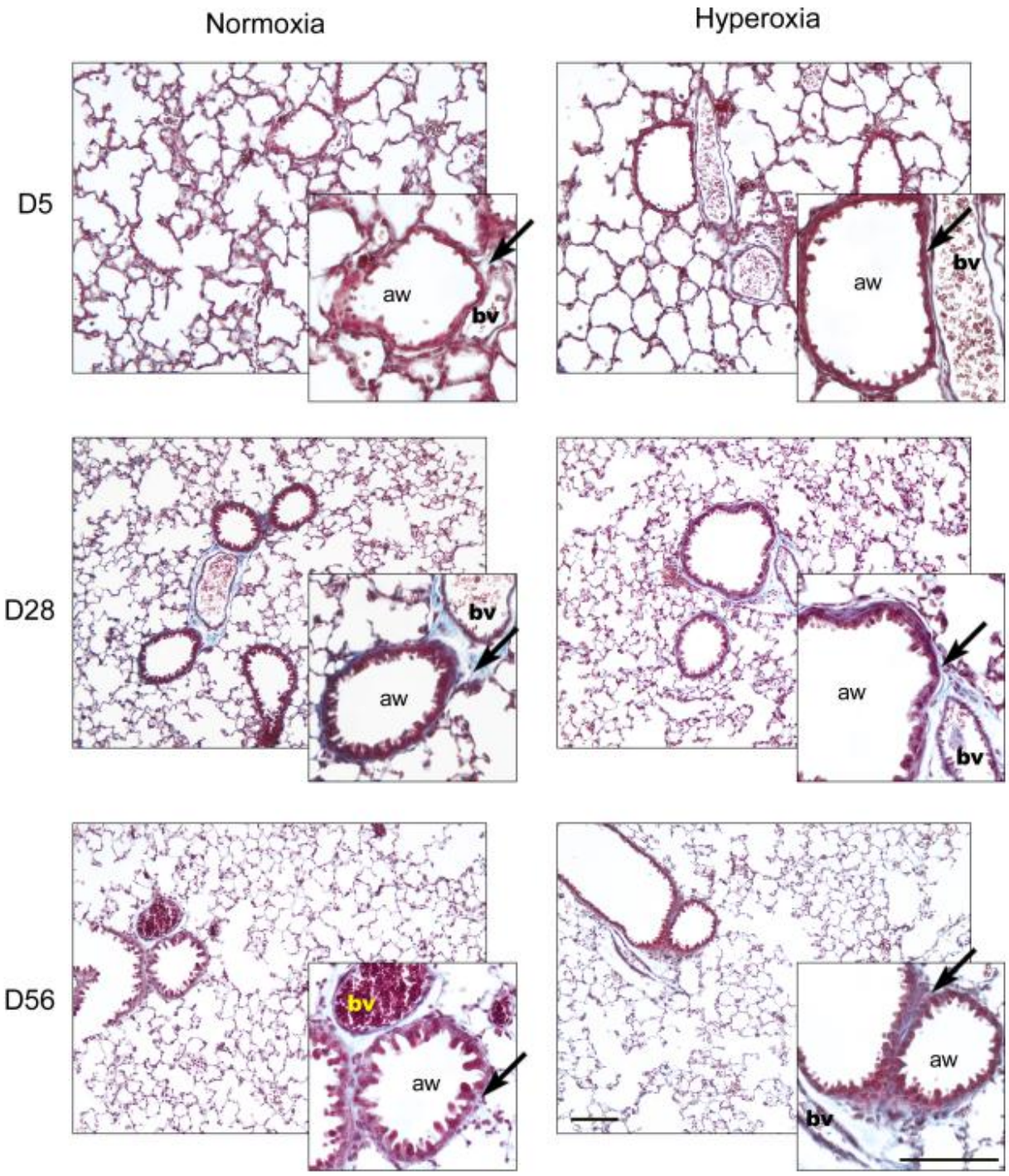

Figure 3.8. Representative Masson's trichrome staining of normoxia and hyperoxia-treated lungs. A collagen layer (stained blue) around the airways (aw) and blood vessels (bv) is present in both normoxia and hyperoxia-treated lungs and is marked with black arrows. Nuclei are stained purple, cytoplasm is stained red. No abnormal collagen deposits (i.e. thickening of lung tissue area) are observed in hyperoxia-treated lungs at any stage. Scale bar = 100 μm.

3.4. Discussion

3.4.1. General Health of Animals

Neither during nor after hyperoxia treatment did animals display any signs of pain or distress, or lose or gain weight in comparison to normoxia mice. Weight loss observed in previous studies could be due to the mother's distress and loss of good health in high oxygen conditions. Our collaborators (Prof. Richard Harding, Dr. Foula Sozo and Ms Sheena Bouch, unpublished) have performed a comparison study, where mothers were either swapped or left with pups during hyperoxia treatment (60% oxygen for seven days). Their study has demonstrated, that pups fed by unswapped mothers in oxygen weighed less than control pups (normoxia with unswapped mothers), whereas when mothers were swapped, there was no significant difference in pup weight. In this study mothers were swapped every 24 hours, so there was no difference between normoxic and hyperoxic food quality that pups received. There was also no difference in observed behavior patterns (moving around the cage), and no hyperoxia-induced mortality. Being born in high oxygen conditions could have affected general survival, as pups did not have to adjust to high oxygen concentrations.

After hyperoxia treatment heavy and loud breathing was noticed in pups during stressful periods, however no mucus was observed in the airways after mucin staining of lung sections, and therefore it was concluded that the reason for noisy breathing was not inflammation or any kind of airway obstruction. Previous studies have shown that the method of paraformaldehyde lung infusion and PAS staining is effective for observing lung mucus (Blackburn, Volmer et al. 2000). There were also no signs of fibrosis observed in the lung after collagen staining of lung sections. Whether the airway noises may have been associated with changes to upper airway structures, for example, larynx, pharynx or nasal structures, was not examined here.

3.4.2. Progress of lung septation

At D5, alveolarisation in mice has been reported to have just started. Therefore secondary septa are beginning to form and reshape the alveolar wall. A lower alveoli number and larger alveolar size were observed during normal development at D5, compared to D28 and D56. This can be explained by the fact that between D5 and D28 the main steps of alveolarisation occur: the number of secondary septa per tissue area reduces as the number of alveoli increases and the size of alveoli becomes smaller due to septation. Between D28 and D56 secondary septation overtly ceases and alveolar size and number do not markedly change. Therefore, after D28 there is sufficient alveolar surface area in contact with air to support the organism with the oxygen available.

At D5, the number of secondary septa per tissue area in hyperoxia treated mice was reduced compared to control levels, as was the number of alveoli, and this was accompanied by a larger alveolar size. During the process of adaptation to normal oxygen conditions, the rate of secondary septation then increased, such that the same number of secondary septa per tissue area as normoxic mice at D5, was reached by hyperoxia treated mice by D28. However, alveoli size remained large and alveoli number did not reach control (normoxic) levels even by D56. This means, that there was a reduced contact area between air and lung tissue at all tested time points, including D56, which would make breathing less efficient. Therefore hyperoxia treatement here caused a chronic lung septation deficit, as deficits persisted to adulthood.

3.4.3. Tissue area

There was significantly more tissue area in both normoxia and hyperoxia treated mice at D28, compared to D5, most likely due to cell growth and division. No difference between tissue area in normoxia and hyperoxia-treated mice at D28 and D56 was observed. Because alveolar size remained high and the number of alveoli remained low (i.e. reduced septation), this suggests that alveolar walls in hyperoxia-treated lungs increased in thickness by D28 in order to compensate for the lack of tissue surface area.

3.4.4. Amount of elastin per tissue area

Less elastin per tissue area was observed at D5 in normoxia mice compared to hyperoxia-treated mice. However elastin levels increased by D28, whereas in hyperoxia-treated mice they were high at all time points examined. It can therefore be concluded that hyperoxia increases elastin levels in the neonatal lung. This confirms earlier studies which demonstrated that elastin depositions in the lungs increase after both ventilation and hyperoxia (Bruce, Bruce et al. 1993; Allison, Crossley et al. 2010). Elastin is produced by vascular smooth muscle cells and surrounds mainly arteries, whereas veins have less elastin, and in small capillaries there is very little or no elastin (Patel, Fine et al. 2006). Elastin is also present on the tips of secondary septa (Burri 2006). Because the total number of blood vessels per tissue area was not altered and secondary septation per tissue area in fact was decreased at D5, the relative increase in elastin levels in the D5 hyperoxia-treated mice, therefore, must be attributable to higher deposits at these sites and also within alveolar walls rather than increases in the number of these sites.

3.4.5. Vascularisation

The number of blood vessels was evaluated in relation to tissue area because tissue area was reduced in hyperoxia-treated mice. As the tissue area increases to control levels at D28 in hyperoxia-treated mice, the number of blood vessels also increases to control levels. However, the increase in blood vessel number per tissue area at D28 indicates the increase in vascular over-stimulation in hyperoxia-treated mice compared to controls. At D56 there was no significant difference observed in any parameters measured aside from the number of alveoli and the alveolar size. Thus these data decouple septation and vascularisation at least to some extent. A reduction of the endothelial marker Pecam1 was further observed at D5 in hyperoxia-treated lungs, which may indicate either less or smaller blood vessels, or a decrease in the number of Pecam1 molecules produced by endothelial cells. Counted elastin-positive vessels do not include all types of vessels, and therefore the number of small capillaries was not evaluated. However, a lack of elastin-positive vessels after hyperoxia at D5 may be related to these reduced Pecam1 levels. In

order to overcome the consequences of hyperoxia, the hyperoxia mouse lung appears to be stimulating blood vessel growth and by D28 both the number of blood vessels per section area and Pecam1 levels reach control levels. Blood vessel number per tissue area increases by D28, suggestive of a “catch-up” compensatory mechanism. In the same manner, the subsequent increase in Pecam1 levels back to control levels is supported by the increase in the number of blood vessels per tissue area, but may also be attributable to the increase in the size of blood vessels per tissue, and/or the increase in the amount of Pecam1 per endothelial cell.

The amount of Vegfa remained unchanged in hyperoxia-treated lungs relative to normoxia lungs at all time points examined, which may indicate that AECII are not affected by hyperoxia at this level. On the other hand, an earlier lack of Vegfa before D5 may not be visible at the stages examined here (Balasubramaniam, Mervis et al. 2007).

It can be concluded, therefore, that both alveolarisation and vascularisation are affected by hyperoxia treatment, but to different degrees and to some extent independently to each other. A reduced rate of secondary septation associates with a reduction in the number of alveoli and an increase in alveolar size, whereas reduced levels of Pecam1 associates with a reduction in the total number of blood vessels per section area, but not with the number of blood vessels per tissue area. Blood vessel number per tissue area undergoes an apparent over-compensatory catch-up phenomenon between D5 and D28 and this associates with a rise in Pecam1 levels. Whether the rapid increase in blood vessel number per tissue area stimulates secondary septation is not known at this stage.

3.4.6. Analysis of cell composition of bone marrow and blood

Previous studies have demonstrated the changes in the number of EPCs, i.e. $Kdr^{+}/Prom1^{+}/Ptprc^{dim/-}$ cells in both the bone marrow and the systemic vascular system following 10 days of hyperoxia treatment of newborn mice (Balasubramaniam, Mervis et al. 2007). Here, however, the number of Kdr^{+} and $Prom1^{+}$ cells in both blood and bone marrow did not change, and neither did the number of $Pecam1^{+}$ (a marker of mature endothelial cells) cells. An increase in the number of $Ptprc^{+}$ cells (which marks both

hematopoietic stem cells and EPC subfractions), however, was observed in the bone marrow of hyperoxia-treated mice relative to controls at D28. Therefore, although preliminary due to the low number of mice examined in this part of the study, hyperoxia affects cell fractions of the bone marrow compartment that may interact with the vascular system of the lung. This hypothesis requires further investigation.

3.5 Conclusion

In conclusion, hyperoxia in newborn mice caused a deficit in both alveolarisation and respiratory vascularisation; however, blood vessel count recovered faster than septation and caught up to (and overtook) control levels by D28. Lung tissue area also reached control levels by D28. However, alveolar number and size remained deficient until adulthood. There was no full recovery by D56 therefore after 4 days of 90% oxygen treatment in newborn mice, despite the absence of (i) weight loss, (ii) mucus in the airways, (iii) inflammation and (iv) fibrosis. A further investigation of possible deformations to upper airway structures in warranted.

Chapter 4. Characterisation of mouse bone marrow endothelial progenitor populations

4.1. Introduction

Bone marrow-derived endothelial progenitor populations are not fully characterised in terms of cell surface markers and differentiation properties. Several EPC populations have been described, i.e. early EPCs and late EPCs (Yoon, Hur et al. 2005; Deschaseaux, Selmani et al. 2007). However, these descriptions vary, making it difficult to isolate the entire EPC population.

It is important to determine the functional qualities of such a cell population before using it for therapeutic purposes. Cultured EPCs have been suggested to improve lung structure after exposure of neonatal mice to high oxygen conditions (Balasubramaniam, Ryan et al. 2010). Vascularisation therapy may therefore represent a useful treatment for structural deficit of the human lung, such as after or during hyperoxia treatment of very preterm birth infants. However, firstly, such cells would have to be demonstrated safe for therapy, and therefore minimum manipulations ought to be used in preparing cells for injection. Secondly, and as alluded to above, the number of cell surface markers that can be used is quite broad, and it still has not been determined, which marker is most suitable for appropriate EPC isolation.

In this study, cell surface markers that are known to be present in EPCs (Kdr, Tek, Prom1, Mcam and Cd34) were used to separate BM-derived cell populations (Bertolini, Shaked et al. 2006). A pilot study using Pecam1 and vWF-immunoreactivity assays was performed to assess differentiation ability of these populations *in vitro*. Individual populations separated based on their immunoreactivity to these EPC markers were then characterised based on individual population immunoreactivity to Kdr, Tek, Prom1, Mcam, Pecam1 and

Ptprc by FACS. The individual populations were further analysed for their ability to form vessel-like structures as a function of plated cells in culture. The population that was most efficient in vessel-like structure formation was selected for further characterisation, such as the presence of GFP in vessel-like structures containing cells isolated from C57Bl6/J GFP mice; GFP fluorescence would enable tracking *in vivo* once used in an injury model. It was hypothesised that by defining a marker that permitted unambiguous and prospective isolation of an efficient Pecam1^{+} blood vessel-like forming BM EPC subpopulation *in vitro*, that this same marker may be optimal for defining a population with similar *in vivo* properties for therapeutic purposes. Cultured EphA3+ cells, previously described to be associated with blood vessel formation (Vail, Tan et al. 2012) were also isolated and characterised in a similar manner to other BM populations, with the view of later examining the potential of these cells to ameliorate the lung structural deficits associated with neonatal mouse hyperoxia treatment. Unsorted plate-adherent cells were also tested in the same way due their known ability to engraft the lung and their previously described therapeutic properties (Silva, Litovsky et al. 2005; Aslam, Baveja et al. 2009; van Haaften, Byrne et al. 2009).

4.2. Materials and methods

4.2.1. Experimental design

Bone marrow was isolated from C57Bl6/J mice as described in General Materials and Methods (Section 2.8). Unsorted bone marrow was plated in culture to examine vessel formation in endothelial differentiation culture medium (EDCM), as described in General Materials and Methods (Section 2.10). Following culture condition optimisation, freshly isolated BM cells were sorted by FACS and MACS (General Materials and Methods, Section 2.9). Both positive and negative fractions were accordingly, differentiated for 14 days and analysed as part of a pilot study for the presence of blood vessel-like structures using immunohistochemistry for Pecam1 and vWF (General Materials and Methods, Section 2.11; Fig 4.1). Experiments were repeated twice (a total of three experiments) in the optimal conditions for statistical analysis of vessel-like structure formation ability.

Unsorted cells were also plated at the same time and under the same conditions to test cell survival indices in the absence of sorting. Freshly-isolated BM was stained for the EPC cell surface markers, hematopoietic marker Ptprc and endothelial marker Pecam1 (General Materials and Methods, Section 2.7).

The BM EphA3+ subpopulation was cultured according to methods provided by our collaborators (General Materials and Methods, Section 2.12). EphA3+ cells were then subjected to the vessel formation assay and FACS characterisation described above.

Chosen fractions that formed vessel-like structures (differentiated from Day 0), as well as: (i) unsorted plate-adherent cells isolated at passage 0 (General Materials and Methods, Section 2.13), (ii) passage 8 and 13 unfrozen EphA3^{+} cells, and (iii) passage 11 frozen EphA3+ cells were analysed for the presence of GFP at two different stages. The first stage was prior to differentiation, with analysis by FACS (General Materials and Methods, Section 2.7). The second stage was after differentiation in EDCM medium, and by analyzing GFP fluorescence and assaying the number of GFP positive cells present in Pecam1^{+} vessel-like structures and the number surrounding these structures (General Materials and Methods, Section 2.14).

4.2.2. Statistical analysis

An ANOVA was used to determine any significant differences between the described characteristics of separate marker-positive fractions, as well as between positive and negative fractions, where $P<0.05$ was considered to represent significant difference.

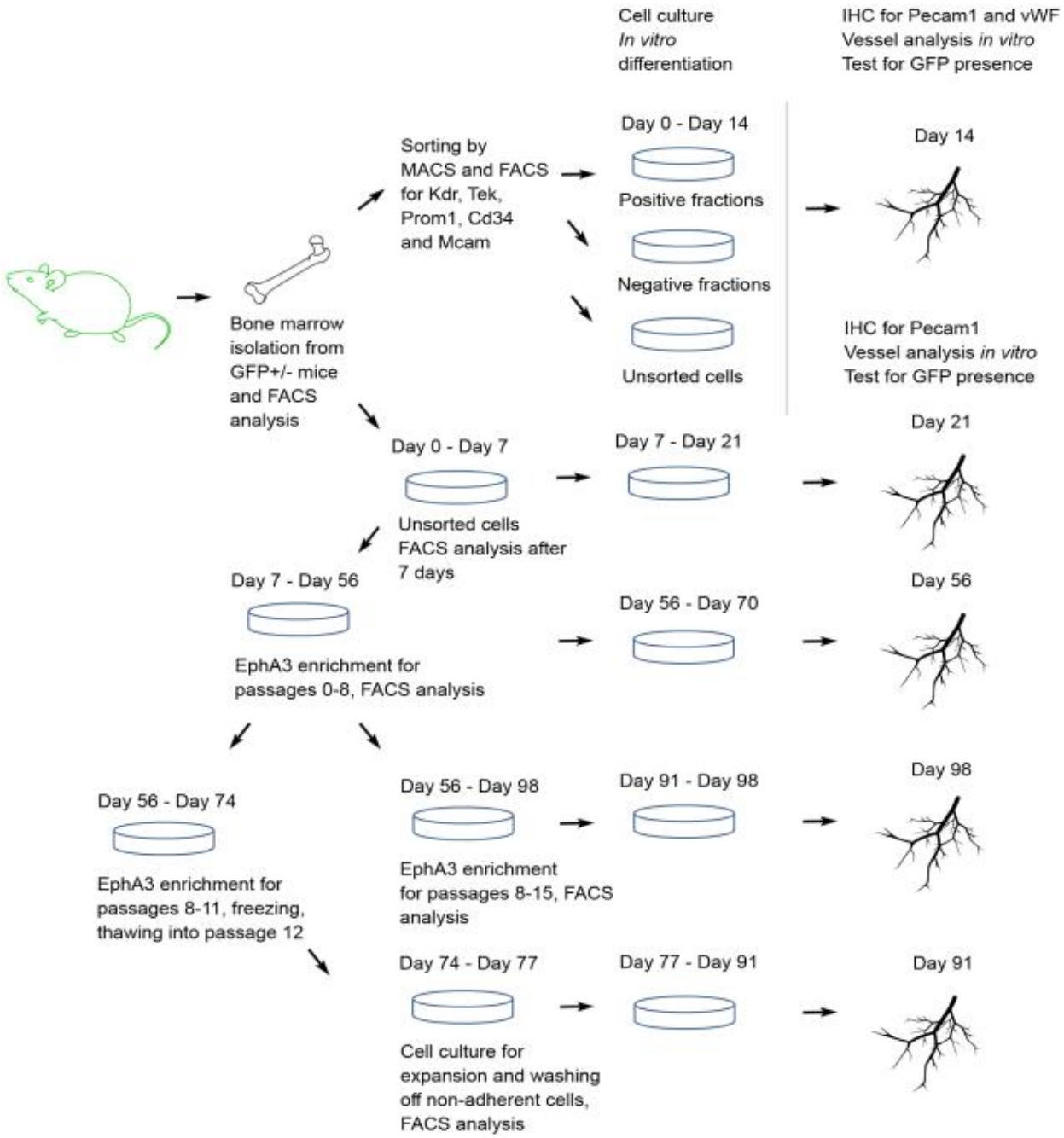

Figure 4.1. Experimental design for the characterisation of different EPC fractions. Cells were isolated from mouse bone marrow and analysed for the presence of surface markers using FACS. A first group of cells was sorted using MACS and FACS, and plated in culture for differentiation into endothelial cells (Day 0-14). A second group was plated in the same manner without sorting. Some of these cells were differentiated straight away (Day 0-14). Others were cultured and expanded for 7-98 days or 0-15 passages. Unsorted plate-adherent cells from passage 0 were differentiated on Day 7-21. Other unsorted cells were cultured in growth medium by Dr. Degu Abebe. Cell aliquots were differentiated and analysed at passage 8 and passage 13. These cells were also frozen at passage 11 and thawed into passage 12, cultured for three days, analysed by FACS and differentiated for *in vitro* analysis. At Day 14 of differentiation all cells were fixed and stained for the presence of endothelial markers.

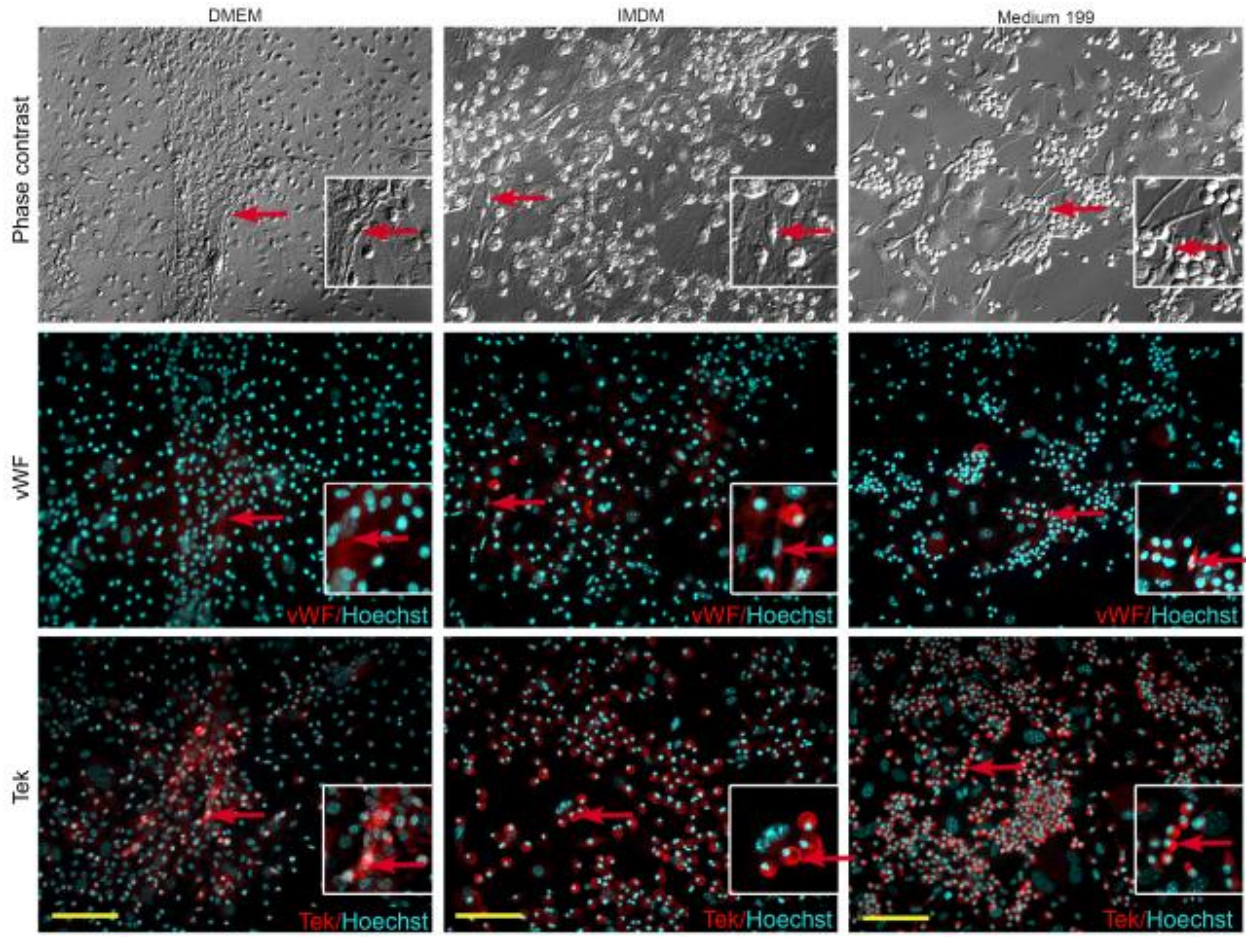

Figure 4.2. Morphology of cells from bone marrow grown in three different media types: DMEM, IMDM and Medium 199. The top row represents cells observed in phase contrast mode. Spindle-shaped cells cultured in DMEM and IMDM were able to group into vessel-like structures, whereas spindle-shaped cells cultured in Medium 199 did not group. Spindle-shaped cells are marked with red arrows. The middle row represents immunoreactivity of spindle-shaped cells to vWF (red) counterstained with Hoechst (blue). Spindle-shaped cells cultured in IMDM and Medium 199 displayed immunoreactivity to vWF, whereas spindle-shaped cells cultured in DMEM displayed low or no immunoreactivity to vWF (red arrows indicate spindle-shaped cells). The bottom row represents immunoreactivity to Tek (red) counterstained with Hoechst (blue). All three groups contained cells that were immunoreactive to Tek (red arrows). Scale bar = 100 μm.

4.3. Results

4.3.1. Media Optimisation

Cells grown in the three different media types (IMDM, DMEM and Medium 199) demonstrated different capacities to differentiate into endothelial-like cells. Cells cultured in IMDM demonstrated the closest resemblance to endothelial cells based on Tek (an endothelial progenitor marker) and vWF (a marker of differentiated endothelial cells) immunoreactivity, as well as their appearance as spindle-shaped cells and their ability to group into vessel-like structures (Fig. 4.2). Spindle-shaped cells cultured in DMEM and IMDM were able to group into vessel-like structures, whereas spindle-shaped cells cultured in Medium 199 did not group (Fig. 4.2). Spindle-shaped cells cultured in IMDM and Medium 199 displayed immunoreactivity to vWF, whereas spindle-shaped cells cultured in DMEM displayed low or no immunoreactivity to vWF (Fig. 4.2). All three groups contained cells that were immunoreactive to Tek. IMDM was therefore selected for use in subsequent experiments.

4.3.2. Pilot study of vessel-like branch formation potential of individual cell populations after FACS and MACS sorting

Positive and negative FACS fractions were plated in culture alongside unsorted cells in EDCM to assay for their potential to organise into vessel-like branching structures and to display immunoreactivity to markers of mature blood vessels. Attachment of cells was visually analysed every day by observing floating and flattening cells, the survival of non-attached (floating) cells was analysed by trypan blue staining. Sorted cells did not survive culture, whereas unsorted cells did. Therefore MACS enrichment was employed in a further attempt to isolate viable cell fractions for *in vitro* culture. Isolated cell fractions were quantitated to enable standardisation of culture input number per 1 cm^2 of the tissue flask area.

Preliminary results indicated that cells from all fractions participated in vessel-like structure formation after *in vitro* differentiation. Most positive fractions had higher vessel-like structure formation activity, compared to negative fractions, according to preliminary calculations (data not shown). However, the $Cd34^+$ fraction demonstrated low plate-adherence and low vessel-like structure formation (less than 2 branches per well, data not shown), compared to the $Cd34^-$ fraction (5-35 branches per well, data not shown), and was therefore excluded from further analysis.

4.3.3. Characterisation of fractions by FACS analysis

The number of BM cells reacting with each antibody varied between the three to five animals analysed. Kdr^+, $Prom1^+$, Tek^+ and $Mcam^+$ cells accounted for 2.42%, 10.4% 2.96% and 34.92%, respectively, of all freshly isolated BM cells analysed by FACS (Fig. 4.3). The $Cd34^+$ fraction accounted for 6.67-13.30% (data not shown).

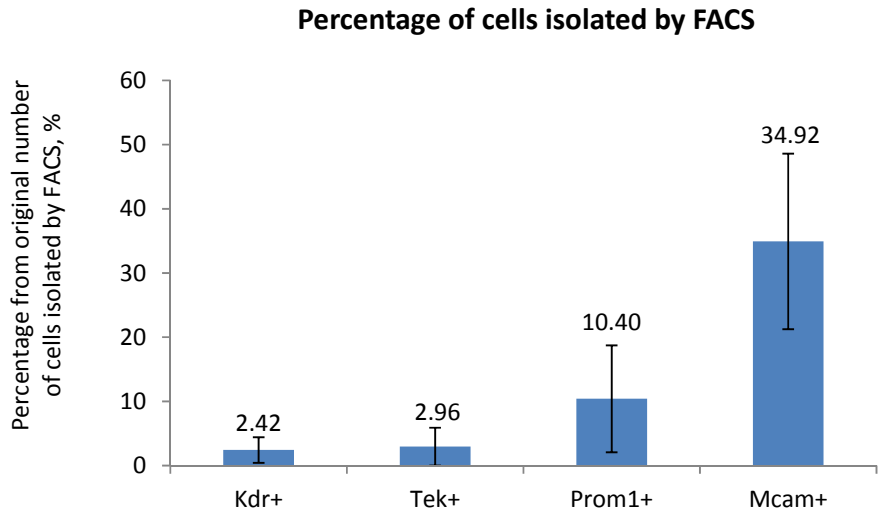

Figure 4.3. Percentage of cells positive for selected surface markers in BM determined by FACS. Error bars represent standard deviation (SD), n=3-5.

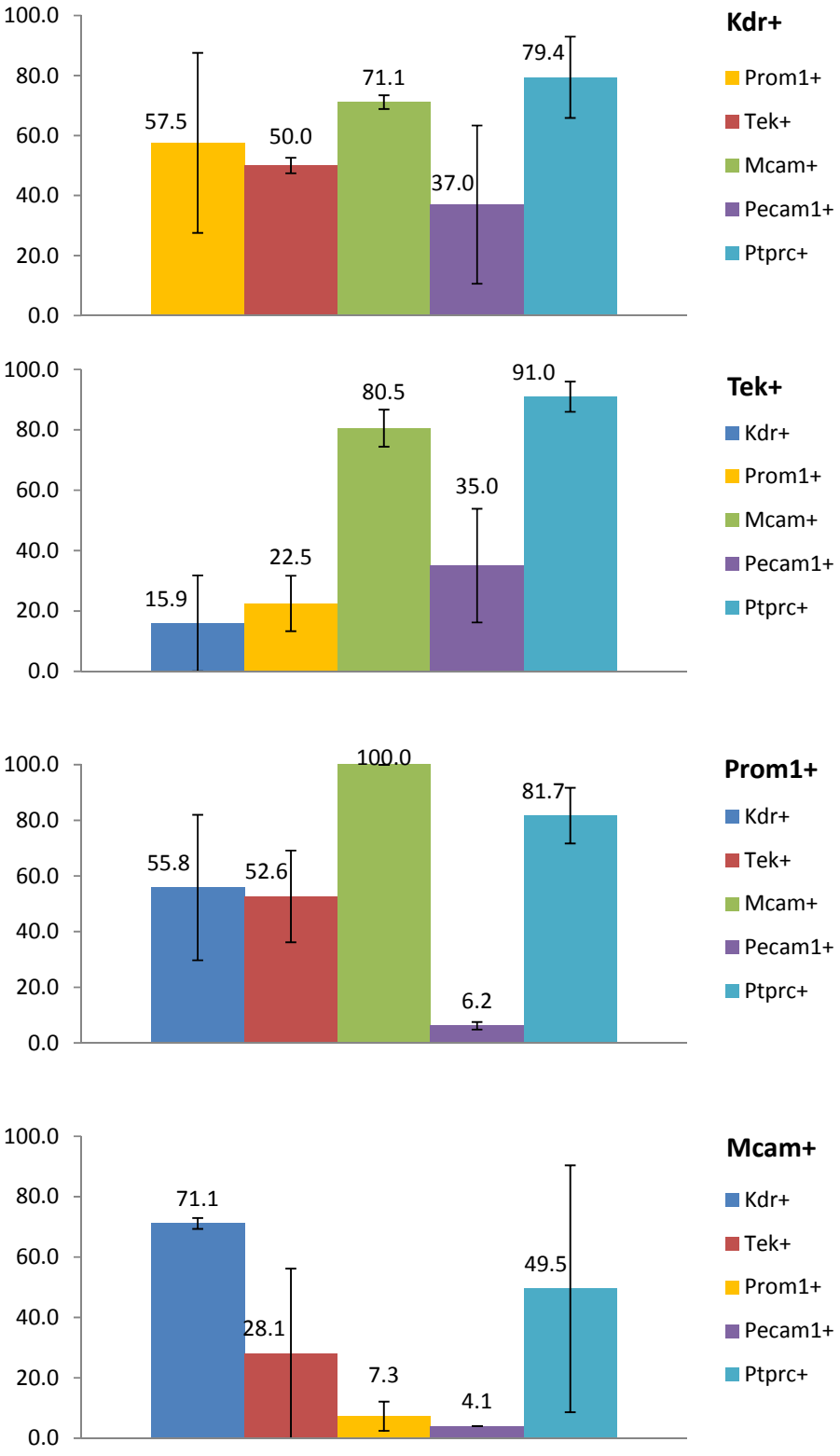

Figure 4.4. Descriptive analysis of different cell fractions from freshly-isolated BM. Error bars represent SD, n=3-5.

Freshly-isolated bone marrow was incubated with Prom1, Tek, Kdr and Mcam antibodies. The Cd34 antibody was not used in this analysis due to the low plate adherence in the preliminary study. Prom1^{+}, Tek^{+}, Mcam^{+} and Kdr^{+} fractions were gated and then these populations were individually characterised for their relative immunoreactivity to Kdr, Tek, Prom1, Mcam, Pecam1 and Ptprc antibodies before cell culture (Fig. 4.4). These data demonstrated that the individually isolated cell fractions represent distinct cell populations. The error bars on the charts represent standard deviation in variation between animals (n=3-5). EphA3^{+} cells were observed at very low levels in freshly-isolated bone marrow cells (<1%, data not shown). This indicates that fresh bone marrow cells do not contain an EphA3+ cell population that can be efficiently isolated.

Long-term cultured cells immunoreactive to EphA3 antibody were frozen at passage 11 and thawed, plated into passage 12 and also characterised for the six markers described above, as well as Pecam1 and Ptprc (Fig. 4.5) Long term cultured EphA3^{+} cells were thus shown to display immunoreactivity to cell markers consistent with other EPC subgroups.

After seven days in culture unsorted plate-adherent cells (passage 0) displayed a 22.23% Kdr^{+}, 1.93% Pecam1^{+}, 31.33% Tek^{+}, 91.03% Ptprc^{+}, 11.07% Mcam^{+} and 22.93% Prom1^{+} subcomposition profile (Fig. 4.6). Short term cultured BM cells were thus shown to display immunoreactivity to cell markers consistent with other EPC subgroups.

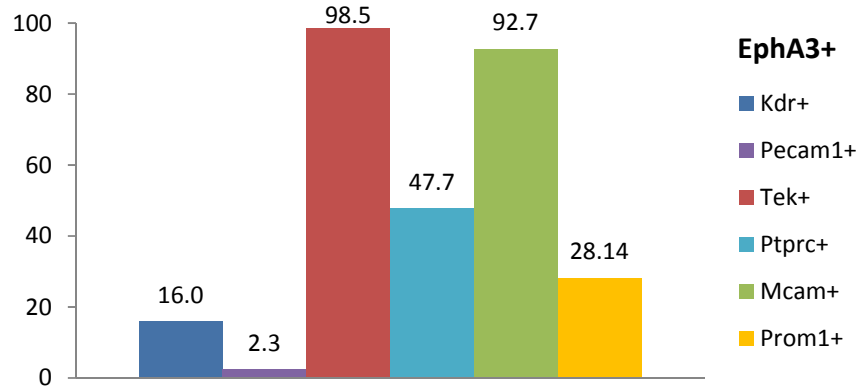

Figure 4.5. Descriptive analysis of long-term cultured EphA3^{+} cells (no error bars were used as these cells have only been isolated once from one mouse).

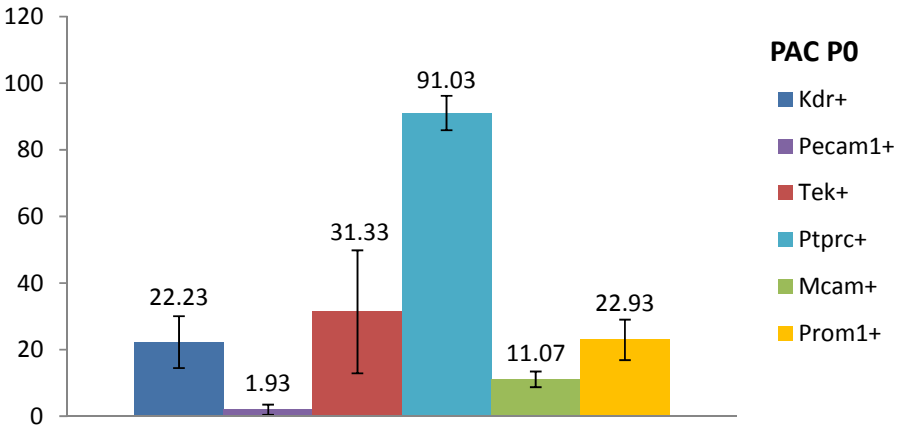

Figure 4.6. Descriptive analysis of unsorted plate-adherent cells at passage 0. Error bars represent SD, n=3-5.

4.3.4. MACS Isolation and cell culture

Individual Kdr$^+$, Kdr$^-$, Tek$^+$, Tek$^-$, Prom1$^+$, Prom1$^-$, Mcam$^+$ and Mcam$^-$ cell populations were separated by MACS in preparation for cell culture to determine the vessel-like branching activity of respective cell populations. These fractions were not 100% pure, but rather enriched for selected markers, and therefore the percentage of isolated cells varied from FACS results (3.5% enriched for Kdr, 3.8% enriched for Tek, 4.9% enriched for Prom1 and 7.7% enriched for Mcam, Fig. 4.7). One to two hundred thousand cells (depending on the number of cells isolated from each animal's bone marrow) were plated per 1 cm^2. Both "positive" and "negative" fractions were plated.

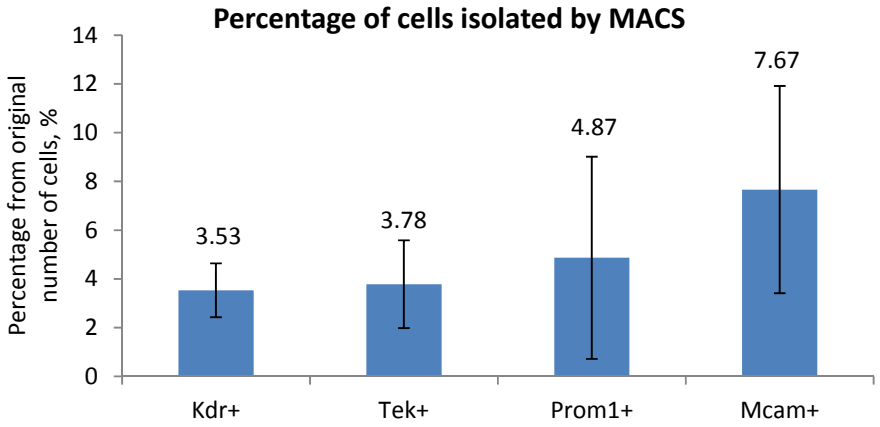

Figure 4.7. The percentage of cells sorted "positive" from the original BM cell number following MACS (magnetic enrichment). Error bars represent SD, n=3-5.

4.3.5. Vessel-like structure formation and endothelial marker immunoreactivity *in vitro* after MACS enrichment

Cells from different fractions formed vessel-like structures that displayed immunoreactivity within the cytoplasm to the mature endothelial cell marker vWF (Fig. 4.8) and in plasma membranes for Pecam1 (Fig. 4.9). The $Pecam1^{+}$ sorted fraction was used as a positive control, and displayed positive immunoreactivity to both Pecam1 (in both plasma membranes and in the cytoplasm) and vWF. Unsorted cells were used as "general cell behaviour" control and also demonstrated vessel-like structure formation capacity. Pecam1 immunoreactivity was used to analyse properties of vessel-like structure formation in more detail. Approximately 5-20% of the cell population in each fraction participated in vessel-like structure formation (data not shown). The number of vessel-like branches immunoreactive to Pecam1 antibody per well per $1x10^{5}$ passaged cells was analysed. The number of these branches in the Kdr^{+} fraction compared to the Kdr^{-} fraction was significantly different (49 vs 2 branches, respectively; n, number of times the cells were isolated from different animals and plated down, was 3; $P<0.05$, Fig. 4.10). All other positive fractions did not display significant differences compared to their negative fractions. Therefore, of all the BM EPC markers tested, Kdr represents the only marker that prospectively delineates the efficiency of a specific EPC BM subpopulation to from Pecam1+ vessel-like structures *in vitro*.

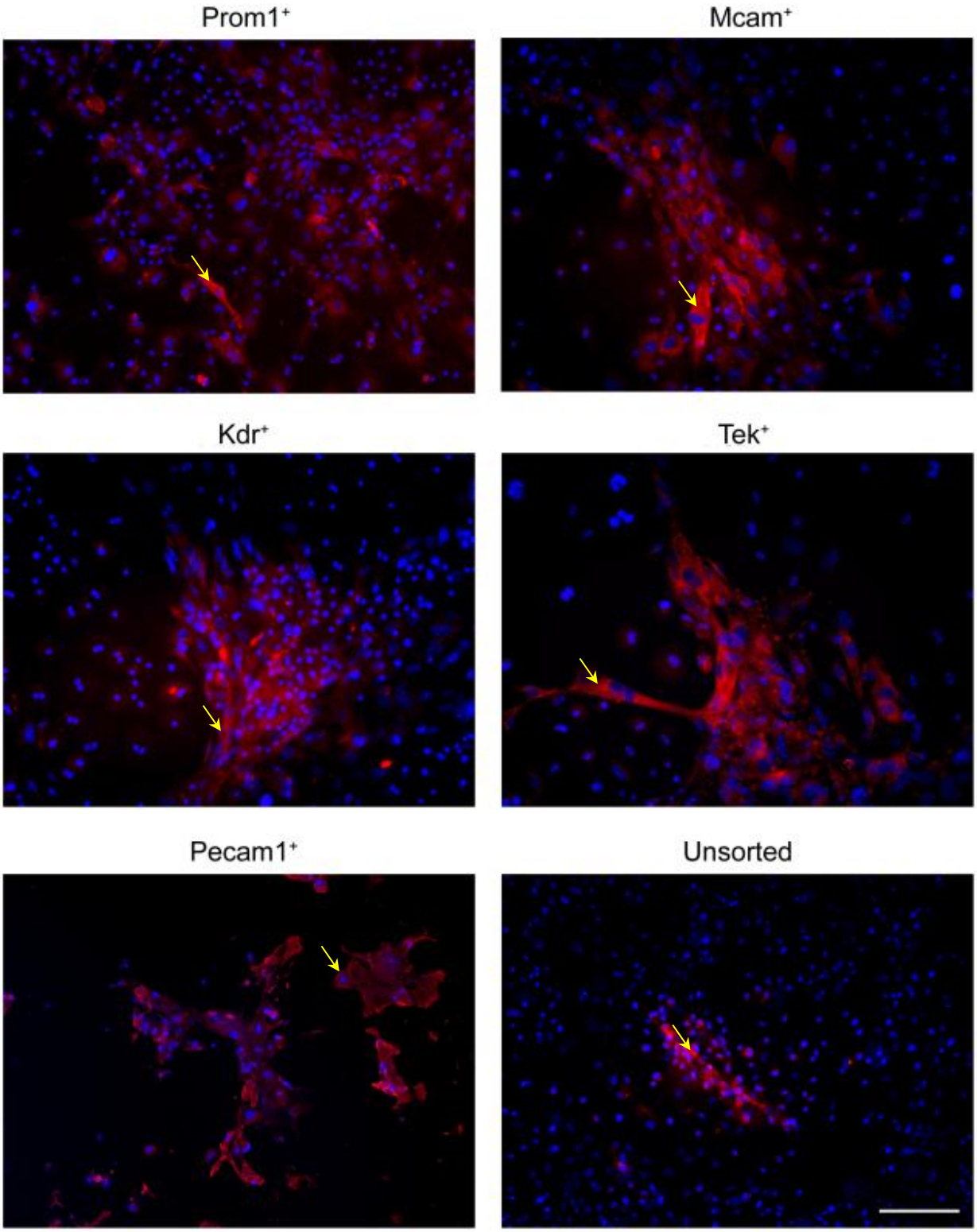

.Figure 4.8. Immunoreactivity of cultured cells for vWF antibody, vWF (red) and nuclei (blue). Localisation of vWF in the cytoplasm is marked with arrows. Scale bar = 100 µm.

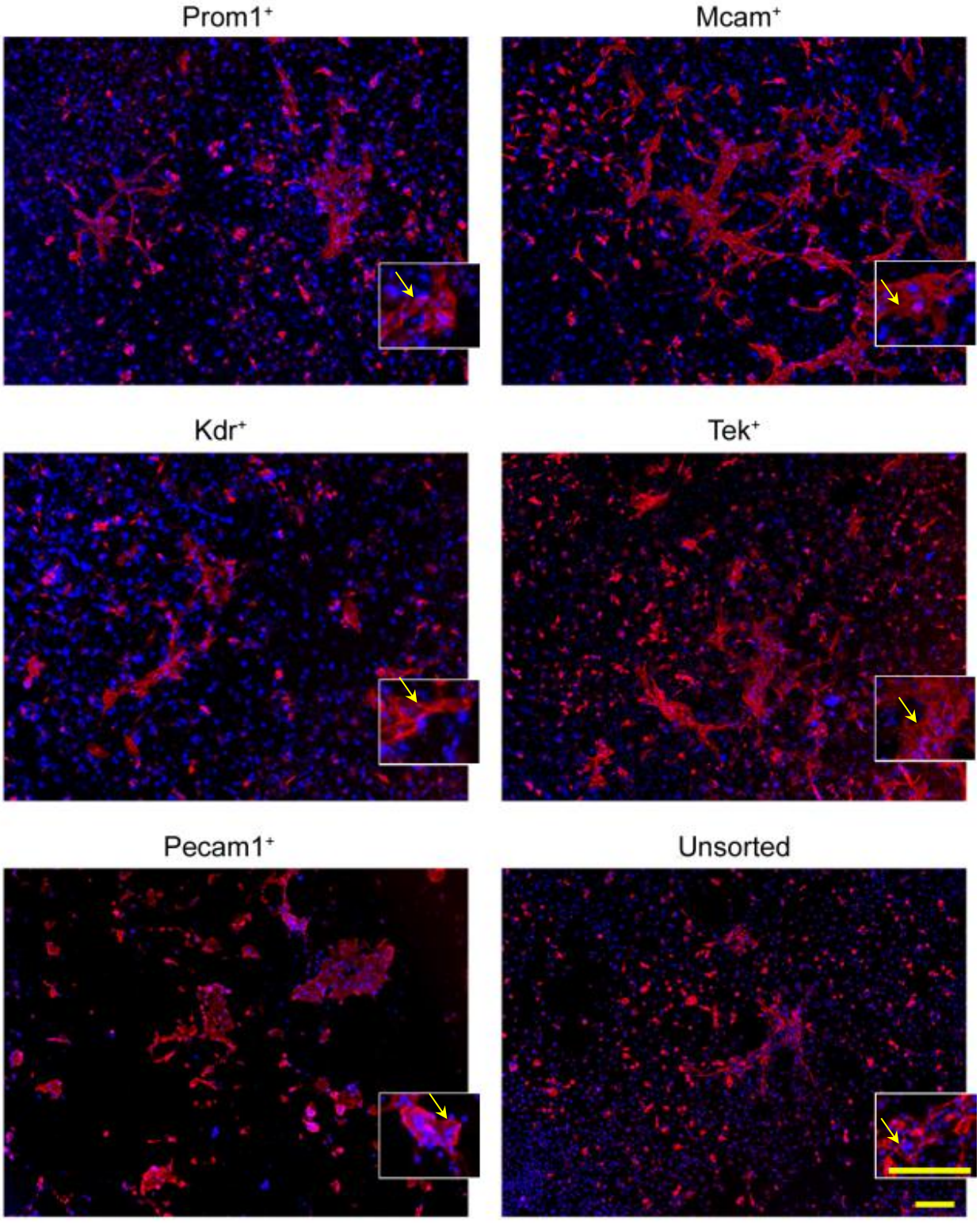

Figure 4.9. Immunoreactivity of cultured cells for Pecam1 antibody, Pecam1 (red) and nuclei (blue). Inserted: localisation of Pecam1 in the plasma membranes is marked with arrows. Scale bar = 100 µm.

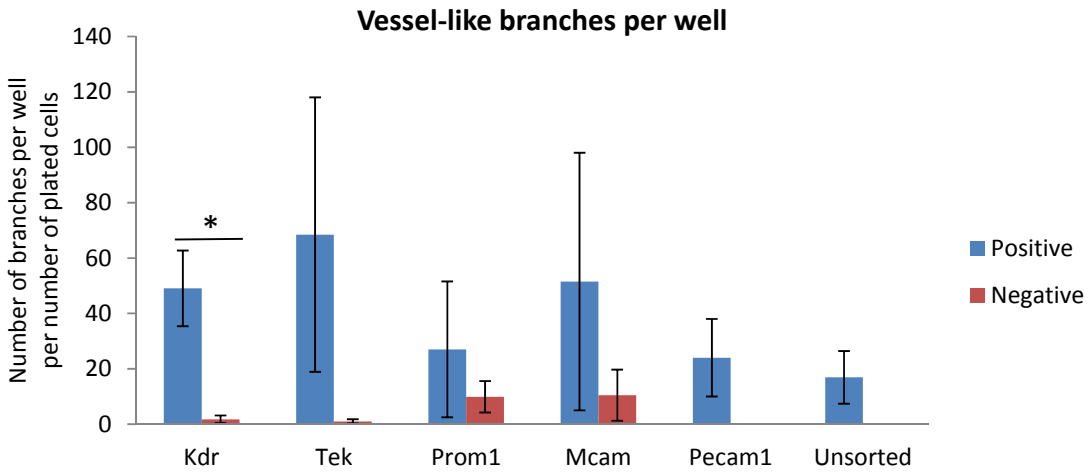

Figure 4.10. Quantification of vessel-like structure formation based on the number of branches immunoreactive to Pecam1 antibody per well for selected fractions of freshly-isolated bone marrow. All observed statistical difference is marked with an asterisk (between Kdr^+ and Kdr^-), $P<0.05$. Error bars represent SEM, n=3.

4.3.6. Vessel-like structure formation and endothelial marker immunoreactivity *in vitro* in $EphA3^+$ cells

$EphA3^+$ cells from passages 8 and 12 did not form vessel-like structures spontaneously in growth or in control medium *in vitro* over the whole seven day passage period (Fig. 4.11). $EphA3^+$ cells from passage 8 formed vessel-like branches when cultured in EDCM for 6-7 days, however, and these structures retained vessel morphology during seven day culture period. Most cells (more than 90%) were involved in vessel-like structure formation (data not shown). Thawed $EphA3^+$ cells from passage 12 formed vessel-like branches when cultured in EDCM for 2-3 days, and these structures retained vessel-like morphology during seven day culture period. Most cells (100%) were involved in structure formation (data not shown). Neither of these branches displayed high immunoreactivity to Pecam1, however, some immunoreactivity was present (Fig. 4.12). $EphA3^+$ cells from later passages (13-15) formed vessel-like structures spontaneously in growth (Fig. 4.13) and control media (data not shown). These cells also showed reduced rates of division, not reaching confluency by passage 14, and also showed an increasing tendency to detach and float (data not shown). These cells further appeared to have undergone senescence

by passage 15 (data not shown). When EDCM was applied at passage 13, these cells have formed rounded clump-like structures after 1-2 days (Fig. 4.13).

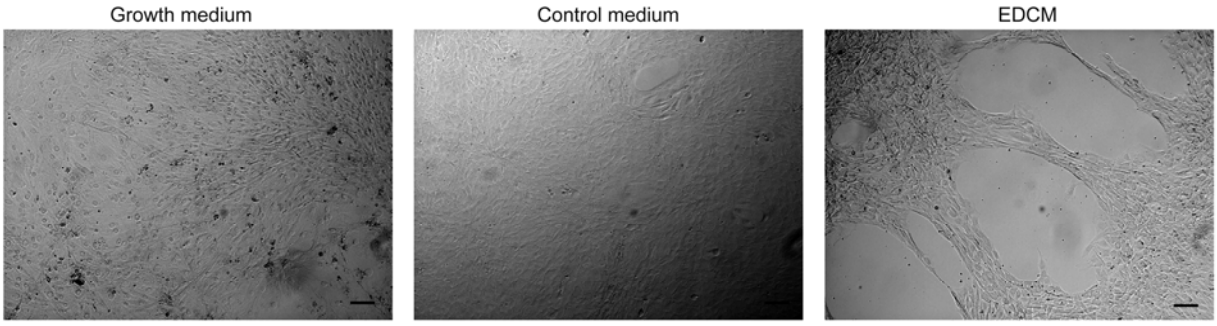

Figure 4.11. Representative morphology of EphA3^{+} cells at passage 8 before (growth medium) and after (control medium and EDCM) they were subjected to differentiation. Due to similarities in morphology passage 12 is not presented. Scale bar = 100 μm.

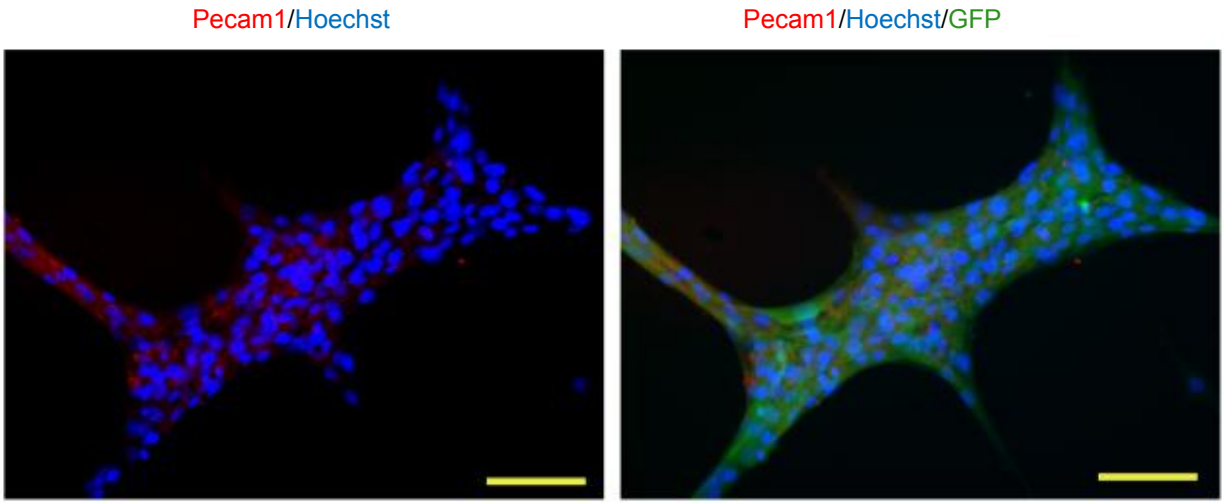

Figure 4.12. Immunoreactivity of cultured EphA3^{+} cells to Pecam1 (red) and nuclear reactivity with Hoechst (blue), GFP (green) x20 magnification. Scale bar = 100 μm.

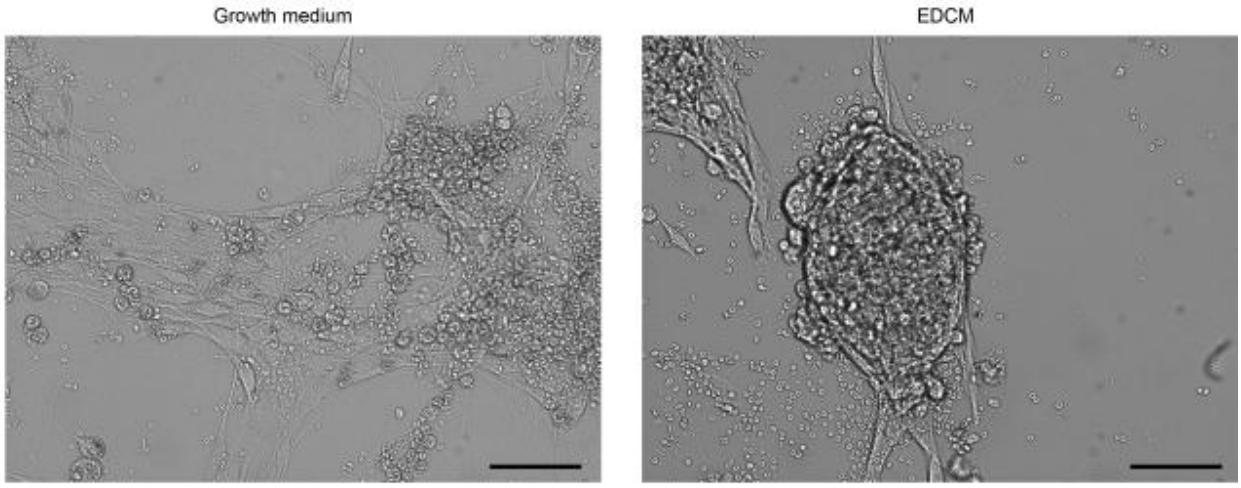

Figure 4.13. Morphology of EphA3$^+$ cells at passage 15 before (growth medium) and after (EDCM) they were subjected to differentiation. Scale bar = 100 µm.

4.3.7. Kdr$^+$ and EphA3$^+$ fraction and unsorted plate-adherent cells FACS GFP analysis

As discussed above, Kdr represents the only BM EPC marker chosen that prospectively delineates the efficiency of a specific EPC BM subpopulation to form Pecam1$^+$ vessel-like structures *in vitro*. Kdr$^+$ cells therefore were chosen for further characterisation. EphA3$^+$ cells were similarly chosen for further analysis due to their ability to form vessel-like structures *in vitro* and to their suggested ability to support blood vessel formation associated with cancer (General Introduction, Section 1.3.1.4). Plate-adherent cells (unsorted) were used as a control based on previous studies (Silva, Litovsky et al. 2005; Aslam, Baveja et al. 2009; van Haaften, Byrne et al. 2009).

According to FACS analysis, the Kdr$^+$ fraction represented 2.42% of all cells isolated from the bone marrow of which 86.8% were GFP$^+$ (data not shown). The total number of GFP$^+$ cells in the fraction enriched magnetically for Kdr was 29.9% (data not shown). With respect to EphA3$^+$ cell culture, according to FACS analysis, the EphA3$^+$ fraction represented 86.31% of all passage 8 BM cells (>95% GFP double positive), 58.9% of all passage 12 BM cells (82.3% GFP double positive) and 30.0% of all passage 13 -15 BM

cells (<50% GFP double positive). Unsorted plate-adherent cells displayed 85.9% of GFP^+ cells after one passage in culture. As such, it was determined, that all these fractions contained GFP^+ cells and could be reliably used for injection *in vivo* in subsequent studies of these cell subpopulations, although the EphA3 studies suggested that fluorescence activity may diminish with time, at least in culture.

4.3.8. Analysis of GFP fluorescence in vessel-like branches from Kdr^+ and $EphA3^+$ fractions and unsorted plate-adherent cell cultures.

As described above, *in vitro* endothelial induction of the Kdr^+ fraction resulted in the appearance of obvious vessel-like branch structures after 14 days that were immunoreactive to Pecam1 antibody (Fig. 4.14). The GFP signal intensity of the cells in culture was variable. Endothelial induction of the $EphA3^+$ fraction similarly resulted in the appearance of $Pecam1^+$ vessel-like structures after 2-7 days, yet GFP fluorescence in these cultures was more uniform (Fig. 4.12). Endothelial induction of plate-adherent cells resulted in fewer and less defined vessel-like structures, observable after 14 days of culture, with more limited Pecam1 immunoreactivity and GFP fluorescence (Fig. 4.15). As such, cell populations retain GFP fluorescence to some extent during vessel-like structure formation, but for future *in vivo* injection studies, it is noted that such fluorescence may diminish with time and differentiation status.

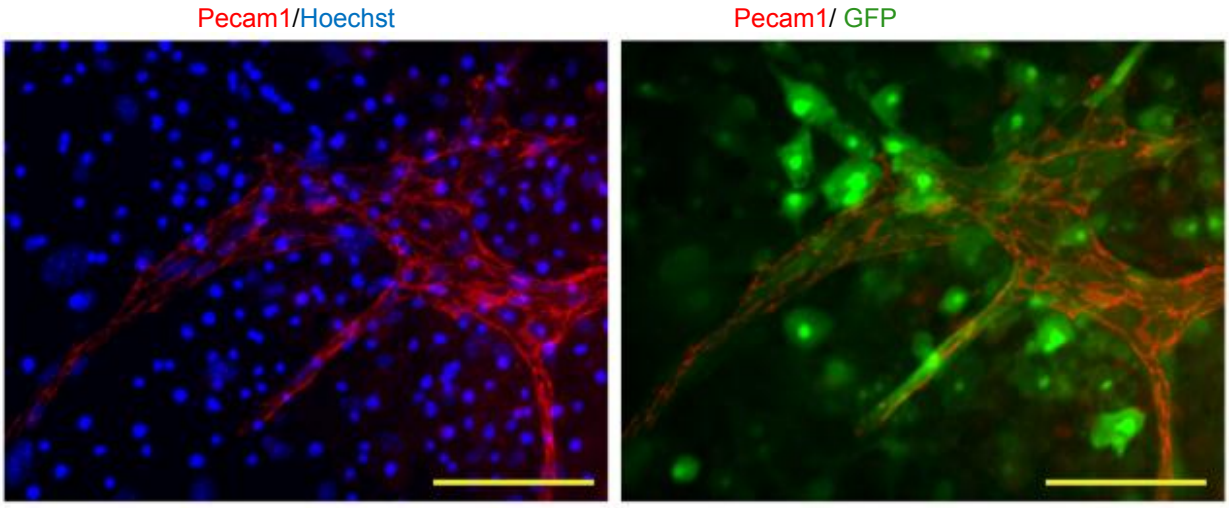

Fig. 4.14. Presence of GFP (green) in vessel-like structures formed from Kdr^+ cells (immunoreactivity to Pecam1 antibody, red) counterstained with Hoechst (blue). Scale bar = 100 µm.

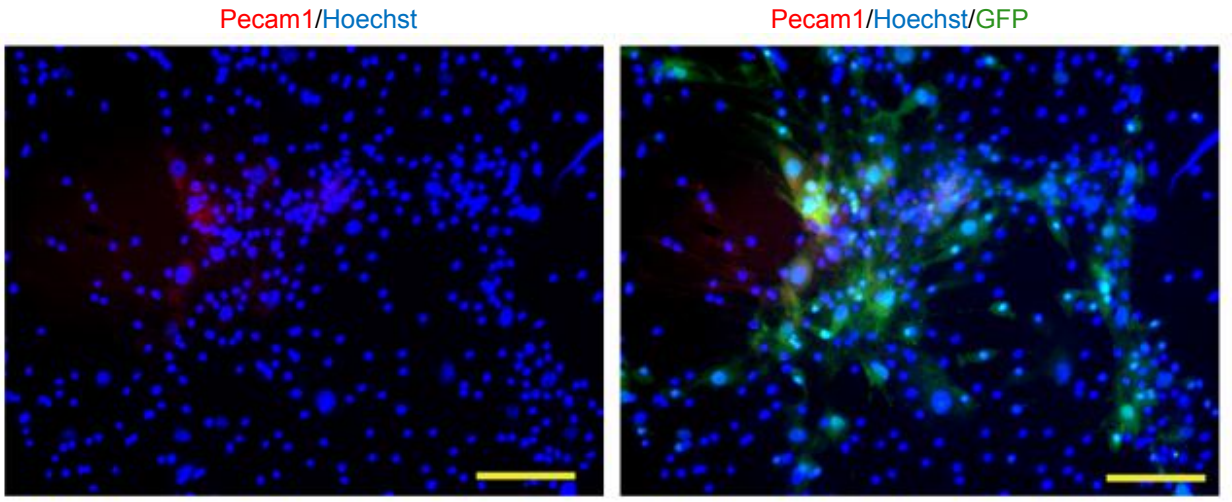

Figure 4.15. Immunoreactivity of unsorted plate-adherent cells to Pecam1 antibody (red) and nuclear reactivity with Hoechst (blue), GFP (green) x20 magnification. Scale bar = 100 μm.

4.3.9. FACS analysis for Kdr in Kdr-enriched cells (by MACS), PACs and P12 EphA3$^+$ cells

Cell fractions were analysed for the presence of Kdr by FACS before differentiation in order to determine its percentage contribution to each group. MACS enrichment for Kdr did not provide a 100% Kdr$^+$ cell population. The freshly-isolated and sorted for Kdr by MACS, cells were 31.36% Kdr$^+$ (Fig. 4.16). Unsorted plate-adherent cells from passage 0 were on average 15.08% Kdr$^+$ (Fig. 4.16). Thawed and plated EphA3+ cells from passage 12 were 16.03% Kdr$^+$ (Fig. 4.16).

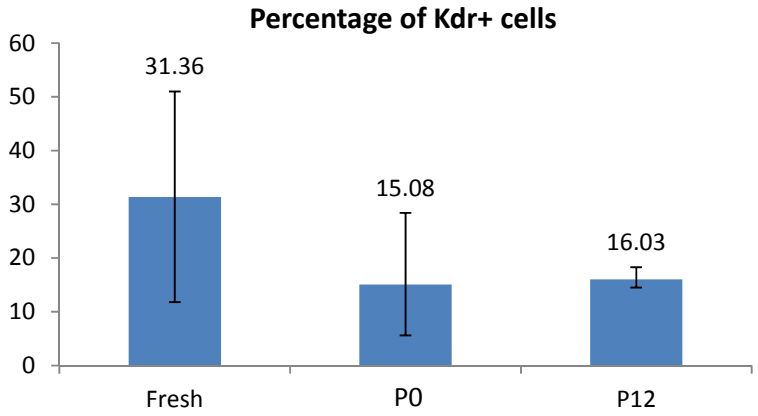

Figure 4.16. Chart indicating average percentage of Kdr$^+$ cells in the EPC fractions of uncultured cells magnetically enriched for Kdr (Fresh), unsorted plate-adherent cells (P0) and unsorted EphA3$^+$ cells (P12). Error bars are descriptive and represent SD, n=3.

4.4. Discussion

4.4.1. Characterisation of fractions

The $Cd34^+$ fraction did not survive in culture after it was isolated by FACS. In the pilot study after MACS enrichment, the $Cd34^+$ fraction was less efficient in vessel-like structure formation, than the $Cd34^-$ fraction. Cd34 was therefore considered an unsuitable EPC marker for the current experiment, as further cell selection was based primarily on vessel-like structure formation *in vitro*. However, recent studies have demonstrated that the $Cd34^+$ cell fraction from peripheral blood contributes to pulmonary angiogenesis and lung regeneration after pneumonectomy *in vivo* (Chamoto, Gibney et al. 2012). This cell fraction could be therefore further investigated in other models, as Cd34 could be a promising endothelial progenitor marker with regenerative potential.

Variation between the numbers of positive cells for each marker confirms that none of the markers used are expressed exclusively in endothelial progenitor cells. Kdr^+ fraction accounted for 2.42% of bone marrow cells was 79.4% $Ptprc^+$ and only 37% $Pecam1^+$, indicating that a significant number of these cells may be HSCs. However, other EPC markers are present in more than a half of Kdr^+ cells, indicating the sufficient general number of EPCs in this fraction. Tek^+ fraction was 91% $Ptprc^+$ and 35% $Pecam1^+$, which also indicates a large number of HSCs in this fraction. Eighty percent of these cells were $Mcam^+$, however less than 25% were Kdr^+ and $Prom1^+$. This could indicate that this fraction is a mixture of EPCs ($Kdr^+/Prom1^+/Mcam^+/Tek^+$), HSCs and lymphocytes ($Tek^+/Ptprc^+/Mcam^-$). $Prom1^+$ fraction contained 87% $Ptprc^+$ cells, but only 6.2% $Pecam1^+$ cells. More than 50% of cells in this fraction were positive for other EPC markers, indicating that this fraction has a high potential in differentiation into endothelial lineage, however, high number of $Ptprc^+$ cells also suggests that up to 81.7% of these cells could be non-endothelial. The $Mcam^+$ fraction contained the lowest number of $Ptprc^+$ cells (49.5%), and also the lowest number of $Pecam1^+$ cells (4.1%). It can be concluded, that this fraction therefore has the highest percentage of MSCs, and the lowest percentage of HSCs. It also had the highest percentage of Kdr^+ cells (71%), but the lowest percentage of $Prom1^+$ cells (7.3%), indicating a higher potential to react to VEGF.

Long-term (12 passages) cultured frozen and thawed EphA3$^+$ cells displayed high immunoreactivity to EPC markers Tek (98.5%) and Mcam (92.7%), but low immunoreactivity to Kdr (16.0%) and Prom1 (28.1%). They were also only 2.3% Pecam1$^+$ and 47.7% Ptprc$^+$. This indicates that some of these cells may be EPCs, MSCs or both. The immunoreactivity of these cells can be called consistent with their characterisation as an EPC subclass.

Unsorted plate-adherent cells at passage 0 displayed high immunoreactivity to Ptprc (91.03%), Tek (31.33%), Kdr (22.23%) and Prom1 (22.93%). In further measurements, however, the number of Kdr$^+$ cells was 15.08% (Fig. 4.16), which indicates slight mouse-to-mouse variations. Mcam$^+$ cells represented 11.07% and Pecam1$^+$ cells represented 1.93% of the population respectively. These measurements suggest that there are MSCs and EPCs present in this fraction; and possibly a relatively high number of HSCs, despite of the plate-adherent qualities. The plate-adherence method used in this study is known to increase the number of EPCs and MSCs, compared to unsorted and uncultured bone marrow (Fig. 4.3). This population of cells therefore has potential to serve as a control for *in vivo* experiments.

In conclusion, all fractions examined contained a certain number of HSCs (which are not plate-adherent, and would have been washed out after a few media changes). Some fractions are likely to contain MSCs, which could be supportive of vascular differentiation and growth. Most fractions contain other endothelial markers, indicating the likely presence of true EPCs.

4.4.2. Comparison of sorting of the freshly-isolated cells by FACS and MACS for further cell culture

To our knowledge, poor plate-adherence and survival in culture after FACS separation of EPC fractions has not been reported previously. Our observations may, however, be explained by the high speed of cell flow usually used in FACS machine and exposure to ultraviolet, which damages cell membranes and potentially other organelles. This

observation may go unnoticed in larger cell populations (i.e. more than $1x10^6$ cells compared to less than $1\text{-}2x10^5$ cells obtained in this study). Magnetic sorting is a less time consuming procedure where the whole cell suspension is separated at once, compared to FACS that separates one single cell at a time. Therefore, if a minimal number of cells is essential for survival due to a requirement for threshold levels of secreted growth factor concentrations or cell-cell contact, it may be expected that cell survival would be higher after MACS. Further, the percentage of specific marker cell populations isolated by FACS and MACS varied (Fig. 4.3, Fig. 4.6). As such, separation reflects 'enrichment', rather than 'sorting'. Because cell survival *in vitro* after MACS was greater than after FACS, MACS was used for further experiments.

4.4.3. Vessel-like structure formation

Individual Kdr^+, Kdr^-, Tek^+, Tek^-, $Prom1^+$, $Prom1^-$, $Mcam^+$ and $Mcam^-$ cell populations were plated down separately in order to analyse how efficient is each of these markers, delineating populations of BM cells that have vascularisation potential. $Pecam1^+$ (endothelial cells) and unsorted fractions were used as positive (endothelial) and negative (non-enriched, general cell behaviour) controls. Most of plated fractions formed relatively similar numbers of vessel-like branches when cultured in the presence of VEGF and FGF2, except for Kdr^- and Tek^- fractions, which formed less branches compared to some other fractions. This result indicates that most fractions contained a sufficient number of EPCs (even without enrichment) to form a number of vessel-like branches, however, some fractions were missing an essential marker for vascular structure formation. The only statistically significant difference between positive and negative fraction of the same marker was observed in Kdr-sorted fractions. Therefore, Kdr could be an essential receptor for vessel formation to proceed. Consistent with this is that Kdr is a VEGF receptor, and VEGF was one factor used in experiments here to induce EPC differentiation, as such promoting vessel-like structure formation mainly in Kdr^+ cells. Tek is known to be an essential molecule for angiogenesis, however, it is not essential for vasculogenesis (Sato, Qin et al. 1993; Dumont, Gradwohl et al. 1994).

EphA3$^+$ cells displayed a high capacity to form vessel-like structures in response to VEGF at all tested passage numbers, but at different rates dependent on passage number. It took 6-7 days to form vessel-like structures after passage 8, 2-3 days after passage 12, and after passage 14 these structures were formed spontaneously after 1-2 days. The passage 12 EphA3$^+$ cell fraction displayed immunoreactivity to Kdr essential for vessel-like structure formation (16.0%) as shown in Figure 4.5. However, the vessel-like structures formed after passage 8 and 12, displayed low immunoreactivity to Pecam1, compared to freshly-isolated cells differentiated for 14 days. This indicates that these structures either did not have enough time in the presence of VEGF to produce Pecam1 at levels sufficient for detection, or they are not blood vessel structures, but another type of vessels. Alternatively, these structures may be composed of cells associated with blood vessels, but not of endothelial origin (i.e. mural cells). In any case, these cells may still be relevant for lung repair, as they grow rapidly, associate with vessel formation and react to VEGF.

Unsorted cells from passage 0 demonstrated a relatively low capacity to form vessel-like structures after 14 days of differentiation, and these structures also displayed low immunoreactivity to Pecam1 antibodies. As this cell fraction was not enriched for any endothelial markers, it was expected to have a lower capacity to form vessel-like structures, compared to enriched fractions. According to previous reports, however, such cells possess the potential to produce vessel-supportive and vessel-associated cells *in vivo* and therefore represent a relevant control cell type here.

4.4.4. Analysis of GFP fluorescence in Kdr$^+$, P12 EphA3$^+$ cells at P12 and unsorted P0 plate-adherent cells.

The GFP signal in differentiated Kdr$^+$ cells was observed in most vessel-like structure derivatives, although at variable brightness. Therefore, if injected into animals to study therapeutic value *in vivo*, these cells might still be tracked in the organism in the case of differentiation and engraftment. EphA3$^+$ and unsorted plate-adherent cells retained GFP in vessel-like structures; however, these structures displayed low immunoreactivity to

Pecam1. These cells if behaving the same way *in vivo*, therefore, may easily be identified. Because GFP signal intensity appears to be affected by time and differentiation status, therefore, any subsequent *in vivo* study testing therapeutic value of these cells ought to involve the use of male cells injected into female mice such that the presence of the Y chromosome may be used to detect the injected cells.

4.4.5. Analysis of presence of Kdr in uncultured Kdr$^+$ cells, EphA3$^+$ cells at P12 and unsorted plate-adherent cells at P0.

Kdr was present in all three populations of tested cells. It was present at various rates in Kdr-enriched cells (31.36% on average), which was expected, and at similar rates in EphA3-enriched cells at P12 (16.03%) and in plate-adherent cells at P0 (15.08%). This makes these fractions more comparable in the *in vivo* studies. These populations have comparable levels Kdr, and therefore its role in endothelial cell differentiation and its functions in lung development in neonatal mice would not influence further *in vivo* treatment results (Ahlbrecht, Schmitz et al. 2008).

4.5. Conclusion

In conclusion, prospectively isolated Kdr$^+$, Tek$^+$, Prom1$^+$ and Mcam$^+$ BM populations all represent potential EPC populations as all are capable to some extent of forming Pecam1$^+$ vessel-like structures *in vitro*. Further, all of these subpopulations display an overlapping phenotype with respect to (i) individual Kdr, Tek, Prom1 and Mcam immunoreactivity, although to apparent different extents, and (ii) Pecam1 immunoreactivity following culture. The Kdr$^+$ subpopulation, however, was the only population that specifically delineated vessel-like structure forming efficiency from the remainder of cells contained within the BM population. It was also concluded, that Kdr is a characteristic molecule of EPC phenotype, and is essential for vascularisation, as negative fraction for this marker formed very few, if any, vessel-like structures. EphA3$^+$

cells similarly displayed immunorectivity to Kdr, Tek, Prom1 and Mcam, consistent with their classification as a potential EPC containing population. Further, and like Kdr^+ cells, cultured $EphA3^+$ cells formed $Pecam1^+$ vessel like structures *in vitro*; however, efficiency was dependent on passage number or time in culture. Higher passage number corresponded to a shorter time to vessel-like structure appearance in culture. Unsorted plate-adherent cells were also characterised in a similar manner and showed a relatively limited ability to form vessel-like structures *in vitro* and to display Pecam1 immunoreactivity. GFP analyses considering all fractions demonstrated that time and differentiation status of the cells affects GFP intensity, at least in culture. As such, if using these cell populations for *in vivo* tracking purposes, care must be taken to avoid false negative detection.

Chapter 5. Injection of progenitor cells from bone marrow into neonatal mice after hyperoxia

5.1. Introduction

Hyperoxia-associated lung-deficit has been widely studied as a common cause of bronchopulmonary dysplasia (BPD) in prematurely born children. In Chapter 3 'Characterisation of a mouse model of hyperoxia and associated long-term respiratory deficit' a mouse model of hyperoxia lung damage was described. Briefly, septation of the hyperoxia-treated lung (i.e. number of alveoli) was significantly reduced compared to the normoxia lung from postnatal day 5 (D5) to postnatal day 56 (D56), and this reduction was accompanied by alveolar enlargement. The number of secondary septa per tissue area was observed to be significantly reduced D5 *postpartum*, but increased by D28 compared to controls and returned to normal control levels by D56. Analysis of parameters of vascularisation indicated that a reduction in the mature blood vessel number, as assessed by elastin staining, and a reduction in the amount of Pecam1, assessed by western blotting, occurred after hyperoxia, yet returned to normal levels by D56. These results indicate that hyperoxia affects both alveolarisation and vascularisation of the neonatal mouse lung. A number of treatments have been previously tested in a number of studies to reduce alveolarisation deficits after hyperoxia, however, they still require optimisation for clinical use, and the specific mechanism of lung repair remains unknown.

It has been hypothesised that some cell types could be applied after hyperoxia for the treatment of the associated deficit with little side effects (van Haaften, Byrne et al. 2009; Balasubramaniam, Ryan et al. 2010). However, long-term culture ought to be avoided in order to reduce the risk of inducing chromosomal mutations within the applied cells and hence reducing the possibility that these cells may lead to neoplasia (Ahrlund-Richter, De Luca et al. 2009).. Freshly-isolated MSCs and/or EPCs may improve vascular structure depending on the type of injury (Asahara, Masuda et al. 1999; Silva, Litovsky et al. 2005).

MSCs have been reported to carry regenerative potential to the lung, by contributing to fibrocytes and supporting mesenchyme, by paracrine activity, and by promoting alveolarisation via mesenchyme-epithelial interactions (Ortiz, Gambelli et al. 2003; Ishizawa, Kubo et al. 2004; Rojas, Xu et al. 2005; Aslam, Baveja et al. 2009). Compared to MSCs, EPC engraftment in lung tissue after injury has not been as popular an area of research, although recent reports have suggested that some types of cultured EPCs may afford some regenerative potential in the lung (Kahler, Wechselberger et al. 2007; Balasubramaniam, Ryan et al. 2010).

The most common and robust technique for isolating MSCs is from bone marrow, by passaging cells on plastic culture dishes and collecting plate-adherent cells (Kotton, Ma et al. 2001). Another common method is by negative selection for $Ptprc^{+}$ (hematopoietic) cells (Ortiz, Gambelli et al. 2003; Anjos-Afonso, Siapati et al. 2004), with plate-adherence being still an essential step. A recent study investigated the injection of MSCs into a mouse lung hyperoxia model and reported the promotion of bronchoalveolar stem cell growth and lung repair (Tropea, Leder et al. 2012).

There is no single technique for isolating EPCs. They can be obtained from bone marrow, umbilical cord blood and major blood vessels. There are a number of characterised EPC markers. In our previous studies (Chapter 4: 'Characterisation of mouse bone marrow endothelial progenitor cells') we have discovered that Kdr delineates vessel-like growth characteristics of BM cells in our culture conditions. Another marker of potential relevance to the repair of hyperoxia-treated lung deficit is EphA3, as $EphA3^{+}$ cells are suggested to be associated with *in vivo* blood vessel formation (Vail, Tan et al., 2012). However, EphA3 is not widely expressed in bone marrow progenitor cells (<1%, Chapter 4, Section 4.3.3), and as such, an *in vitro* technique for their enrichment has been created to facilitate their characterisation (General Materials and Methods, Section 2.12).

Therefore, BM-derived Kdr^{+} and cultured $EphA3^{+}$ cells were investigated here to determine their potential to alter morphometric parameters of neonatal lung affected by hyperoxia (defined in Chapter 3). Unsorted plate-adherent cells (PACs) at P0 were

included in this study as a therapeutic positive control based on previous reports (Ortiz, Gambelli et al. 2003; Ishizawa, Kubo et al. 2004; Rojas, Xu et al. 2005; Aslam, Baveja et al. 2009).

5.2. Materials and methods

5.2.1. Experimental design

Pregnant females were separated into two groups. Mice in the first group were placed in 90% oxygen conditions the night before giving birth, while those in the second were left at room air. Hyperoxia experiment was performed as described in General Materials and Methods, Section 2.1. After four days in oxygen, mice were allowed to recover in room air, and tissues were collected from seven pups in both hyperoxia and normoxia groups (from four pups for morphometric analysis and from three pups for protein analysis). Cell isolation was performed in advance to further inject the hyperoxia-treated and normoxia mice. Bone marrow was isolated from a male GFP+/- mouse as described in General Materials and Methods, Sections 2.8, 2.12 and 2.13. Hyperoxia-treated pups were separated into four groups to be injected with either PBS (no cells), Kdr-enriched cells (uncultured), plate-adherent cells (passage 0, or P0), or EphA3-enriched cells (passages 8, 12, and 13-15) (General Materials and Methods, Section 2.15). EphA3-enriched cells were first injected to collect preliminary data for a pilot study. Frozen cells were then used at P12 for a further and more comprehensive study. Normoxic mice were also separated into four groups and also injected in the same manner (Fig. 5.1). Mice were weighed and measured (crown to rump length) once a week starting from week 1 (day 7 *postpartum*). Lungs were pressure-fixed, as described in General Materials and Methods, Section 2.2, or snap-frozen for protein analysis. After pressure-fixing, but before paraffin-embedding, lungs were weighed (with solution inside) and lung volume was measured by water displacement (by placing lungs in a tube with water) at day 28 and day 56 *postpartum*. Following 5 µm serial sectioning, as described in General Materials and Methods, Section 2.2, two tissue sections (50-55th and 95-100th) from each mouse were collected on one slide for staining. Only two stains (Mayer's hematoxyllin-eosin and Weighert's elastin

stains) were used on lung tissue for morphometric analysis (General Materials and Methods, Sections 2.2 and 2.3).

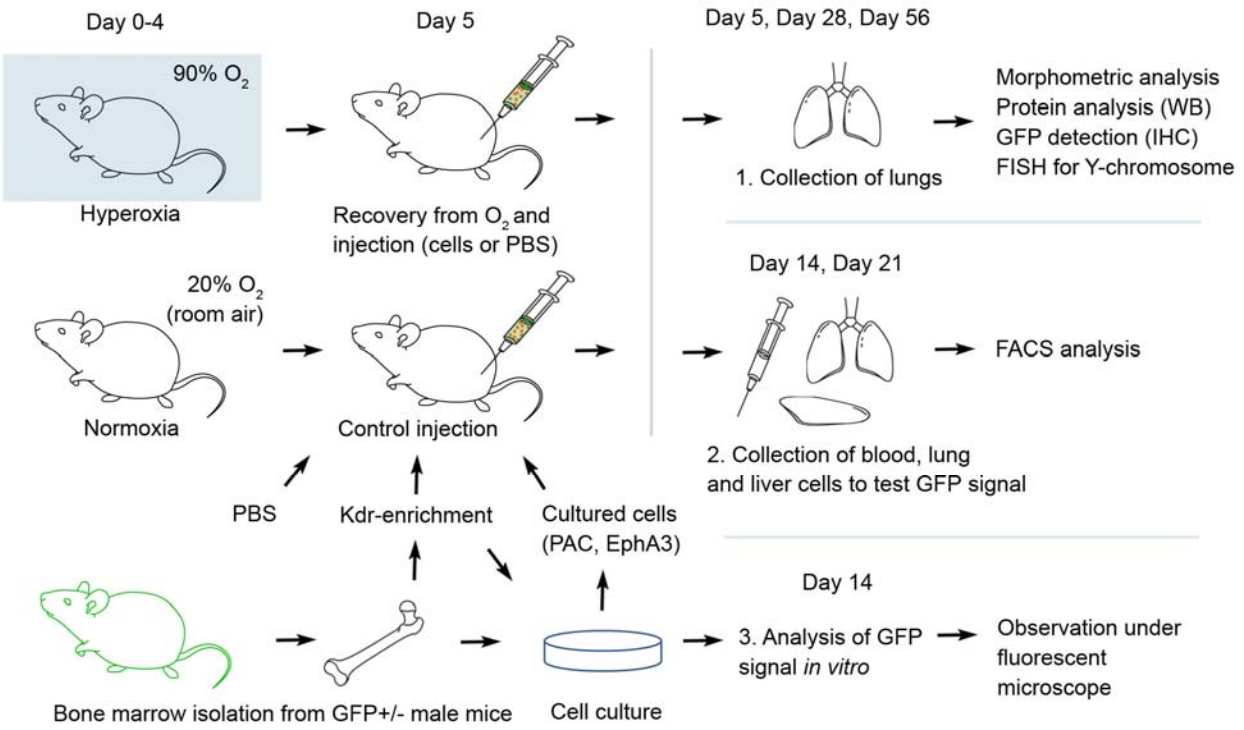

Figure 5.1. Experimental design for cell injection and analysis after hyperoxia. PBS – phosphate buffer saline, Kdr-enrichment – Kdr-enriched cell fraction from bone marrow without culture, PAC – plate-adherent cells at P0, EphA3 – EphA3-enriched plate-adherent cells at P8, P12 (thawed) or P13-15, WB – western blotting, GFP – green fluorescent protein, IHC – immunohistochemistry, FISH – fluorescent *in situ* hybridisation.

All morphometric measurements were performed according to methods used in Chapter 3. Lungs were analysed for alveolar size (400 measurements per mouse), alveoli number per 3.63 mm (five measurements per mouse), lung tissue area per image of the lung section of 0.564 mm^2 (five measurements per mouse), the number of secondary septa per square millimetre of lung tissue (five measurements per mouse) and the number of blood vessels per lung section area image of 0.564 mm^2 area (five measurements per mouse). Western blotting was used to assess the Pecam1, Vegfa and Sftpc protein levels as described in General Materials and Methods, Section 2.5. Blood, lung and liver were collected for FACS analysis as described in General Materials and Methods (Section 2.16), and analysed for the presence GFP by FACS (General Materials and Methods,

Section 2.14). One hundred thousand of each injected cell type: Kdr-enriched cells (uncultured), plate-adherent cells (P1) and EphA3-enriched cells (P12), was plated in culture on the injection day in Control medium (described in General Materials and Methods, Section 2.12) for 14 days, to assess GFP fluorescence. Immunohistochemistry for GFP on lung sections frozen at day 28 was performed as described in General Materials and Methods, Section 2.4, using Tyramide signal enhancement. Paraffin lung sections from female mice injected with male cells were further tested for the presence of the Y chromosome using fluorescent *in situ* hybridisation (FISH) as described in General Materials and Methods, Section 2.17.

5.2.2. Statistical analysis

For morphometric analysis, a univariate general linear model was applied for analysis of variance, where “group” (a group of mice with the same oxygen treatment and cell injection) was allocated to be the main factor, and “animal” (values from a single mouse) and “litter” (values from mice within one litter) were allocated to be the random factors (five measurements per animal were taken, two to four animals per litter were analysed at each time point). It was followed by a Dunnett’s posthoc test, which was used to determine significant differences between morphometric characteristics of all treated lungs relative to control (Normoxia PBS) lungs at different stages. A Student Newman-Keuls posthoc test was also used to determine significant differences between all other groups. Error bars indicate standard error (SEM), calculated from average values per mouse, without taking into account variations within each animal.

An ANOVA test followed by Dunnett’s and Student Newman-Keuls posthoc was performed to determine significant differences between protein levels in the lungs, mouse body weight and length, lung weight and lung volume in relation to control (Normoxia PBS) group, and between all other groups, respectively. All posthoc tests were performed using the SPSS statistical package. Data charts were drawn in Microsoft Excel. Error bars indicate standard error (SEM), calculated from average values per mouse, without taking into account variations within each animal.

5.3. Results

5.3.1. Pilot experiment for EphA3$^+$ cell injection

EphA3 cells were injected at passage 8 (P8, 56 days in culture) and passage 13-15 (P13-15, 91-113 days in culture), without freezing, into hyperoxia-treated and normoxia mice. PBS was injected as a control. There were four to five mice in each group (both males and females). Mice were observed for the first 4-5 weeks of age. There were no significant changes observed in mouse weight and length, when P8 cells were injected.

After injection of P13-15 cells, male mouse weight was significantly reduced (compared to the control, Normoxia PBS group) in normoxia mice at one week of age and in hyperoxia-treated mice at four weeks (Fig. 5.2). Female mouse weight was significantly reduced at one week in both normoxia and hyperoxia-treated groups, and at four weeks in the normoxia group (compared to Normoxia PBS group). Mouse length was significantly reduced in hyperoxia-treated males and females at three and four weeks *postpartum* after P13-15 cells were injected, as well as at one week *postpartum* in females, compared to Normoxia PBS. Normoxia female mice injected with P13-15 cells also had reduced length at four weeks compared to Normoxia PBS (Fig. 5.2).

At three weeks of age mice injected with P13-15 cells started to display signs of pain and distress (slower movements), and developed small red spots at the site of injection above the right hip. PBS-injected mice did not have any spots at the injection site. By four weeks of age, mice injected with P13-15 cells developed red lumps (~15 mm in diameter) at the site of injection. Most mice were culled to avoid further distress by five weeks of age. Mice injected with P8 cells did not demonstrate any signs of pain, and moved normally around the cage. Like in the PBS-injected group, no lumps or redness were ever observed at the site of injection in the P8 EphA3$^+$ cell injected mice.

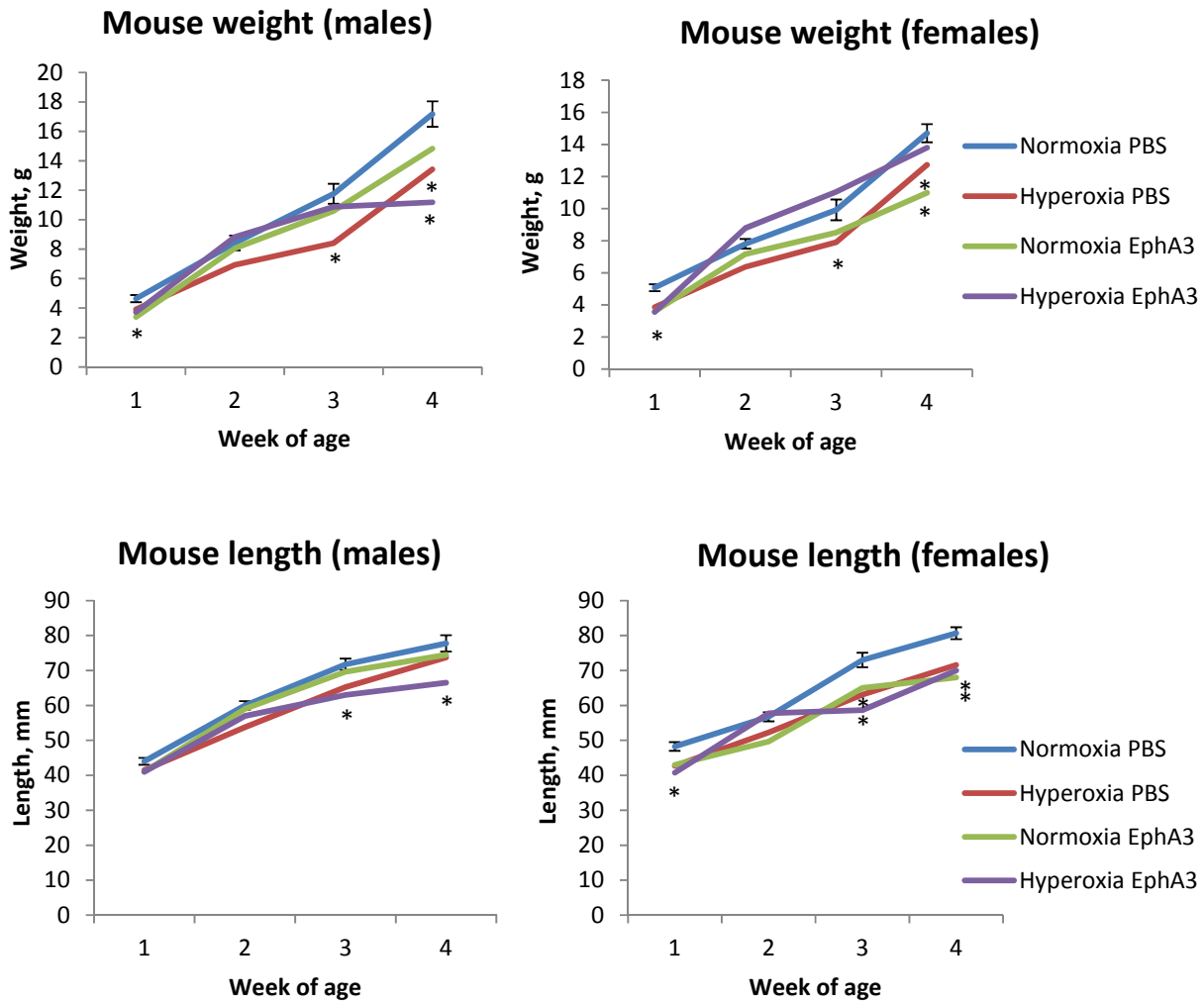

Figure 5.2. Mouse weight and length after P13-15 EphA3 cell injection compared to Normoxia PBS. Hyperoxia PBS data are presented in the charts for comparison. Average SEM is demonstrated as error bars in control (Normoxia PBS) group. Asterisks indicate significant difference compared to the Normoxia PBS control group ($P<0.05$; n=2-4).

Lung samples from mice injected with P8 cells and PBS, respectively, at four weeks of age (D28 *postpartum*) were pressure-fixed and embedded in paraffin for morphometric analysis. Lung samples from mice, injected with P13-15 cells were also fixed, together with the lumps from the site of injection, embedded in paraffin and analysed for pathological conditions.

Alveolar size in the lungs of both normoxia and hyperoxia-treated mice injected with P8 cells and hyperoxia-treated mice injected with PBS was significantly increased, compared to control (Normoxia PBS, $P<0.05$, n=4, Dunnett's posthoc, Fig. 5.3). Alveolar size in both the hyperoxia-treated and normoxia groups injected with P8 cells was significantly smaller compared to the Hyperoxia PBS group, when the four groups were compared using Student Newman-Keuls posthoc ($P<0.05$; n=4, data not shown). The number of alveoli in both hyperoxia-treated and normoxia groups injected with P8 cells was not different to the control (Normoxia PBS) group; however, the number of alveoli in the Hyperoxia PBS group was significantly reduced ($P<0.05$, n=4, Dunnett's posthoc, Fig. 5.3). The lung tissue area and the number of elastin-positive blood vessels were not significantly different to the control (Normoxia PBS) in any of these groups (Fig. 5.3). The number of secondary septa per tissue area in both hyperoxia-treated and normoxia groups injected with P8 cells was not significantly different to the control (Normoxia PBS) group, however, the Hyperoxia PBS group had significantly increased number of secondary septa per tissue area ($P<0.05$, n=4, Dunnett's posthoc, Fig. 5.3). The Normoxia PBS and Hyperoxia PBS groups at D28 showed the same changes in all measured morphometric parameters observed in Chapter 3.

Histological analysis of the lungs from mice injected with P13-15 cells demonstrated aberrant growth in some areas, represented with condensed tissue containing small cells of predominantly mesenchymal (i.e. spindle-like) morphology (Fig. 5.4). There was an abnormally high number of nucleated cells observed in the lumen of pulmonary blood vessels after P13-15 cell injection, which was not observed after other cell types or PBS were injected (Fig. 5.5). Lumps from the injection site were represented with a few tissue types: condensed tissue areas containing small spindle-like cells, abnormal vascular-like formations with erythrocytes, and skin mesenchymal-like cells surrounding the lumps (Fig. 5.6).

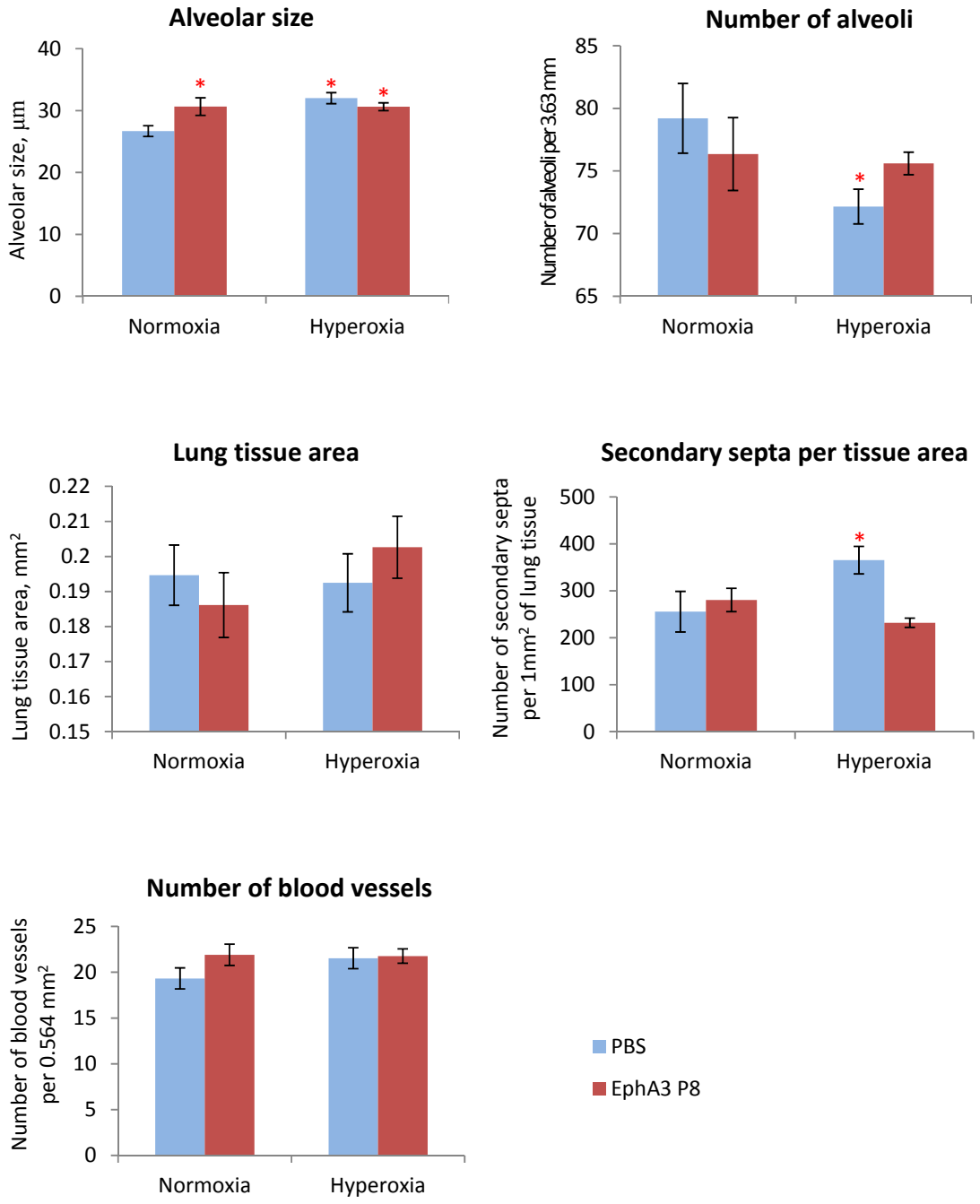

Figure 5.3. Morphometric lung parameters at D28 after the injection of PBS (blue) or EphA3^{+} cells from P8 (red). Significant differences compared to the controls (Normoxia PBS) are marked with red asterisks (P<0.01). Error bars indicate SEM from average values per mouse in each group, n=4. Lung tissue area and the number of blood vessels are presented per lung section image area, i.e. per 0.564 mm^2. The number of alveoli is presented per 3.63 mm line (vertical and horizontal) drawn across an image of each lung section.

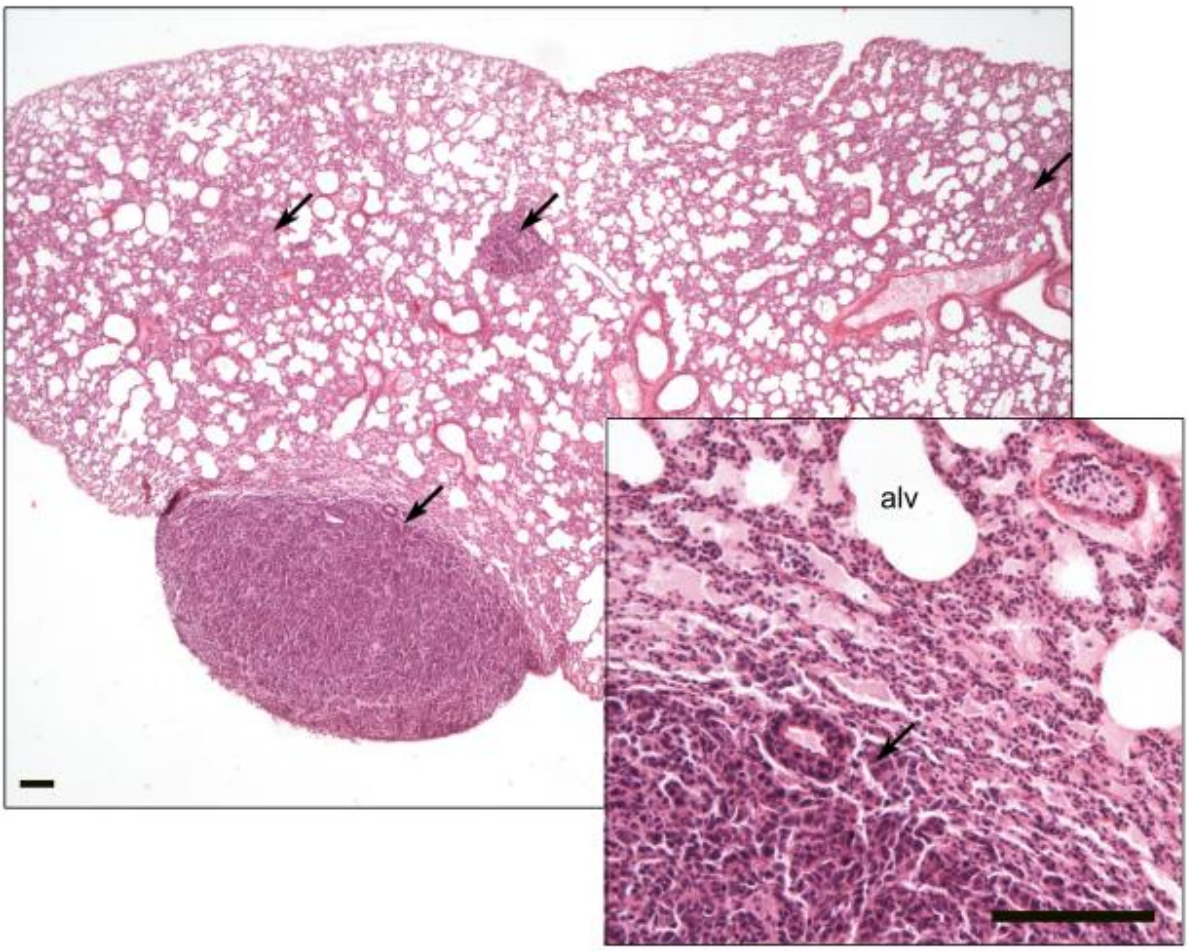

Figure 5.4. Mayer's hematoxyllin and eosin stain of a representative lung section from mouse injected with P13-15 EphA3 cells. Lumps of condensed tissue are indicated with arrows, alv – alveolus. Scale = 100 μm.

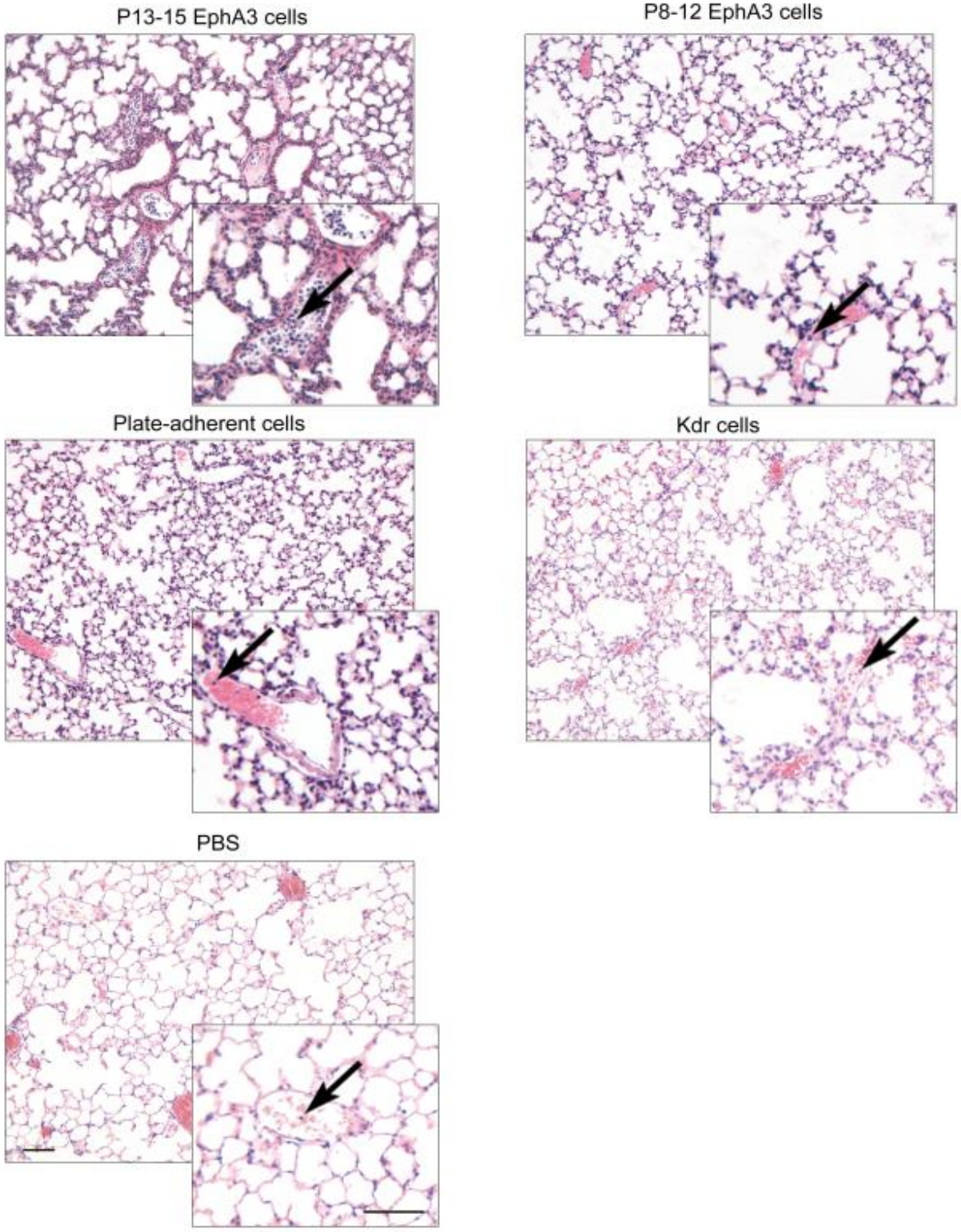

Figure 5.5. Hematoxyllin and eosin staining of nucleated cells in the lungs of mice injected with either late (P13-15) or early (P8-12) passages of EphA3-enriched cells, as well as plate-adherent cells, Kdr-enriched cells and PBS. There is an increase in nucleated cell number in blood vessel lumen in the lungs of P13-15 EphA3 cell injected mice, compared to all other groups. Nucleated cells in the blood vessel lumens are marked with arrows. Scale = 100 μm.

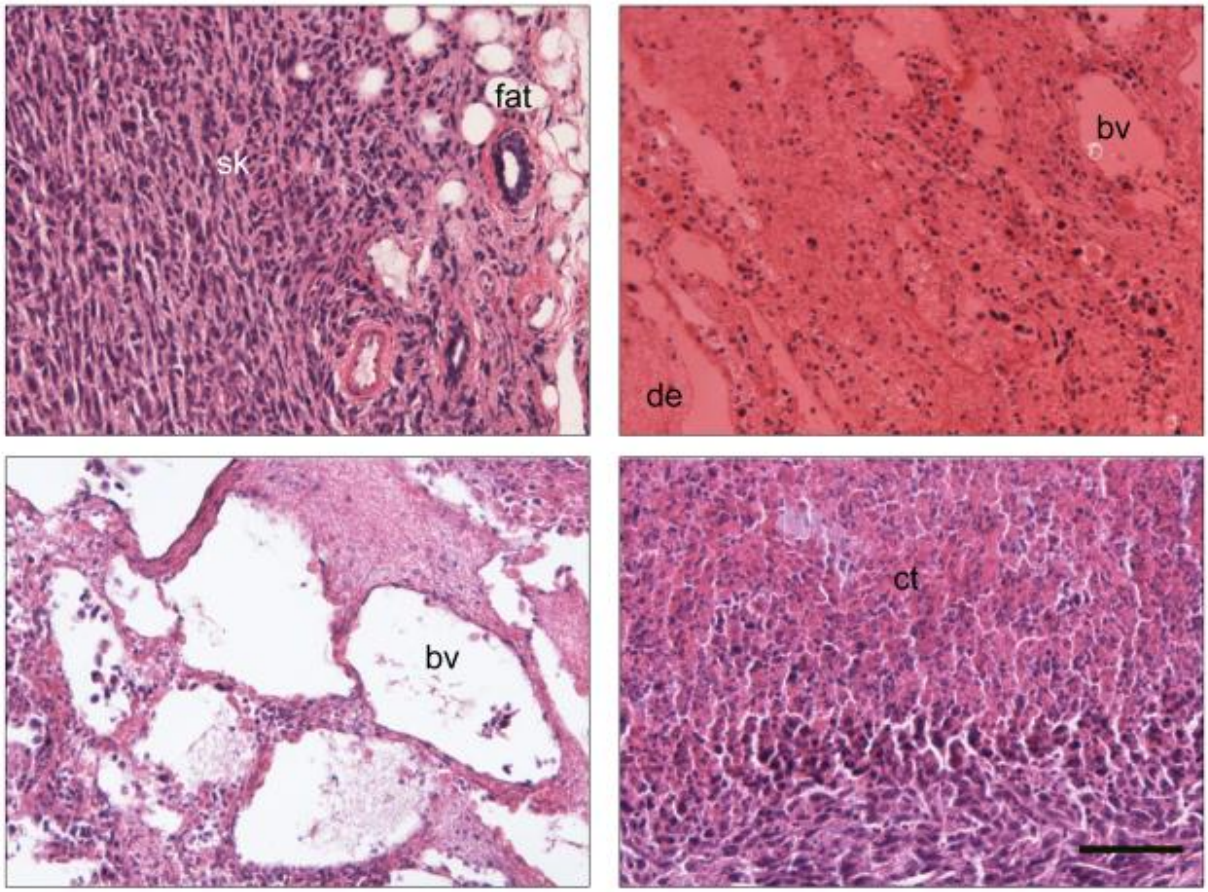

Figure 5.6. Representative types of tissue in the aberrant structures (lumps) from the site of injection, stained with hematoxyllin and eosin. Sk – skin mesenchymal-like spindle-shaped cells, fat, de – degrading erythrocytes and necrosis areas, bv – blood vessel, ct – condensed tissue. Scale = 100 μm.

Immunohistochemistry for GFP was performed on the lung and lump samples from mice, injected with P13-15 cells, as described in General Materials and Methods, Section 2.3. Strong donor-derived GFP signals were observed throughout the lung sections in condensed (hypercellular) tissue areas (Fig. 5.7). GFP signal was also present in the lumps. No hypercellular regions or aberrant growth were observed in mice injected with P8 cells.

This pilot study has therefore demonstrated that injection of P8 EphA3 enriched cells into hyperoxia-treated mice had a positive effect upon the changes observed in PBS-injected hyperoxia-treated mice with respect to lung alveolar size, alveolar number and secondary septa formation, normalizing the values of these parameters to control levels.

Furthermore, no aberrant effects upon lung tissue architecture were observed. Conversely, injection of P13-15 EphA3 enriched cells into both hyperoxia treated and normoxia mice had a detrimental effect upon lung architecture and animal health, highlighting the need for caution when injecting long term cultured cells into animals.

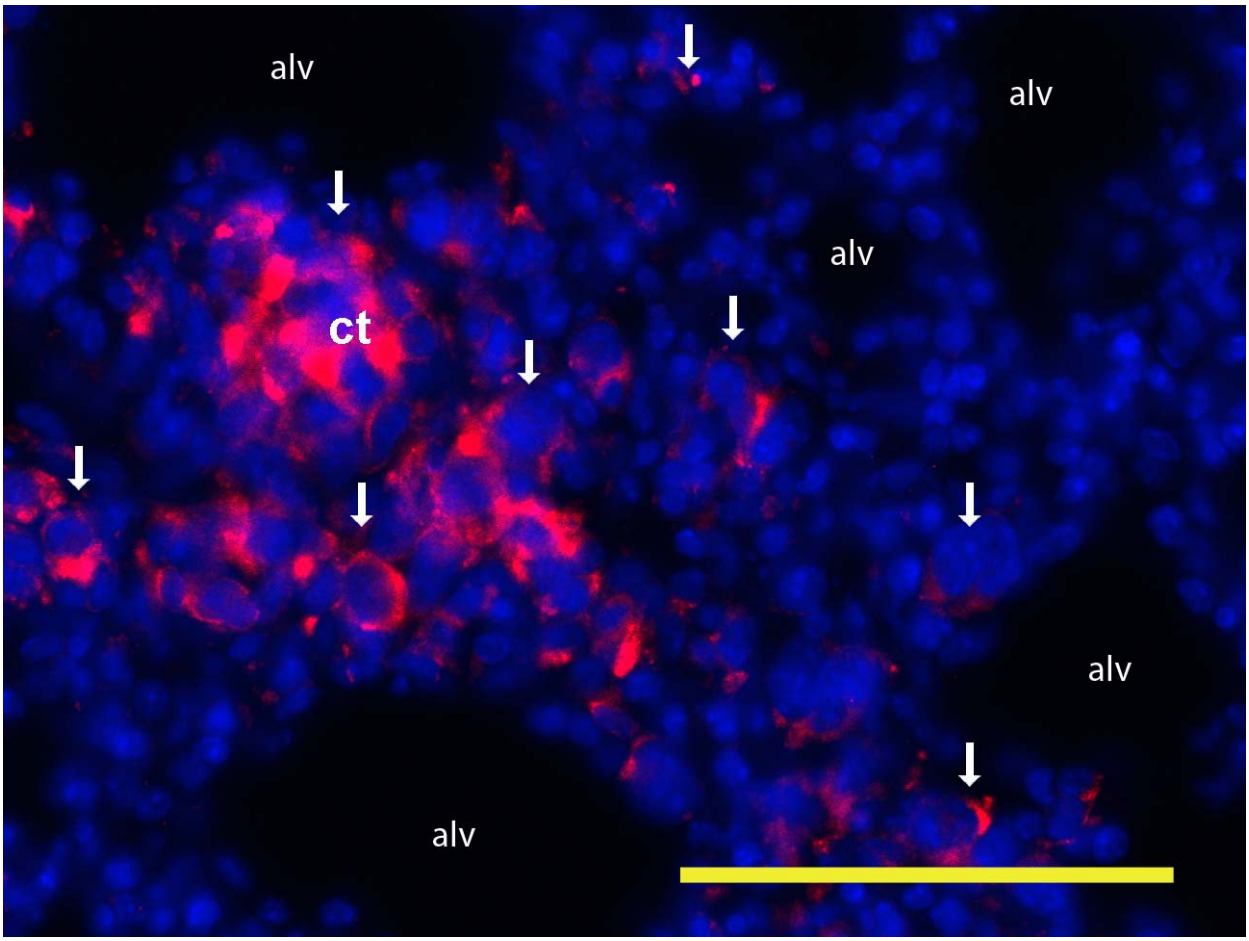

Figure 5.7. Immunohistochemistry for GFP (red) of representative lung section from a mouse injected with late culture stage EphA3 cells (P13-15), counterstained with Hoechst to demonstrate nuclei (blue). Condensed tissue regions (ct) and alveoli (alv) areas are marked on the image. Arrows point at GFP-immunoreactive (red) cells localised in condensed tissue and occasionally in the alveoli. Scale = 100 μm.

5.3.2. General animal health after injection of other cell types

In the pilot study, aberrant structures and hypercellular regions, as well as signs of pain and distress, were observed in the animals injected with P13-15 EphA3 enriched cells

(cells were 91-113 days in culture), but not with earlier passage cells. Further experiments for comparing the therapeutic value of EphA3 enriched cells with Kdr^+ and plate-adherent cells (PACs) following hyperoxia injury were therefore performed with EphA3 enriched cells from earlier passages. More specifically, cell suspensions used in the following larger scale study included: (i) uncultured cells freshly isolated from bone marrow and enriched for Kdr by MACS (Kdr cells), (ii) unsorted plate-adherent cells from P0 cultured for 7-10 days (PACs) and (iii) EphA3-enriched cells (EphA3 cells) cultured for 11 passages, frozen, thawed into P12 and kept in culture for three days (insufficient expansion of EphA3-enriched cells by passage 8 meant that cells were grown further such that enough cells were available for this experiment). All mice did not demonstrate any signs of pain or distress, they moved around the cage normally, and they gained weight. No red spots or lumps were observed at the site of injection in any mice at any time examined. All lung samples were analysed under the microscope and did not display any signs of aberrant growths, hypercellular regions or condensed tissue areas, and there was a small number of nucleated cells observed in blood vessel lumens, which was similar to PBS-injected mice (Fig. 5.5).

5.3.3. Sample collection at different time points

At postnatal day five (D5), 24 hours after hyperoxia treatment was completed, three non-injected mice per group were subjected to lung molecular analysis, and four non-injected mice per group were used for lung morphometric analysis. All other mice were injected with either PBS or cell suspensions. One to two mice per group were used to analyse the presence of GFP in the blood, the liver and the lungs at D14 and D21. At D28 and D56 three to four mice per group were used for molecular analysis of lungs, and four to five mice per group were used for morphometric analysis of the lungs. As a result, there was a total of two groups (Normoxia and Hyperoxia) of mice before injection (D5) and eight groups of mice after injection (D14-D56). The eight groups were the following: Normoxia PBS (normoxic mice, injected with PBS), Normoxia Kdr (normoxic mice, injected with fresh Kdr-enriched cells), Normoxia PAC (normoxic mice, injected with plate-adherent cells from P0), Normoxia EphA3 (normoxic mice, injected with EphA3-enriched cells at P12), Hyperoxia PBS (hyperoxia-treated mice, injected with PBS), Hyperoxia Kdr

(hyperoxia-treated mice, injected with fresh Kdr-enriched cells), Hyperoxia PAC (hyperoxia-treated mice, injected with plate-adherent cells from P0), and Hyperoxia EphA3 (hyperoxia-treated mice, injected with EphA3-enriched cells at P12).

5.3.4. Mouse weight and length

Mice were weighed and measured each week, and their weight and length were compared to the control group (Normoxia PBS) at each time point using Dunnett's posthoc. Male and female mice were compared separately. The Hyperoxia PBS male group body weight was significantly lower than that of the male control group at three (8.41 g vs 10.87 g; $P<0.05$; n=4) weeks of age, yet returned to control levels by the fourth week (Fig. 5.8-A). In Chapter 3, mouse weight differences were not observed between male hyperoxia-treated and normoxic mice. The Hyperoxia EphA3 male group body weight was significantly lower than that of the control group at six (22.31 g vs 24.72 g; $P<0.05$; n=4-5) and eight (23.93 g vs 27.02 g; $P<0.05$; n=4-5) weeks of age, yet it was not significantly different from that of the control group at any other stage (Fig. 5.8-A). All other groups (Hyperoxia Kdr, Normoxia Kdr, Hyperoxia PAC, Normoxia PAC and Normoxia EphA3) were not significantly different from the control in male mouse weight at any time point.

Male mouse length (crown to rump) was significantly reduced in the Hyperoxia Kdr group compared to control, or Normoxia PBS group at week one (39.00 mm vs 44.00 mm; $P<0.05$; n=3), two (51.60 mm vs 59.67 mm; $P<0.05$; n=3-4) and three (61.50 mm vs 71.75 mm; $P<0.05$; n=4). Male mouse length was also significantly reduced in the Hyperoxia EphA3 group compared to the control group at two (50.88 mm vs 59.67 mm; $P<0.05$; n=3-8) and three (59.83 mm vs 71.75 mm; $P<0.05$; n=4-8) weeks of age (Fig. 5.8-B). The Normoxia EphA3 (53.31 mm) and Normoxia PAC (54.28 mm) groups crown-rump length was also significantly reduced when compared to the control group measurements (59.67 mm) at two weeks of age (Fig. 5.8-B; $P<0.05$, n=3-8). This length reduction persisted in the Normoxia EphA3 group at three weeks of age (63.55 mm vs 71.75 mm; $P<0.05$; n=4-8). At four weeks male mouse length in these injected groups had returned to control levels. Crown-rump length in Normoxia PAC group (90.00 mm), however, was

significantly increased compared to the control group measurements (82.00 mm) at five weeks (Fig. 5.8-B; $P<0.05$; n=2-5), yet returned to control levels by week six. All other groups (Hyperoxia PBS, Normoxia Kdr and Hyperoxia PAC) were not significantly different from the control male mouse weight at any time point.

Female mouse body weight was significantly reduced in the Hyperoxia EphA3 group compared to the control group at week one (3.68 g vs 5.07 g; $P<0.05$; n=4-6) and two (6.21 g vs 8.10 g; $P<0.05$; n=4-6), according to Dunnett's posthoc (Fig. 5.9-A). The Hyperoxia PBS (3.85 g; n=7) and Normoxia PAC (3.93 g; n=8) female mouse body weight was significantly reduced compared to the control group (5.07 g; n=4) at one week of age ($P<0.05$; Fig. 5.9-A). There was no difference in female mouse body weight after two weeks of age. There was no significant difference in female mouse body weight observed in Hyperoxia Kdr, Normoxia Kdr, Hyperoxia PAC and Normoxia EphA3 groups compared to control at any time point tested (Fig. 5.9-A). Therefore, compared to Chapter 3 results, where no significant difference was observed in female mouse body weight between hyperoxia-treated and normoxia groups at any time point tested, in this experiment the difference was observed after PBS injection at one week of age.

Crown to rump length of female mice was significantly reduced in Hyperoxia EphA3, Hyperoxia PAC, Hyperoxia PBS and Normoxia PAC groups when compared to that of the control group at one (41.17 mm, 42.33 mm, 42.71 mm and 41.88 mm respectively vs 48.25 mm; $P<0.05$; n=4-8) and four (68.00 mm, 71.75 mm, 71.57 mm and 71.17 mm respectively vs 80.67 mm; $P<0.05$; n=3-8) weeks of age, (Fig. 5.9-B). Crown to rump length in the Hyperoxia EphA3 group was also significantly reduced when compared to the control group measurements (57.40 mm vs 73.00 mm; $P<0.05$; n=4-5) at three weeks of age (Fig. 5.9-B). Crown to rump length of female mice was again significantly reduced in Hyperoxia PAC and Hyperoxia PBS groups when compared to that of the control group at seven weeks of age (84.5 mm and 84.4 mm respectively vs 91.00 mm; $P<0.05$; n=2-5). There was no significant difference in female mouse length observed in Hyperoxia Kdr, Normoxia Kdr and Normoxia EphA3 groups compared to control at any time point tested.

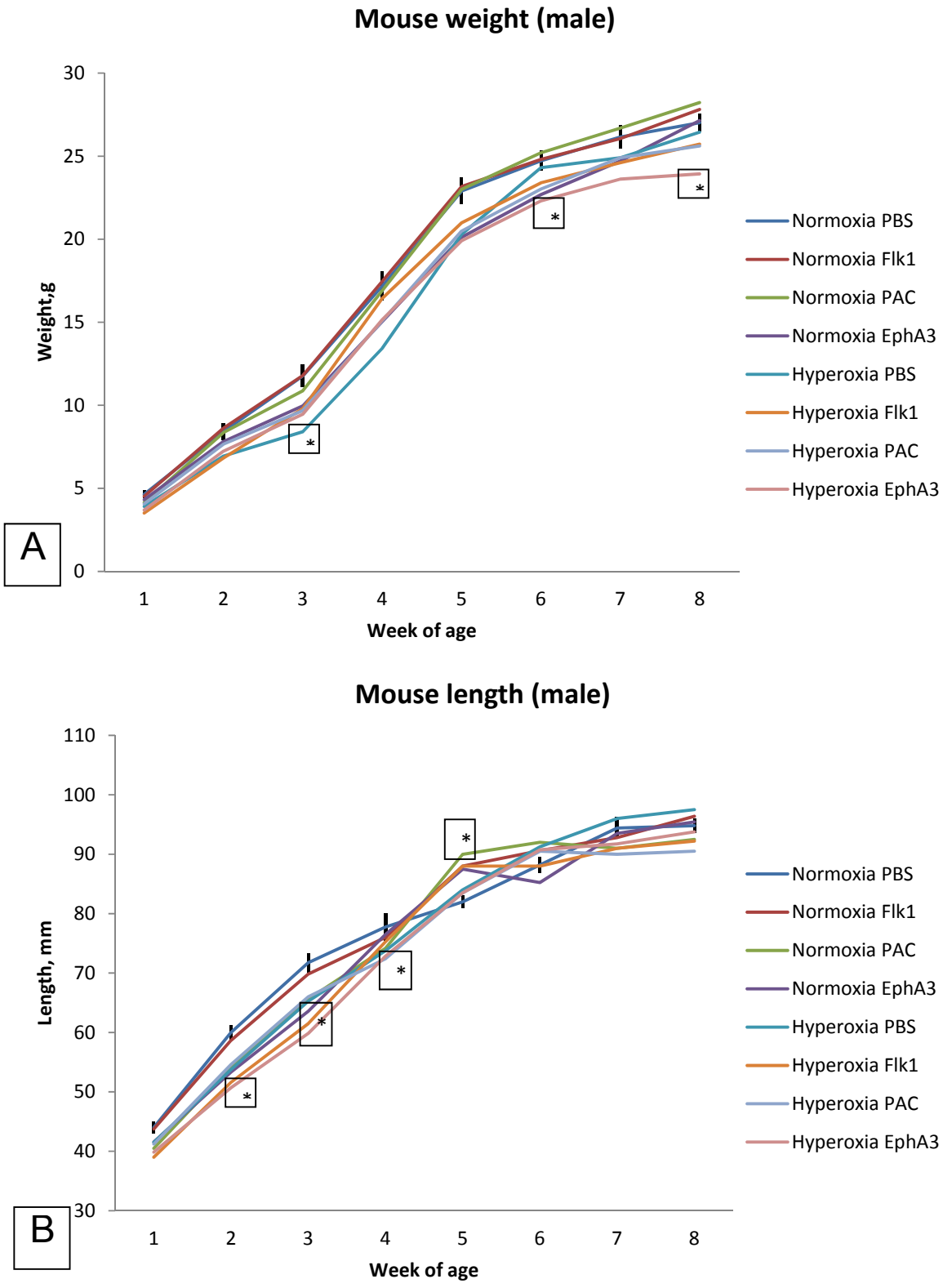

Figure 5.8. A. Male body weight. B. Male crown-rump length. Averaged error bars marked on the control group (Normoxia PBS), as all other groups were compared to this group. These exemplar error bars can be visually applied to each value to compare the groups. Asterisks in boxes represent significant differences from control group ($P<0.05$), n=4-6. Boxes include only groups that are different from control.

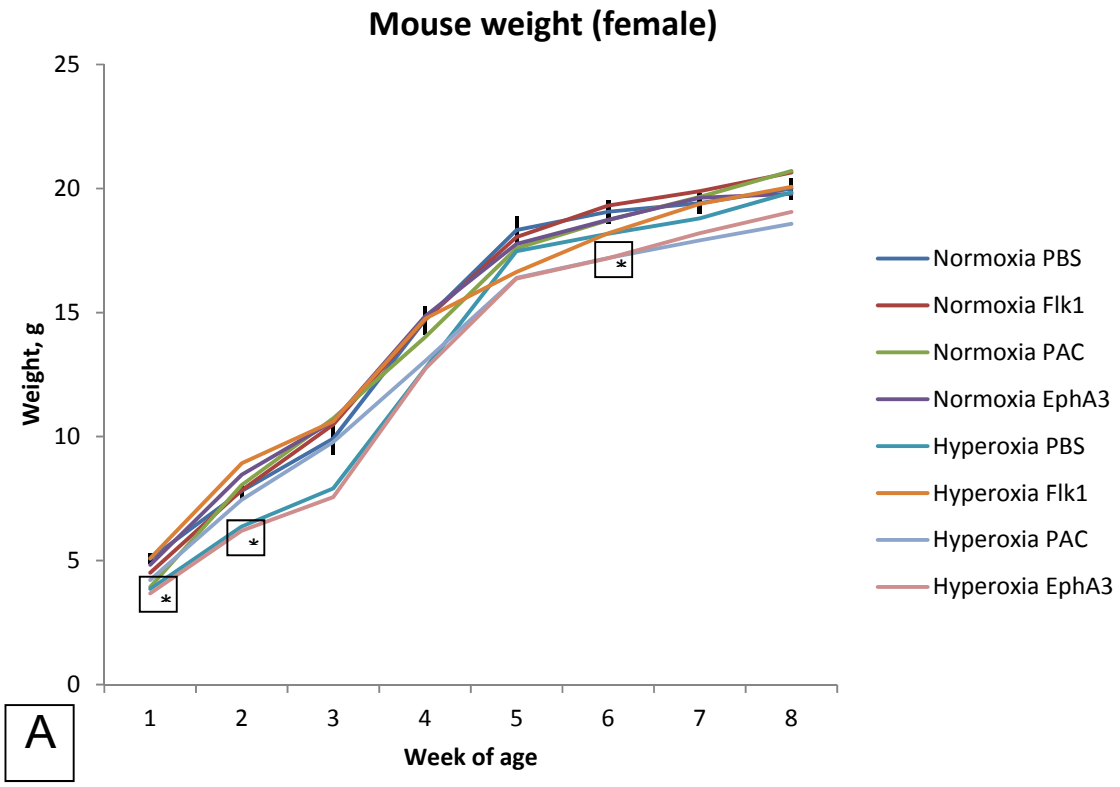

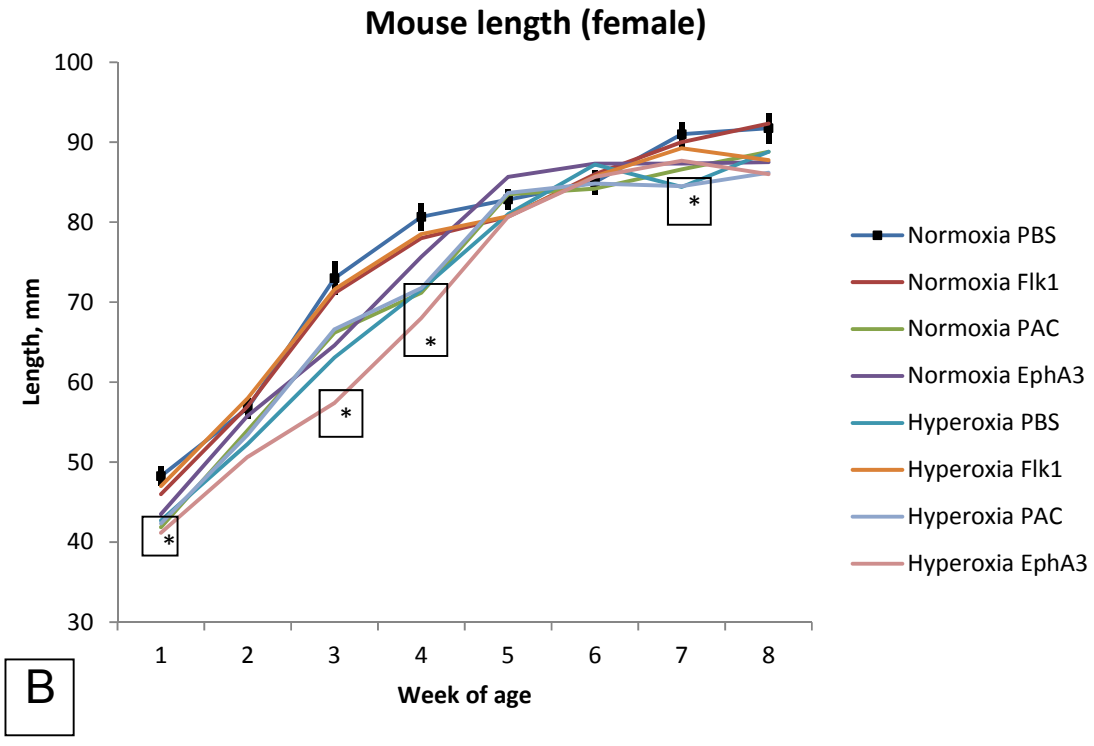

Figure 5.9. A. Female body weight. B. Female crown-rump length. Averaged error bars marked on control group (Normoxia PBS), as all other groups were compared to this group. These exemplar error bars can be visually applied to each value to compare the groups. Asterisks in boxes represent significant differences from control group ($P<0.05$), n=4-6. Boxes include only groups that are different from control.

5.3.5. Lung weight and volume

The lungs were weighed and measured in volume by water displacement after pressure-fixing. According to Dunnett's posthoc, there was no significant difference between control and other groups in either parameter at any time point (Figure 5.10).

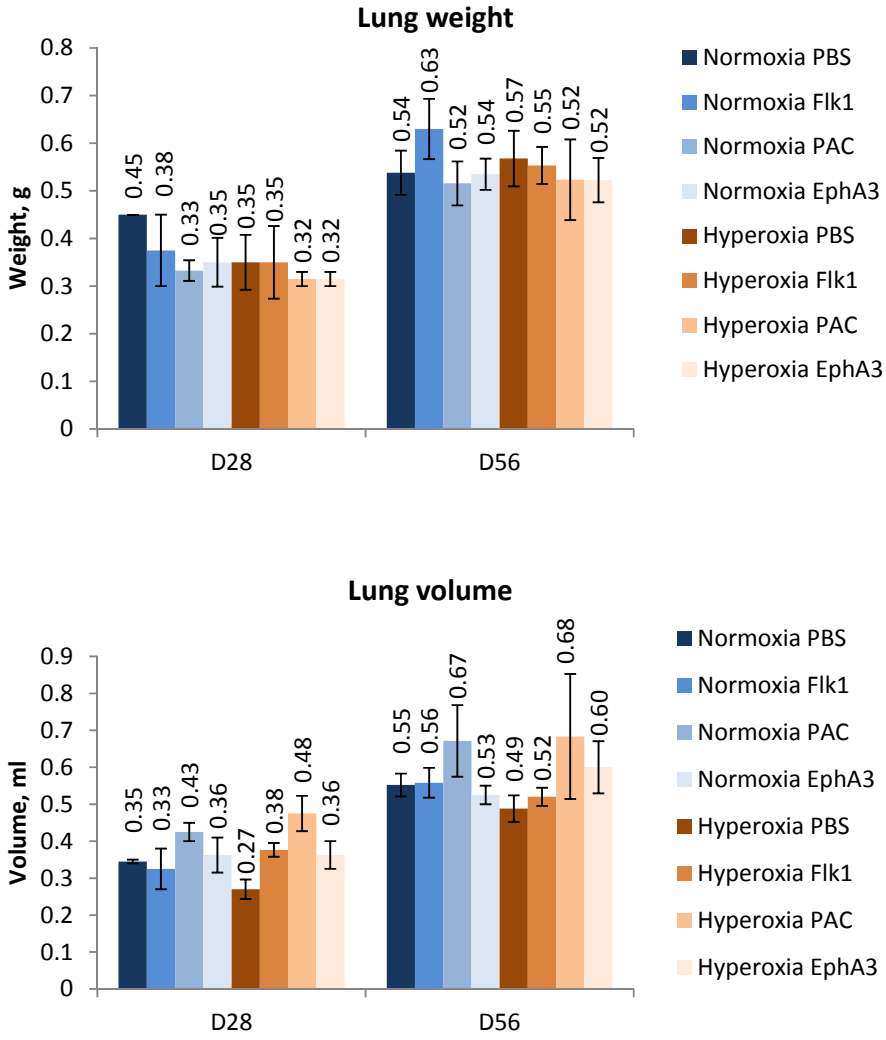

Figure 5.10. Lung weight and volume after pressure-fixing. No significant differences compared to the control group were observed. Error bars represent SEM, n=3-4.

5.3.6. Morphometric and vascular analyses of the lungs after hyperoxia treatment

Morphometric data from normoxia and hyperoxia-treated mice injected with EphA3 cells from P8 (from the pilot study) were included in the respective Normoxia EphA3 and Hyperoxia EphA3 groups in this section.

Paraffin lung sections stained with haematoxylin and eosin were analysed for alveolar size and number (Fig. 5.11-A). Alveolar size was increased after hyperoxia treatment at D5 (hyperoxia 57.13 μm vs normoxia 45.02 μm) and remained increased in all hyperoxia-treated groups at D28 (29.85 μm in Hyperoxia Kdr, 31.06 μm in Hyperoxia PAC, 32.25 μm in Hyperoxia EphA3 and 32.01 μm in Hyperoxia PBS group) compared to control (26.69 μm in Normoxia PBS group), according to Dunnett's posthoc. At D56 all hyperoxia-treated groups retained increased alveolar size (more than 32 μm), except for the Hyperoxia Kdr group (30.09 μm) compared to the control group (30.43 μm), according to Dunnett's and Student Newman-Keuls posthoc (Appendices, Section I). At D28, the Hyperoxia Kdr group alveoli were also significantly reduced in size, compared to the Hyperoxia PBS group, according to Student Newman-Keuls posthoc. Alveolar size in the Normoxia EphA3 (29.53 μm) group was significantly increased compared to the control group (Dunnett's posthoc, Fig. 5.11-A), but significantly reduced compared to the Hyperoxia PBS and Hyperoxia EphA3 groups' alveoli at D28 (Student Newman-Keuls posthoc, Appendices, Section I). The Normoxia Kdr group had significantly larger alveoli (32.57 μm), than the control and Hyperoxia Kdr groups at D56, yet was not different from Hyperoxia PBS group (32.78 μm), according to Student Newman-Keuls posthoc (Appendices, Section I).

At D5, and prior to the injection of cells, the number of alveoli in the hyperoxia treated lungs had decreased relative to normoxia lungs (50.09 airspaces per 3.63 mm of line drawn across the image vs 58.75 airspaces in the Normoxia group). Alveolar number was also significantly reduced in all hyperoxia-treated groups at D28 (71.97 airspaces in Hyperoxia Kdr, 72.16 in Hyperoxia PBS, 72.50 in Hyperoxia EphA3 and 72.76 in

Hyperoxia PAC groups) compared to the control group (78.84 airspaces, Normoxia PBS group), according to Dunnett's posthoc (Fig. 5.11-A). The Hyperoxia PBS group animals had significantly less alveoli (72.16) compared to the mice in the Normoxia PBS (78.84) and Normoxia Kdr (78.20) groups, but no significant differences were observed when compared to the Normoxia EphA3 (73.95) and Normoxia PAC (76.95) groups at D28 (Appendices, Section I). There was no significant difference in alveoli number between any groups at D56 according to both Dunnett's and Student Newman-Keuls posthoc tests (Appendices, Section I), which contradicted the results in Chapter 3. However, when data from Chapter 3 (normoxia and hyperoxia groups) were included in this study (in Normoxia PBS and Hyperoxia PBS groups, respectively), there was a significant reduction in the number of alveoli observed at D56 in the Hyperoxia PBS, Hyperoxia EphA3, Hyperoxia PAC, Normoxia PAC and Normoxia Kdr groups , but not in the other groups (data not shown).

Paraffin lung sections stained with Weighert's elastin were analysed for lung tissue area, the number of secondary septa per 1 mm^2 of lung tissue area and the number of blood vessels per lung secion area of 0.564 mm^2 (Fig. 5.11-B,C). Lung tissue area was significantly reduced in all hyperoxia-treated groups at D5 (in hyperoxia-treated lungs 0.145 mm^2 per 0.564 mm^2 of lung section area vs normoxia lung 0.164 mm^2 per 0.564 mm^2), but returned to control levels by D28, similarly to previously described data (Chapter 3). The Normoxia EphA3 (0.183 mm^2) and Hyperoxia EphA3 (0.181 mm^2) groups had significantly reduced total lung tissue area compared to the Normoxia PAC (0.201 mm^2), Hyperoxia PAC (0.209 mm^2) and Normoxia Kdr (0.203 mm^2) groups at D28 (Appendices, Section I). Lung tissue area in the Hyperoxia PBS (0.193 mm^2) and Hyperoxia Kdr (0.187 mm^2) groups was significantly reduced when compared to the Hyperoxia PAC (0.209 mm^2) group at D28. There was no significant difference between groups at D56 (Appendices, Section I).

The number of secondary septa per square millimetre of lung tissue area was significantly reduced at D5 (259.94 septa per mm^2 of lung tissue area in hyperoxia-treated lungs vs 377.12 septa per mm^2 in normoxic lungs). At D28 there was no difference in the number

of secondary septa per lung tissue area in the Hyperoxia Kdr and Hyperoxia PAC groups, but it was significantly increased in the Normoxia EphA3 (344.8 septa), Hyperoxia PBS (365.3 septa) and Hyperoxia EphA3 (443.5 septa) groups, compared to the control group (255.6 septa), according to Dunnett's posthoc. No significant differences between these groups were observed at D56, except for the Hyperoxia EphA3 group, which retained an increased septa number per lung tissue area than all other groups (Student Newman-Keuls posthoc, Appendices, Section I). At D28, the Hyperoxia PBS group (365.3) had significantly more septa per lung tissue area than all other groups (less than 303 septa), except for the Hyperoxia EphA3 (443.5) and Normoxia EphA3 (344.8) groups (Student Newman-Keuls posthoc, Appendices, Section I). The Normoxia PAC group had significantly less septa per lung tissue area compared to all hyperoxia-treated groups, except for the Hyperoxia PAC group (Student Newman-Keuls posthoc, Appendices, Section I).

The number of blood vessels per 0.564 mm^2 of lung section area was significantly reduced at D5 (12.41 vessels in hyperoxia-treated group vs 14.6 vessels in normoxia group), and returned to the control levels in all groups at D28, according to Dunnett's posthoc. However, the numbers of blood vessels per area in the Normoxia PAC (24.60) and Hyperoxia PAC (25.24) groups were observed to be significantly higher compared to that of the control (19.38) at D28, according to Dunnett's posthoc. At D56 these values returned to control levels, however, Hyperoxia PBS group had significantly less blood vessels (17.84) compared to the control group (22.24). When data from hyperoxia and normoxia groups (Chapter 3 data) was included into Hyperoxia PBS and Normoxia PBS respectively into this study, there was no significant difference in blood vessel number between any groups (including Hyperoxia PBS group), according to Student Newman-Keuls posthoc; however, there was still a reduction in the number of blood vessels in Hyperoxia PBS group, compared to control, according to Dunnett's posthoc (data not shown).

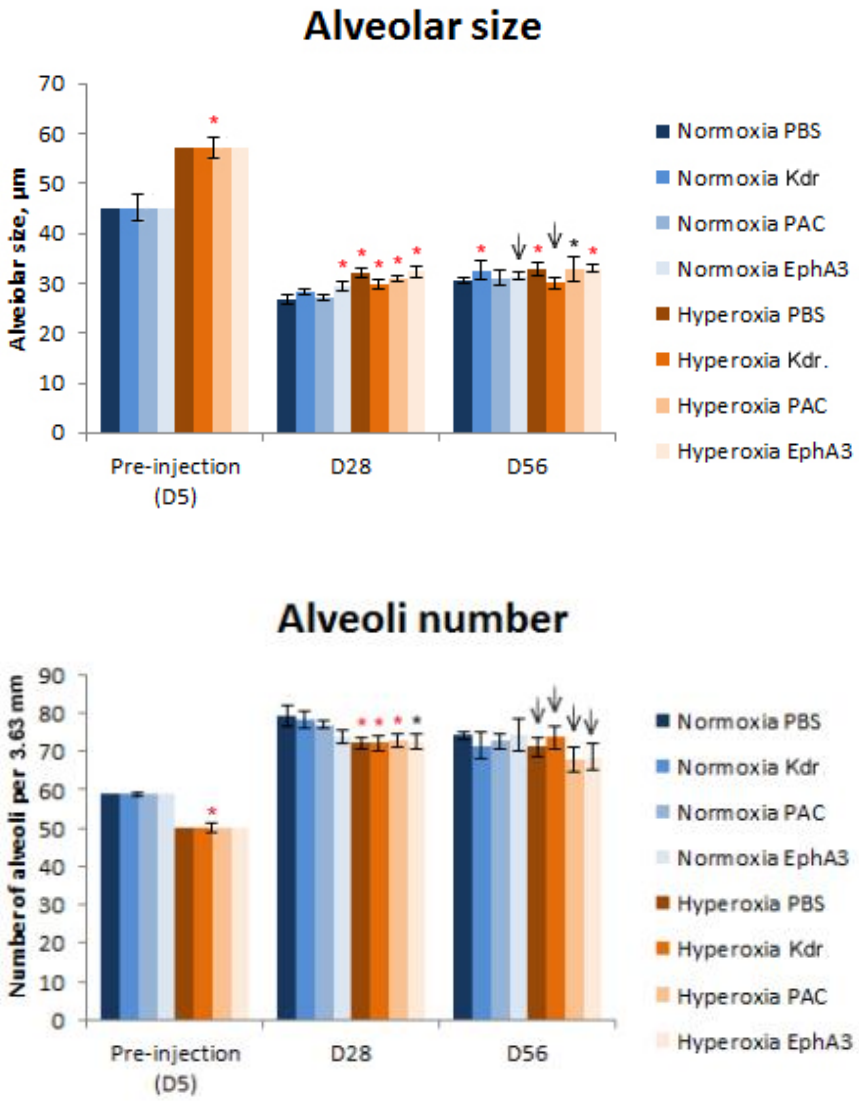

Figure 5.11-A. Morphometric lung parameters at D5 (before the injection), D28 and D56. Day 5 data are presented in two groups (Normoxia in blue and Hyperoxia in brown), as injection of cells has not been performed at that stage. Significant differences compared to the controls (Normoxia at D5 or Normoxia PBS at D28 and D56) are marked with black asterisks ($P<0.05$) and with red asterisks ($P<0.01$). Arrows indicate the earliest point when the group has no significant difference compared to control group after the significant difference was observed in a previous time point. Error bars indicate SEM from average values per mouse in each group, n=4-5. The number of alveoli is presented per 3.63 mm line (vertical and horizontal) drawn across an image of each lung section.

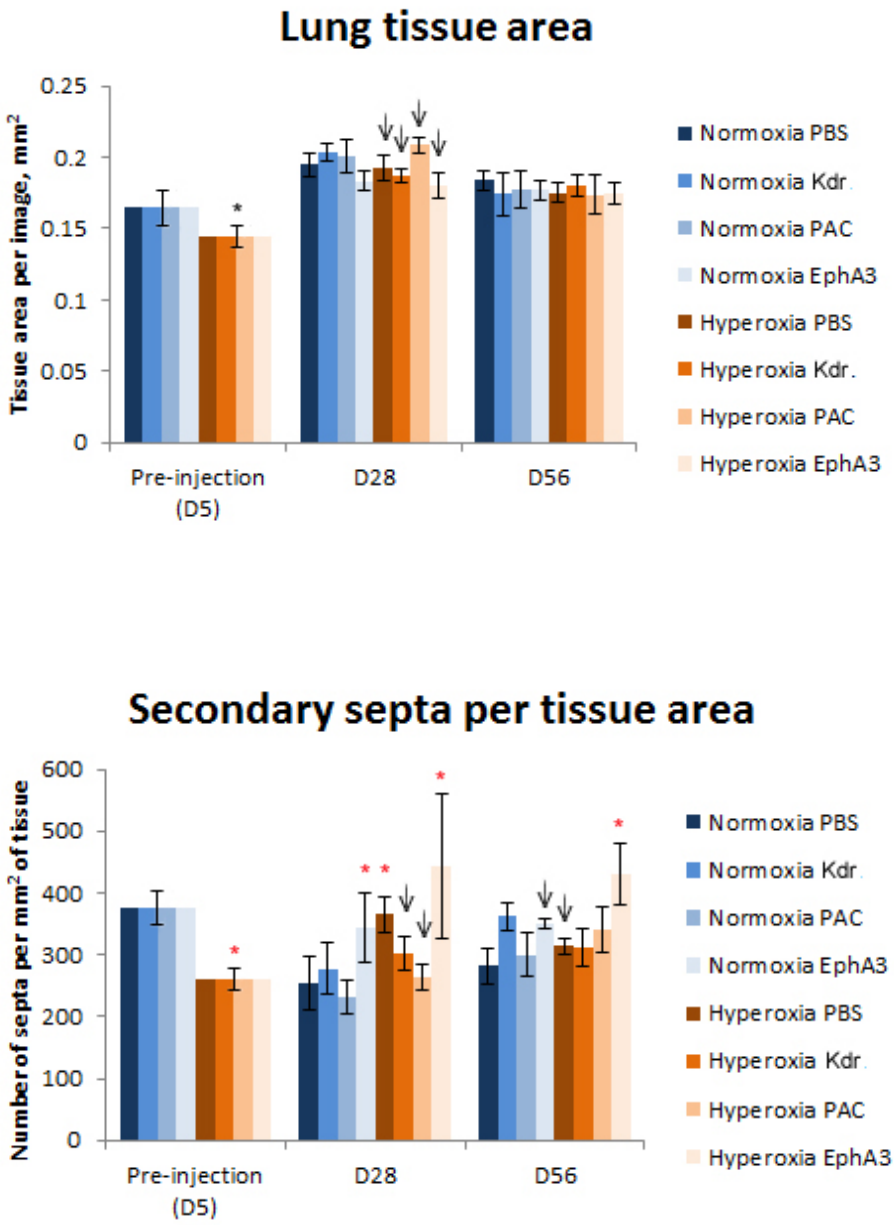

Figure 5.11-B. Morphometric lung parameters at D5 (before the injection), D28 and D56. Day 5 data are presented in two groups (Normoxia in blue and Hyperoxia in brown), as injection of cells has not been performed at that stage. Significant differences compared to the controls (Normoxia at D5 or Normoxia PBS at D28 and D56) are marked with black asterisks ($P<0.05$) and with red asterisks ($P<0.01$). Arrows indicate the earliest point when the group has no significant difference compared to control group after the significant difference was observed in a previous time point. Error bars indicate SEM from average values per mouse in each group, n=4-5. Lung tissue area is presented per lung section image area, i.e. per 0.564 mm^2.

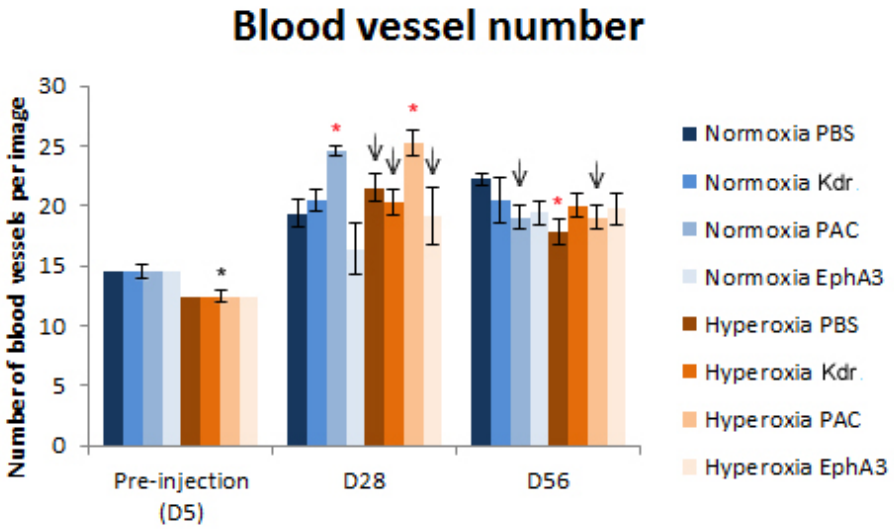

Figure 5.11-C. Vascular lung parameters at D5 (before the injection), D28 and D56. Day 5 data are presented in two groups (Normoxia in blue and Hyperoxia in brown), as injection of cells has not been performed at that stage. Significant differences compared to the controls (Normoxia at D5 or Normoxia PBS at D28 and D56) are marked with black asterisks ($P<0.05$) and with red asterisks ($P<0.01$). Arrows indicate the earliest point when the group has no significant difference compared to control group after the significant difference was observed in a previous time point. Error bars indicate SEM from average values per mouse in each group, n=4-5. The number of blood vessels is presented per lung section image area, i.e. per 0.564 mm^2.

5.3.7. Analysis of protein levels in the lungs following injections

Levels of Pecam1 (CD31), Vegfa and Sftpc were measured by western blotting and compared to the control group (Normoxia PBS) at each time point (Fig. 5.12) using one-way ANOVA followed by Dunnett's posthoc. There was no significant difference at any time point in the levels of Pecam1 (Fig. 5.13-A), which was observed as a single 140 kDa band. There was a high variability between the samples in the levels of Pecam1 at D28 (Fig. 5.12-B). Vegfa was observed as a 21 and 42 kDa double band. There was a reduction in the levels of the 42 kDa Vegfa band in the Normoxia EphA3 (0.13 units), Hyperoxia Kdr (0.06 units) and Hyperoxia PAC (0.20 units) groups compared to the control group (1 unit) at D28 (Fig. 5.13-A). Levels of the 42 kDa Vegfa band returned to control levels in all groups at D56. There was a reduction in the levels of the 21 kDa Vegfa band in Normoxia Kdr (0.35 units) and Normoxia PAC (0.29 units) groups compared to the control group (1 unit), however, no reduction was observed at D56. Sftpc was

observed as a 21 and 25 kDa double band. There was no significant difference observed in the protein levels of either size of Sftpc between control and any other group at any time point examined (Fig. 5.13-B).

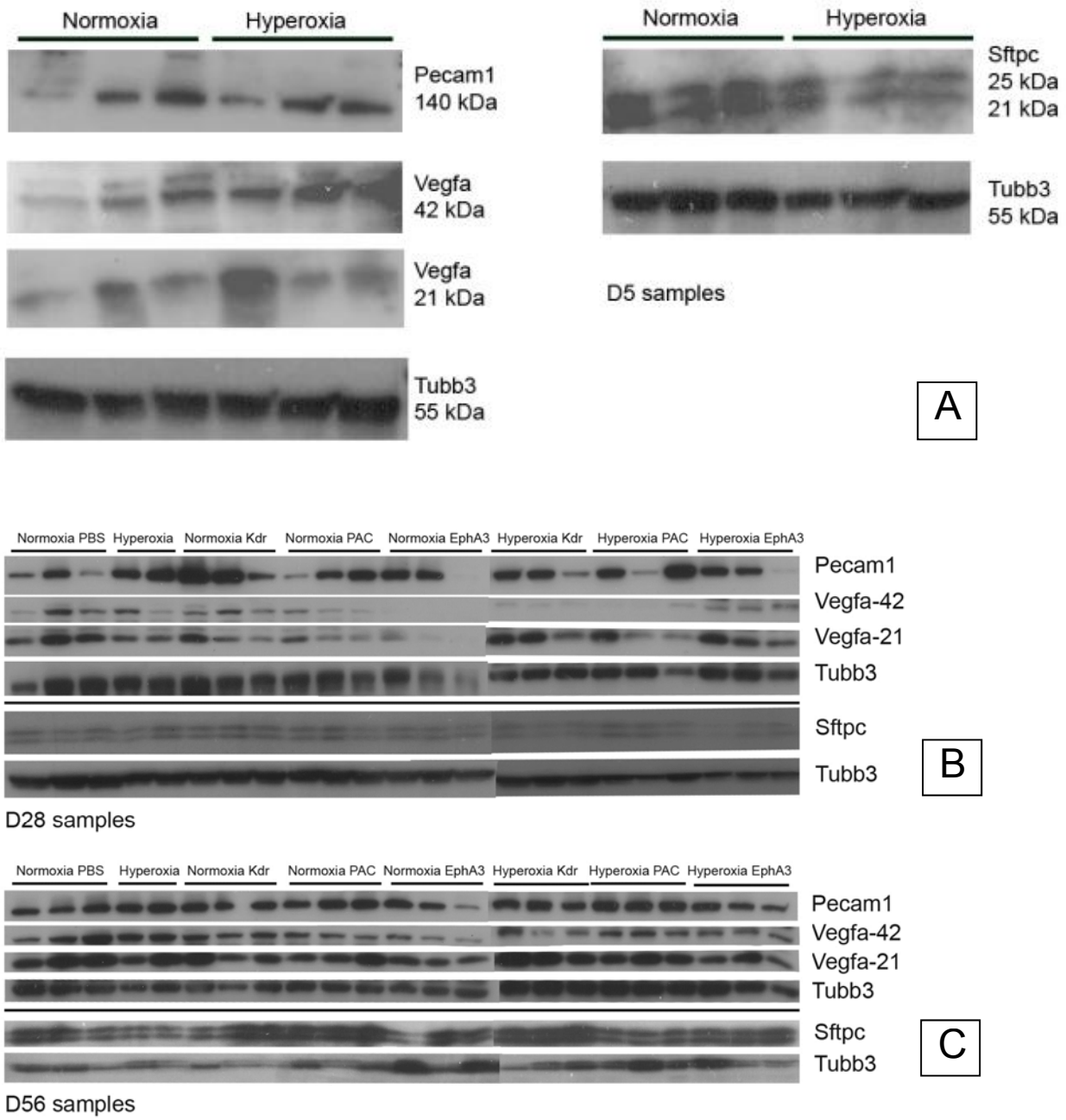

Figure 5.12. Western blotting protein analysis of lungs at three time point. A – at D5, B – at D28, C – at D56. Tubulin beta 3 (Tubb3) was used as a loading control. Loading amount: 8-10 µg of protein. Film exposure time: 3-15 secs.

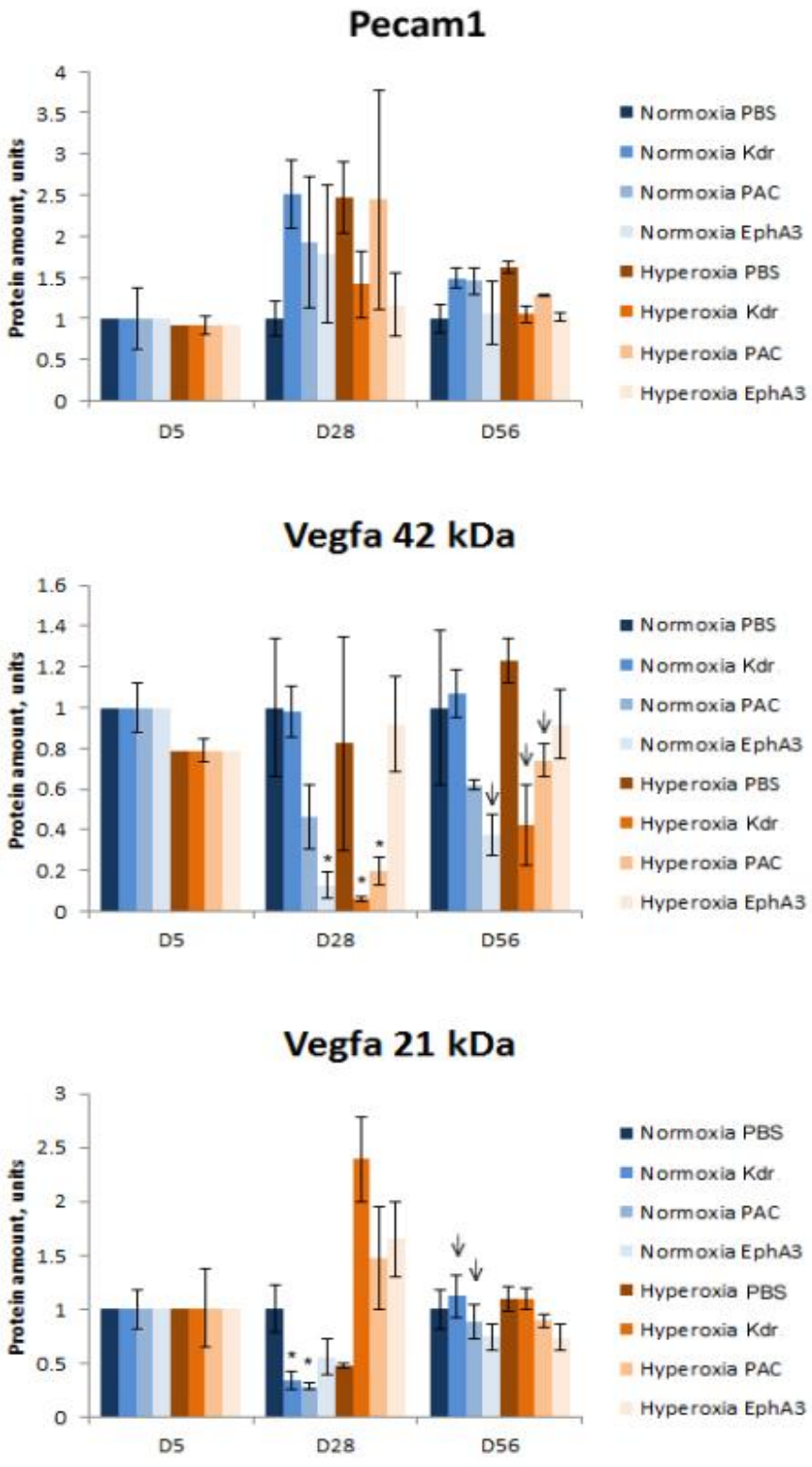

Figure 5.13-A. Statistical analysis of western blots. Charts indicate the amount of each protein (units) in relation to the loading control (Tubb3), where Normoxia PBS values are taken as one unit. Asterisks indicate significant difference from Normoxia PBS group, $P<0.05$, $n=3$. Error bars represent SEM.

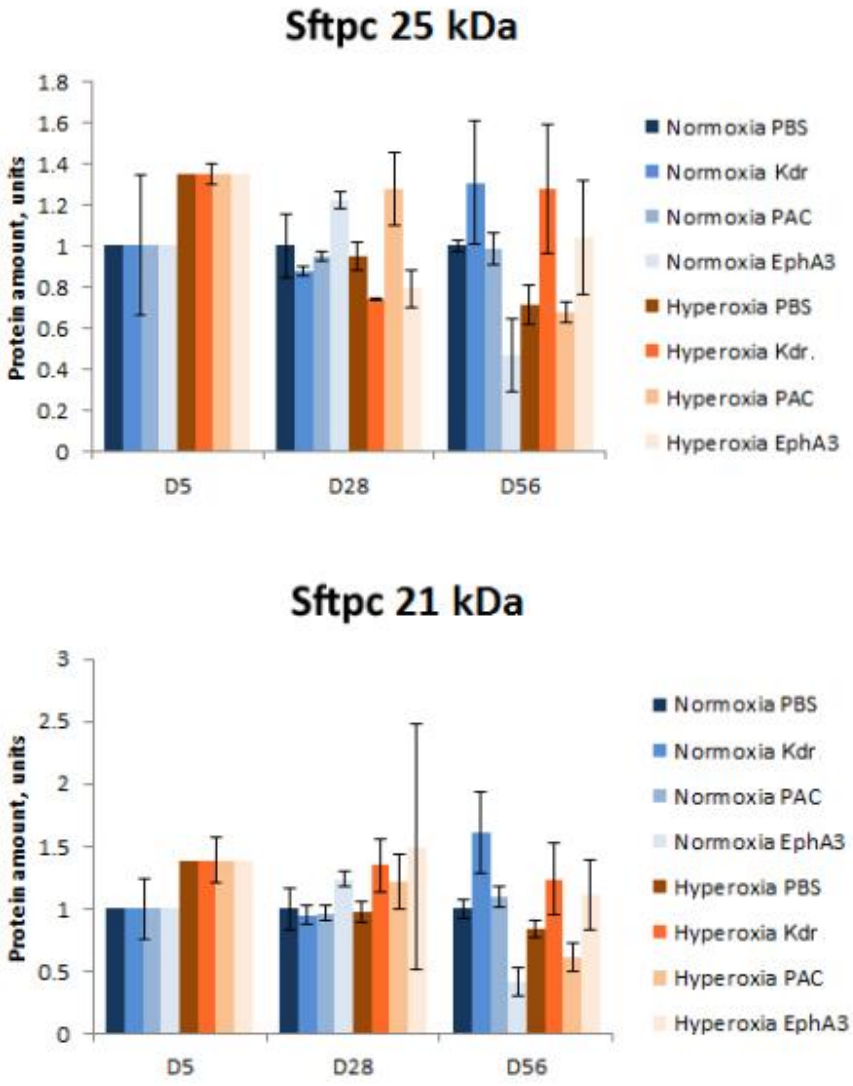

Figure 5.13-B. Statistical analysis of western blots. Charts indicate the amount of each protein (units) in relation to the loading control (Tubb3), where Normoxia PBS values are taken as one unit. Asterisks indicate significant difference from Normoxia PBS group, $P<0.05$, n=3. Error bars represent SEM.

5.3.8. Analysis of the presence of GFP$^+$ cell engraftment following injections

Lung, liver and blood cell suspensions from injected mice were analysed for the presence of GFP by FACS. There was no significant increase observed in the number of GFP$^+$ cells above the uninjected control levels in the mouse lungs and blood (less than 0.5%) at D14 and D21 (Fig. 5.14). There was no significant increase in GFP$^+$ cells above the control

levels in the liver (less than 2%) at both D14 and D21 (Fig. 5.14). Plated aliquots from samples of cell populations taken prior to injection retained GFP fluorescence in culture (control medium, General Materials and methods, Section 2.12), however, during the same 14 days (Fig. 5.15). Immunohistochemistry for GFP with signal enhancement on D28 lung sections did not show any GFP^+ signal in any lung tissues of cell-injected mice (Fig. 5.16). No increase in GFP fluorescence above background levels was detected at D28.

Day 14

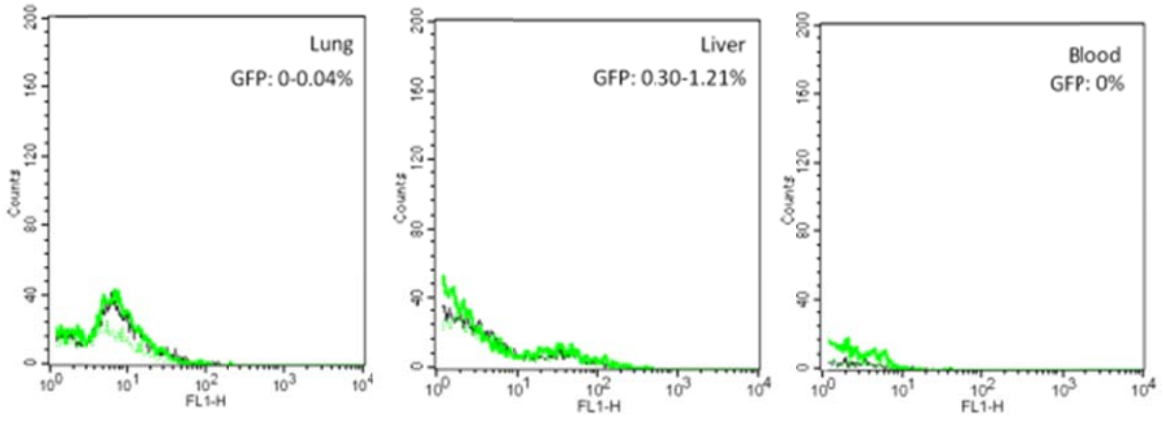

Day 21

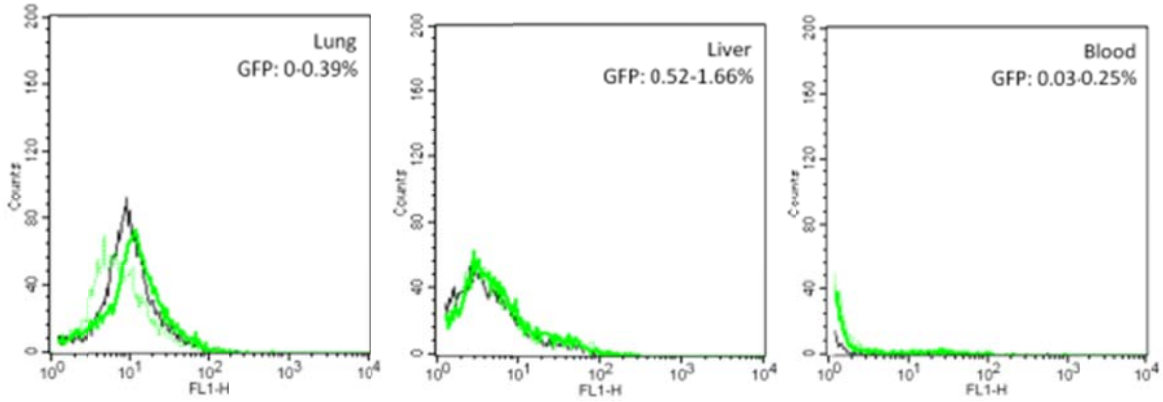

Figure 5.14. FACS analysis for the presence of GFP^+ cells in the cell suspensions of the lung, liver and blood of the injected mice (green lines) in comparison to control (non-injected mice, black line) at D14 (top row) and D21 (bottom row). X axis (FL1-H) indicates green fluorescence. There is no significant increase in fluorescence in the injected mice (amount of GFP is indicated by how far to the right from control black peak are the green peaks) in lung, liver and blood. Percentage of GFP^+ cells is indicated on the top right of each chart.

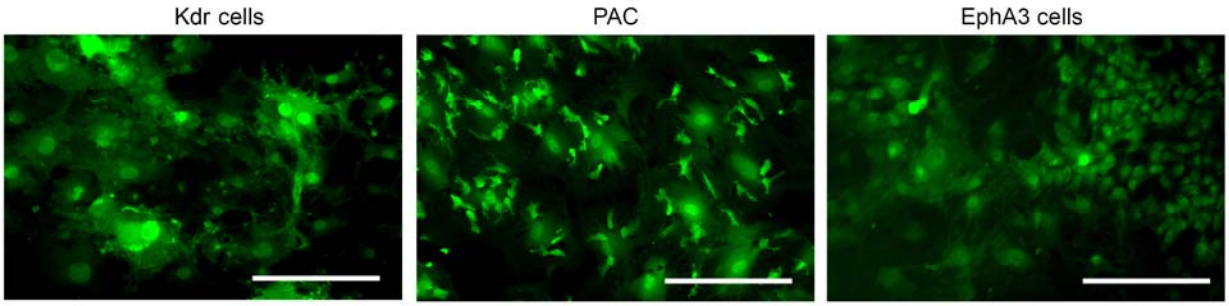

Figure 5.15. Samples of representatives of each injected cell type cultured in control medium analysed for the presence of GFP (green signal) at the same time point as the samples were collected from the injected mice for FACS (D14). GFP was present in each cell type. Negative control (GFP^- cells) was negative. Scale bar = 100 µm.

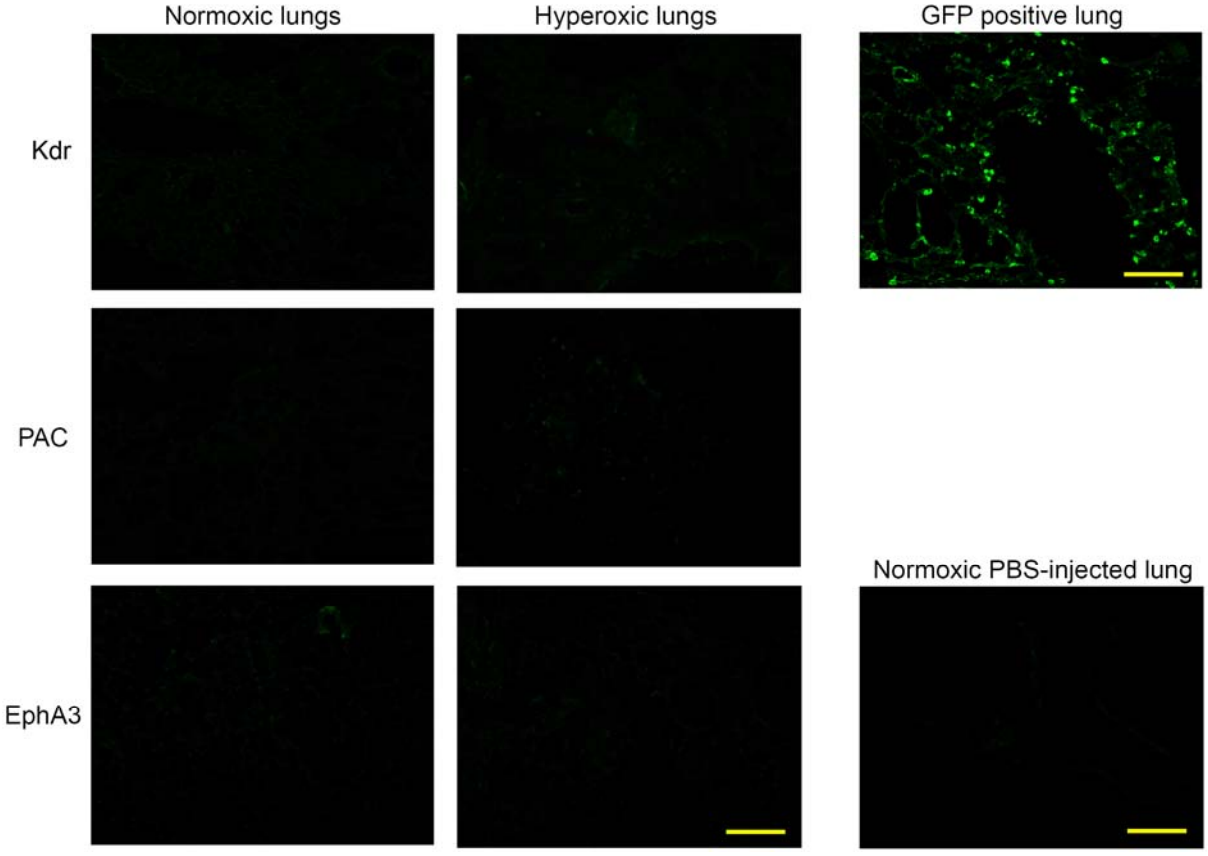

Figure 5.16. No positive signals were observed using immunohistochemistry for GFP on lung sections from injected mice at D28. Lung from GFP+/- mouse was used as a positive control; lung from mouse injected with PBS was used as a negative control. Scale bar = 100 µm.

5.3.9. FISH for the detection of the Y-chromosome

A fluorescent probe was used to observe the presence of the Y-chromosome containing cells in the lungs of female mice that were injected with cells isolated from male mouse bone marrow. Two sections from each group were randomly taken and assessed under a fluorescent microscope. No Y-chromosome signals were observed in selected samples per 5-10x10^4 cells analysed (Fig. 5.17).

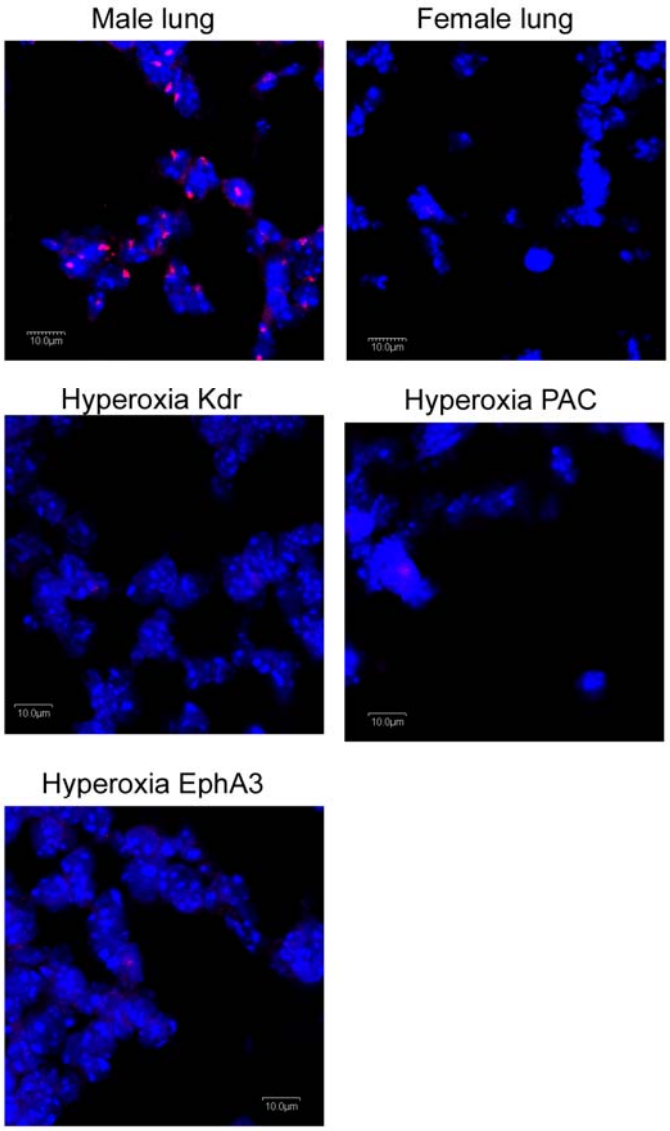

Figure 5.17. Lung sections stained for the Y-chromosome (red) and counterstained with DAPI (blue). Positive control: male lung, negative control: female lung. No positive staining was observed in the cell-injected lung samples. Scale bar = 10 μm.

5.4. Discussion

5.4.1. Comparison of lung parameters after injection of EphA3-enriched cells from different cell passages

EphA3-enriched cell fractions were injected at three different passage numbers. Firstly, passage 8 (P8) cells that were 56 days in culture, were injected into hyperoxia-treated and normoxia mice, followed by P13-15 (91-113 days in culture) cells and finally P12 (77 days in culture) cells. Observations of the lung parameters indicated that the injection of the earlier passages (P8, P12) of cells did not lead to any lump, nodule, abnormal growth, redness or other aberrant structure formation by at least 28 postnatal days (and 56 postnatal days when P12 cells were injected), whereas these structures did develop after the injection of later cell passages (P13-15). Immunohistochemistry for GFP demonstrated sparse GFP signals in hypercellular and condensed tissue areas in the lungs and at the site of injection, after P13-15 cells were injected. This indicates that injected cells have participated in the formation of these lumps. Also these cells had reached the lung via the peritoneum or blood stream and became incorporated into the lung tissue, participating potentially in hyperproliferative activity. Histological analysis of aberrant structures led to the conclusion that these structures are pathological, mostly represented as hyperproliferation and the formation of a disorganised vasculature system (Fig. 5.5), as well as due to the observed high amount of nucleated cells in the blood vessels (Fig. 5.6), which could indicate inflammation. The EphA3 molecule itself could have played a role in this pathological process, since it is associated with vascularisation in cancer (Vail, Tan et al., 2012) and other cancerous tissues (Vearing, Lee et al. 2005). After these findings, it was concluded, that the P13-15 cells cannot be used for cell therapy.

Morphometric parameters of the lung after the injection of EphA3-enriched cells from P8 and P12 were compared (in one set with all other groups) at D28, and variation in these parameters was observed. The number of alveoli after P8 injection was not different from control (Normoxia PBS) in the lungs of hyperoxia-treated mice. However, the number of alveoli after P12 injection into hyperoxia-treated mice was significantly reduced, similarly

to Hyperoxia PBS and all other hyperoxia-treated groups. This could indicate that P8 cells have a greater potential to reduce the hyperoxia-induced decrease in alveolar number (i.e. one of the septation parameters) compared to P12 cells.

Alveolar size was significantly increased, when compared to the control group, in both injected normoxia and hyperoxia-treated mice when either of these two passages of cells was injected. However, when compared to the Hyperoxia PBS group, after P8 cell injection alveolar size was significantly reduced in hyperoxia-treated mice, whereas after P12 cell injection, it was similar. This again indicates, that P8 cells might have a slightly higher potential than P12 cells in restoring septation (in this case, alveolar size reduction) after hyperoxia treatment.

At D28 the number of secondary septa per tissue area was increased after hyperoxia treatment in PBS-injected mice, as well as in hyperoxia-treated and normoxia mice injected with P12 cells, compared to the control group. However, after the injection of P8 cells, the number of secondary septa per tissue area in hyperoxia-treated and normoxia mice was similar to that in the control group. The number of secondary septa represents the progress of septation, which is reduced by hyperoxia treatment, and has been demonstrated to catch up with the control septa number in the adulthood (Chapter 3, Section 3.3.3.2). Therefore, it can be suggested, that the progress of septation slows down and then gradually increases after P12 cells are injected, but returns more quickly to the control number of septa after P8 cell injection.

There were no differences in lung tissue area and blood vessel numbers after P8 and P12 cells were injected into hyperoxia-treated and normoxia mice, compared to the Normoxia PBS group. The other septation parameters (i.e. alveolar size and number) however are essential for indicating the degree of lung structure restoration after hyperoxia, and it can therefore be concluded, that P8 cells could have influenced the process of alveolarisation, as discussed above.

In conclusion, a gradual decrease in therapeutic parameters of EphA3-enriched cells is observed as cells age. Cells from P8 improve some parameters of lung architecture, whereas cells from P12 do not, and cells from P13-15 induce aberrant growth and lump formation. However, enrichment of bone marrow cell population for EphA3 requires a certain period in culture, and aberrant effects of earlier-passaged cells injected in mice were not studied beyond 56 days of age. A balance between cell expansion and enrichment for the desired marker has to be considered, but generally for any possible and associated therapeutic applications long-term cell culture of this cell type should be avoided.

5.4.2. Comparison of lung parameters and protein levels after injection of Kdr cells, EphA3 cells, PACs and PBS

Three different bone marrow-derived cell types have been injected into hyperoxia-treated mice together with control normoxic mice to test for any therapeutic effect and any potential side effects. Some groups displayed partial or full recovery of some morphometric parameters of lung deficit, and this is discussed below.

Out of all the hyperoxia-treated groups, the Hyperoxia Kdr group was the only group that demonstrated a restored alveolar size by D56 compared to control levels (Fig. 5.11). However, in the Normoxia Kdr group alveolar size was increased and this occurred with a parallel reduction in the levels of the 21 kDa Vegfa protein at D28. Reduced Vegfa here may be causal to increased alveolar size. Reduced 42 kDa (dimer) Vegfa levels in the Hyperoxia Kdr group at D28, however, did not cause a reduction in septation at D56. All other morphometric parameters, however, remained normal in the Normoxia Kdr group at all time points. These data could indicate that Kdr cells behave differently in normoxia and hyperoxia-treated mice, potentially inducing septation after hyperoxia treatment, and inhibiting it in normoxia mice.

The injection of plate-adherent cells (PACs) was not associated with changes in lung alveolar size following hyperoxia treatment, although these cells assisted in the recovery of other morphometric parameters. When PACs were injected into normoxic mice, an

increase in the number of blood vessels and a reduction in the amount of 21 kDa Vegfa at D28 were observed. The two events could be related, as the build-up of blood vessels could provide feedback to the organism to reduce the amount of Vegf molecules.

Both hyperoxia-treated and normoxia mice responded quite differently to the injection of EphA3 cells compared to the two other cell types. There was a trend in animal body weight and length reduction from the first to the eighth week of age, as well as an increase in the number of secondary septa. There was an increased alveolar size in both normoxia and hyperoxia-treated mice after EphA3 cell injection at D28, which can explain the increase in secondary septa number that was even higher, than in the Hyperoxia PBS group. These results may indicate that EphA3 cells independently slow down alveolarisation, and after hyperoxia treatment a double-effect can be observed. The Normoxia EphA3 group also had reduced 42kDa Vegfa levels at D28, which might also be related to an increase in secondary septa number.

Generally, most morphometric parameters have recovered in the majority of groups, including Hyperoxia PBS, except for alveolar size. In this parameter Kdr cells were required to slowly achieve recovery after hyperoxia, but had adverse effect in the normoxia group. The Hyperoxia Kdr group also demonstrated recovered alveoli number by D56 (similar to other groups), lung tissue area by D28 (similar to other groups), secondary septa per tissue number by D28 (similar to Hyperoxia PAC group) and blood vessel number by D28 (similar to all other groups). This group therefore can be considered fully recovered in all tested parameters.

5.4.3. Comparison of mouse weight, lung morphometric parameters and protein levels to previous results

Compared to previous experiments in earlier chapters, after PBS injection into hyperoxia-treated mice there was an occasional (for example, week one and week three) reduction in animal weight (and length) during the first weeks after treatment. This suggests that the

hyperoxia treatment reduces body weight in a fashion dependent on other factors. Whether this may be eating habits or general health remains to be investigated.

The number of alveoli and the number of blood vessels per lung section area demonstrated different outcomes in Chapter 3 (normoxia vs hyperoxia) and Chapter 5 (Normoxia PBS vs Hyperoxia PBS) at D56. The number of alveoli was significantly reduced after hyperoxia treatment compared to control; however, was not significantly different, when PBS was injected into both groups. Statistical analysis that included both data sets demonstrated that the significant difference was provided by the large number of alveoli in the normoxia group (Chapter 3), whereas in the Normoxia PBS group (Chapter 5) this number was lower. The number of blood vessels per lung section area was significantly lower in Hyperoxia PBS group, compared to Normoxia PBS group (Chapter 5), but there was no difference between hyperoxia and normoxia groups in this parameter (Chapter 3) at D56. Statistical analysis that included both data sets demonstrated that these results appeared due to mouse-to-mouse variation, and there is no significant difference in blood vessel number at D56, according to the general linear model. These results indicate that in these parameters a higher number of mice might be required for analysis, as individual mouse and litter variations could increase or decrease the standard deviation in the groups.

There was no reduction in the level of Pecam1 at D5, which could be explained by the time of sample collection. It is possible, that Pecam1 protein levels returned to control levels quickly after hyperoxia treatment had stopped. Therefore, a few hours difference between sample collections may influence the observable increase or decrease in the levels of certain proteins, such as Pecam1.

5.4.4. Tracking injected cells *in vivo*

Injected cells could not be observed in the lungs at any time point. No signal from the injected cells (GFP or Y-chromosome) was observed in the lungs three or four weeks after injection, which indicates that the cells had not stayed or engrafted in the lung, but

rather modified lung morphometric characteristics indirectly, for example, by stimulating alveolarisation by promoting septation (EphA3 cells increased the number of secondary septa per lung tissue area at D28 in both normoxia and hyperoxia-treated mice, Kdr cells decreased alveolar size after hyperoxia treatment and increased it in normoxia mice) or vascularisation (plate-adherent cells increased the number of blood vessels by D28 in both normoxia and hyperoxia-treated mice). However, the mechanism that affects lung structure alterations by these cell types remains unknown. It is possible to speculate that secreted cytokines and factors may have assisted recovery *in vivo*, as it was demonstrated or hypothesised in previous studies of the therapeutic application of BM-derived progenitor cells in the lung (Rojas, Xu et al. 2005; Aslam, Baveja et al. 2009). However, it can be assumed, that fresh cells (i.e. freshly isolated from bone marrow, like Kdr cells) assist this recovery faster and more reliably than cultured cells (PAC and EphA3 cells).

In conclusion, freshly-isolated cells, enriched for Vegf receptor 2, Kdr (Flk1), may represent a good candidate for treating the consequences of hyperoxia, such as lung deficit, by improving alveolarisation. The injection of these cells also had no effect on Sftpc levels, and as such from this perspective may be considered a safe treatment.

Chapter 6. General Discussion

In this study, a mouse model of neonatal hyperoxia was developed to assist further studies for the treatment of lung deficit in prematurely born children. The hyperoxia-induced lung deficit described here resulted in a permanent reduction in alveolarisation and a temporary reduction in vascularisation. Relative to untreated controls, alveolar size of hyperoxia-treated mice was increased at all time points examined, while the number of alveoli was correspondingly decreased, which confirms previous findings on alveolar size and number after hyperoxia treatment (Dauger, Ferkdadji et al. 2003). The number of secondary septa (crests) per tissue area significantly decreased at five days of age, and then significantly increased by 28 days of age after hyperoxia treatment, compared to normoxia mice. Studies published earlier report either a decrease (Ozer, Kumral et al. 2005) or no changes (Masood, Yi et al. 2009) in the number of secondary septa per area analysed, but an increase in the number of secondary septa per tissue area after 10-14 days of hyperoxia. According to the current study, the number of secondary septa varies with time after hyperoxia treatment, and indicates a response of the lung to a reduced alveolarisation, that returns to the control levels by D56, demonstrating a compensatory effect at D28. These findings suggest that the number of secondary septa should be analysed in a time-dependent manner, at least until early adulthood.

The number of blood vessels per lung section area (0.564mm^2) in hyperoxia-treated mice decreased relative to untreated controls only at five days of age with an apparent over-compensatory catch-up phase between D5 and D28, when measured per tissue area. There are studies, describing both a reduction (Balasubramaniam, Mervis et al. 2007) and no effect (Ozer, Kumral et al. 2005) on the number of blood vessels per section area after neonatal hyperoxia exposure. However, these differences might be observed due to variations in the methods used, i.e. different time in hyperoxia (ten days) as well as different approach to blood vessel detection (vWF or Pecam1 immunoreactivity, respectively). In the current study not only were both parameters described (the blood vessel number per section area and per tissue area), but also the recovery process

between D5 and D56 *postpartum* (Chapter 3, Section 3.3.5). In Chapter 5, however, data at D56 displayed a significant decrease in the number of blood vessels per section area (Section 5.3.6), according to Dunnett's posthoc, which was not applied in Chapter 3. Therefore, it can be concluded, that there is a trend in blood vessel number reduction after hyperoxia at D56, and increasing the number of animals per group to further verify this should be considered.

No significant reduction in animal body weight was observed after hyperoxia treatment without injections, and occasional weight loss was observed after PBS injection. However, there are reports of both weight loss with the mother rotation procedure (Ozer, Kumral et al. 2005) and no weight loss without the rotation procedure (Balasubramaniam, Mervis et al. 2007) after longer hyperoxia exposure (more than ten days). As discussed in Chapter 5 (Section 5.4.3), in this study the occasional differences in animal body weight could be assigned to animals personal eating habits, which would depend on animal stress levels during the week. Stress might be caused by various conditions (i.e. animal handling methods, litter size or the number of times the cages were opened), and it is therefore essential to keep them consistent between animal groups. However, it can be concluded, that hyperoxia has no long-term effect on animal body weight, since occasional weight reduction in this study did not persist to adulthood, which was reported in the previous studies mentioned above.

Furthermore, after four days of 90% oxygen treatment, no lung fibrosis or collagen deposits were observed, unlike in other published reports, where long-term treatment (i.e. 11-20 days of hyperoxia) does result in fibrosis (Ozer, Kumral et al. 2005; Mataloun, Rebello et al. 2006). The novelty of the current study was the examination of alveolarisation and vascularisation at different stages during the 56 day post-treatment period. This has provided a dynamic picture of the injury model and thus permitted a greater reconciliation of the changes to vascularisation and alveolarisation deficits. This model can be considered ethically safe as it represents the effects of hyperoxia on the most important parameters of lung architecture, but does not involve overt pathologic changes to the animal lung, or animal weight loss or death.

Various therapeutic approaches have been considered during the current study. Based on previous publications and studies published during the course of this work, it was considered, that endothelial progenitor cells (EPCs) may represent a good therapeutic tool for treating hyperoxia-induced neonatal lung deficit (Balasubramaniam, Mervis et al. 2007; Balasubramaniam, Ryan et al. 2010). Isolation and enrichment of bone marrow cells for specific EPC markers were first optimised. BM cells were magnetically sorted for the four well-known EPC markers (Kdr, Tek, Mcam and Prom1), as well as for a hypothesised EPC and mesenchymal marker (EphA3), and then tested for their capacity to differentiate into endothelial cells and form blood vessel-like structures *in vitro*. Kdr was selected as the most relevant EPC marker for freshly-isolated cells, based on (i) the consistency of Kdr^+ cells in $Pecam1^+$ vessel-like structure formation *in vitro* in reaction to Vegf and (ii) its ability to specifically delineate a BM cell subpopulation with significantly greater vessel-like forming capability compared to remaining BM cells. $EphA3^+$ cells were selected based on their previously discovered association with vascularisation (Vail, Tan et al. 2012). EphA3 is also known to bind to ephrin-B2 molecule, which is expressed in the lung, and of relevance, it has been recently discovered that ephrin-B2 is essential in protecting the lung from alveolar deficiency and promoting alveolar growth after hyperoxia treatment (Cerretti, Bos et al. 1995; Vadivel, van Haaften et al. 2012). To compare cell engraftment efficiency, plate-adherent cells (PACs) from passage 0 were used, based on previous reports regarding the potential of these cells for therapeutic purposes (Silva, Litovsky et al. 2005; Aslam, Baveja et al. 2009; van Haaften, Byrne et al. 2009). All selected cell types (Kdr^+, $EphA3^+$ and PACs) demonstrated *in vitro* vessel-like structure formation in response to Vegf, and these cells when isolated from $GFP^{+/-}$ mice retained GFP activity (although to varying extents) in differentiated cells during culture.

Kdr+, EphA3+ and PAC cell suspensions were applied to the neonatal hyperoxia-treated and normoxia neonatal mouse lungs by intraperitoneal injection. The effects of these cell groups were subsequently assayed by comparing lung morphometric and molecular parameters at different post-treatment stages to PBS (sham) injected controls by either ANOVA or general linear model followed by Dunnet's posthoc, and comparing groups to each other by the same tests followed by Student Newman-Keuls posthoc. It was demonstrated that earlier passage $EphA3^+$ cells (P8) assist morphometric lung recovery

more efficiently than later passage EphA3$^+$ cells (P12, P13-15), i.e. assist the increase in the number of alveoli after hyperoxia (Table 6.1). All younger cell types (uncultured Kdr$^+$ cells, P0 and P8 cells) assisted the decrease in the number of secondary septa per tissue area, returning to control levels by D28, whereas P12 cell injection resulted in the increased number of secondary septa per tissue area after both hyperoxia treatment and normoxia (Table 6.1). Moreover, older cell populations (P13-15) reached senescence *in vitro* and induced abnormal growth and aberrant structure formation when injected *in vivo*. These findings confirm, that the longer cells are expanded in culture, the higher is their chance to undergo chromosomal mutations or loss of tumour suppression function (Ahrlund-Richter, De Luca et al. 2009). A comparison of uncultured (Kdr$^+$) and cultured cells (all other types) demonstrated alveolar size reduction after uncultured cell injection which indicates the increase in alveolarisation (Table 6.1). This confirmed the hypothesis that even a short time in culture might influence certain cellular properties, such as marker expression and the capacity of cells to grow and differentiate, which was suggested in earlier studies (Boquest, Shahdadfar et al. 2005). In comparing earlier (P0) and later (P8, P12, P13-15) passages, it could be suggested that differentiation potential is reduced over time in culture (lower Pecam1 immunoreactivity in vessel-like structures or abnormal structures) and corresponds with a tendency of cells to senesce (Table 6.1), which also confirms previous findings in adipose stem cells (Noer, Boquest et al. 2007). EphA3 might be a promising marker; however, given the difficulties of cell enrichment for EphA3, it could be a challenge to isolate EphA3$^+$ cells for therapeutic purposes, as they would require a constant cytogenetic control.

Kdr+ cells injection into mice treated with hyperoxia led to promising results in terms of lung architecture recovery, i.e. alveolar size reduction. However, when injected into normoxic mice, these cells had a reversed effect on this parameter. These cells therefore could be therapeutically valuable only in the presence of lung deficit, but in its absence further considerations are required.

Cell type/ Cell characteristics	Uncultured and enriched (Kdr^+)	Passage 0 (PAC)	Passage 8 ($EphA3^+$)	Passage 12 (frozen/thawed/ $EphA3^+$)	Passage 13-15 ($EphA3^+$)
In vitro characteristics					
Time in culture (Days)	0	7-10	56	77	91-98
Vessel formation	Medium	Low	High	High	Abnormal (aggregates)
Pecam1-immunoreactivity in vessel-like structures	High	Medium	Low	Low	N/A
In vivo characteristics					
Alteration of alveolar size after normoxia or hyperoxia	Decrease (hyperoxia), increase (normoxia)	No changes	Increase (normoxia)	Increase (normoxia)	N/A, aberrant growth formation, increase in the number of nucleated cells in the bloodstream
Alteration of the number of alveoli after normoxia or hyperoxia	No changes	No changes	Increase (hyperoxia)	No changes	
Alteration of the lung tissue area after normoxia or hyperoxia	No changes	No changes	No changes	No changes	
Alteration of the number of secondary septa per tissue area after normoxia or hyperoxia	Decrease (hyperoxia)	Decrease (hyperoxia)	Decrease (hyperoxia)	Increase (hyperoxia and normoxia)	
Alteration in the number of pulmonary blood after normoxia or hyperoxia	No changes	Increase (hyperoxia and normoxia)	No changes	No changes	

Table 6.1. Characteristics of all tested cell types depending on their time in culture. For passage 8 and passage 13-15 cells only 28 day *in vivo* analysis is presented, for all other groups – 28 and 56 day *in vivo* analysis is presented. All *in vivo* alterations are indicated in relation to either Normoxia PBS (normoxia) or Hyperoxia PBS (hyperoxia) groups. A potential therapeutic effect, i.e. returning a specific parameter from hyperoxia to control level, is underlined.

Plate-adherent cells that were cultured for a short period of time, affected vascularisation parameters, but did not assist in the recovery of alveolarisation after hyperoxia, as compared parameters were always similar to those in the Hyperoxia PBS group

(Appendices, Section I), which contradicts previous findings (Aslam, Baveja et al. 2009; van Haaften, Byrne et al. 2009). This could be explained by the relatively low number of cells used for injection in the current study (less than $2x10^4$ cells per animal) or by a different delivery method (intraperitoneal rather than intratracheal or intravenous injection). However, PACs served ultimately as a relevant control group testing method efficiency in terms of the delivery of other cell types, such as Kdr^+ cells, which assisted recovery of lung parameters (i.e. same cell number and type of injection were used).

The mechanism of structural improvements in the lungs after EPC injection remains unknown. Our studies shed some light on this mechanism, suggesting that EPCs might influence alveolarisation via paracrine effects, as the injected cell signals for GFP and the Y chromosome, and therefore the engraftment, were not detected in the lung, blood, or liver. Since vascularisation (i.e. the number of blood vessels per area) recovers shortly after hyperoxia treatment (by 28 days) it can be expected that EPCs might engraft into developing pulmonary blood vessels between D5 and D28. However, this effect is not observed, possibly due to low cell numbers injected or an efficient response to hyperoxia treatment prior to cell injection. Moreover, it was previously demonstrated, that BM-derived cells play mainly a supporting role in growing vasculature, but do not incorporate into the vessels (Ziegelhoeffer, Fernandez et al. 2004). However, they might still assist alveolarisation via the production of differentiation factors for alveolar type II cells and by inducing alveolar growth (Yamamoto, Yun et al. 2007). Initial vascular deficit is likely to be replaced by host own EPCs, and therefore injection of additional EPCs might re-fill EPC pools and promote lung recovery via additional stimulating of septation.

Despite the fact that injected cells were not detected engrafting in the lung, the significant alterations in morphometric parameters were still observed. Some cell types have affected lung structure by returning morphometric parameters to the control (normoxia) levels after mice were treated with hyperoxia, such as the reduction in the number of secondary septa per tissue area at D28 (Kdr^+, P0 and P8 $EphA3^+$ cells), the increase in the number of alveoli at D28 (P8 $EphA3^+$ cells) and the reduction in the alveolar size at D56 (Kdr^+ cells; Table 6.1, underlined). All other parameter alterations are likely to have been induced as

an over-reaction or under-reaction to the injected cells, for example the increase in the alveolar size in normoxic mice after Kdr^+, P8 and P12 $EphA3^+$ cells were injected, the increase in the number of secondary septa per tissue area in both normoxic and hyperoxic mice, after P12 $EphA3^+$ cells were injected, and finally, the increase in the number of blood vessels, after P0 PACs were injected (Table 6.1, *in vivo* parameters that are not underlined). It can therefore be concluded, that all tested cell types demonstrate certain side effects after injection into normoxia mice. However, Kdr^+ and P8 $EphA3^+$ cells assist alveolarisation after hyperoxia, returning important parameters of lung architecture (i.e. alveolar size and number) to the control levels, and therefore providing a therapeutic benefit to the hyperoxia-treated lung.

In this study, a neonatal hyperoxia model was established, and the associated lung deficit and its long-term recovery process were characterised. BM-derived Kdr^+ and early (P8) $EphA3^+$ EPC subpopulations were demonstrated to promote the recovery of the long-term effects of hyperoxia, such as lung alveolarisation. Further analysis of such cell types may lead to their clinical application for the treatment of hyperoxia-induced pulmonary deficit or injury in prematurely born children.

References

Abe, S., C. Boyer, et al. (2004). "Cells Derived from the Circulation Contribute to the Repair of Lung Injury." Am J Respir Crit Care Med **170**(11): 1158-1163.

Abe, S., G. Lauby, et al. (2003). "Transplanted BM and BM side population cells contribute progeny to the lung and liver in irradiated mice." Cytotherapy **5**(6): 523-533.

Aguilar, S., E. Nye, et al. (2007). "Murine but not human mesenchymal stem cells generate osteosarcoma-like lesions in the lung." Stem Cells **25**(6): 1586-1594.

Ahlbrecht, K., J. Schmitz, et al. (2008). "Spatiotemporal Expression of flk-1 in Pulmonary Epithelial Cells during Lung Development." American Journal of Respiratory Cell and Molecular Biology **39**(2): 163-170.

Ahrlund-Richter, L., M. De Luca, et al. (2009). "Isolation and production of cells suitable for human therapy: challenges ahead." Cell Stem Cell **4**(1): 20-26.

Albelda, S. M., P. D. Oliver, et al. (1990). "EndoCAM: a novel endothelial cell-cell adhesion molecule." The Journal of Cell Biology **110**(4): 1227-1237.

Albera, C., J. M. Polak, et al. (2005). "Repopulation of human pulmonary epithelium by bone marrow cells: a potential means to promote repair." Tissue Eng **11**(7-8): 1115-1121.

Albertine, K. H., Pysher, T.J. (2004). Pulmonary consequences of preterm birth. The Lung: Development, aging and environment. P. Harding R., K.E., Plopper, C.G. London, Elsevier Academic Press**:** 237-251.

Alcorn, D. G., T. M. Adamson, et al. (1981). "A morphologic and morphometric analysis of fetal lung development in the sheep." Anat Rec **201**(4): 655-667.

Aliotta, J. M., M. Passero, et al. (2005). "Stem cells and pulmonary metamorphosis: New concepts in repair and regeneration." Journal of Cellular Physiology **204**(3): 725-741.

Allison, B. J., K. J. Crossley, et al. (2010). "Ventilation and oxygen: dose-related effects of oxygen on ventilation-induced lung injury." Pediatr Res **67**(3): 238-243.

Altin, J. G. and E. K. Sloan (1997). "The role of CD45 and CD45-associated molecules in T cell activation." Immunol Cell Biol **75**(5): 430-445.

Anjos-Afonso, F., E. K. Siapati, et al. (2004). "In vivo contribution of murine mesenchymal stem cells into multiple cell-types under minimal damage conditions." Journal of Cell Science **117**(23): 5655-5664.

Asahara, T., H. Masuda, et al. (1999). "Bone Marrow Origin of Endothelial Progenitor Cells Responsible for Postnatal Vasculogenesis in Physiological and Pathological Neovascularization." Circulation Research **85**(3): 221-228.

Asahara, T., T. Takahashi, et al. (1999). "VEGF contributes to postnatal neovascularization by mobilizing bone marrow-derived endothelial progenitor cells." EMBO J **18**(14): 3964-3972.

Aslam, M., R. Baveja, et al. (2009). "Bone marrow stromal cells attenuate lung injury in a murine model of neonatal chronic lung disease." Am J Respir Crit Care Med **180**(11): 1122-1130.

Balasubramaniam, V., C. F. Mervis, et al. (2007). "Hyperoxia reduces bone marrow, circulating, and lung endothelial progenitor cells in the developing lung: implications for the pathogenesis of bronchopulmonary dysplasia." American Journal of Physiology - Lung Cellular and Molecular Physiology **292**(5): L1073-L1084.

Balasubramaniam, V., S. L. Ryan, et al. (2010). "Bone marrow-derived angiogenic cells restore lung alveolar and vascular structure after neonatal hyperoxia in infant mice." Am J Physiol Lung Cell Mol Physiol **298**(3): L315-323.

Baumhueter, S., N. Dybdal, et al. (1994). "Global vascular expression of murine CD34, a sialomucin-like endothelial ligand for L-selectin." Blood **84**(8): 2554-2565.

Beck, H., R. Voswinckel, et al. (2003). "Participation of Bone Marrow-Derived Cells in Long-Term Repair Processes After Experimental Stroke." J Cereb Blood Flow Metab **23**(6): 709-717.

Berenson, R. J., R. G. Andrews, et al. (1988). "Antigen CD34+ marrow cells engraft lethally irradiated baboons." J Clin Invest **81**(3): 951-955.

Bernanke, D. H. and R. R. Markwald (1982). "Migratory behavior of cardiac cushion tissue cells in a collagen-lattice culture system." Developmental Biology **91**(2): 235-245.

Bertolini, F., Y. Shaked, et al. (2006). "The multifaceted circulating endothelial cell in cancer: towards marker and target identification." Nat Rev Cancer **6**(11): 835-845.

Blackburn, M. R., J. B. Volmer, et al. (2000). "Metabolic Consequences of Adenosine Deaminase Deficiency in Mice Are Associated with Defects in Alveogenesis, Pulmonary Inflammation, and Airway Obstruction." The Journal of Experimental Medicine **192**(2): 159-170.

Boquest, A. C., A. Shahdadfar, et al. (2005). "Isolation and Transcription Profiling of Purified Uncultured Human Stromal Stem Cells: Alteration of Gene Expression after In Vitro Cell Culture." Molecular Biology of the Cell **16**(3): 1131-1141.

Bruce, M. C., E. N. Bruce, et al. (1993). "Hyperoxic exposure of developing rat lung decreases tropoelastin mRNA levels that rebound postexposure." Am J Physiol **265**(3 Pt 1): L293-300.

Burnham, E. and M. Moss (2006). "Progenitor cells in acute lung injury." Minerva Anestesiol **72**(6): 369-374.

Burri, P. H. (1974). "The postnatal growth of the rat lung. 3. Morphology." Anat Rec **180**(1): 77-98.

Burri, P. H. (1997). Structural aspects of prenatal and postnatal development and growth of the lung. Lung Growth and Development. New York, Marcel Decker**:** 1-35.

Burri, P. H. (2006). "Structural aspects of postnatal lung development - alveolar formation and growth." Biol Neonate **89**(4): 313-322.

Burri, P. H. and V. Djonov (2002). "Intussusceptive angiogenesis—the alternative to capillary sprouting." Molecular Aspects of Medicine **23**(6, Supplement): 1-27.

Cerretti, D. P., T. V. Bos, et al. (1995). "Isolation of LERK-5: A ligand of the eph-related receptor tyrosine kinases." Molecular Immunology **32**(16): 1197-1205.

Chamoto, K., B. C. Gibney, et al. (2012). "CD34^sup +^ Progenitor to Endothelial Cell Transition in Post-Pneumonectomy Angiogenesis." American Journal of Respiratory Cell and Molecular Biology **46**(3): 283-289.

Chang, J. C., R. Summer, et al. (2005). "Evidence that bone marrow cells do not contribute to the alveolar epithelium." Am J Respir Cell Mol Biol **33**(4): 335-342.

Chun-mao, H., W. Su-yi, et al. (2007). "Human bone marrow-derived mesenchymal stem cells differentiate into epidermal-like cells in vitro." Differentiation **75**(4): 292-298.

Covas, D. T., R. A. Panepucci, et al. (2008). "Multipotent mesenchymal stromal cells obtained from diverse human tissues share functional properties and gene-expression profile with CD146+ perivascular cells and fibroblasts." Experimental hematology **36**(5): 642-654.

Dauger, S., L. Ferkdadji, et al. (2003). "Neonatal exposure to 65% oxygen durably impairs lung architecture and breathing pattern in adult mice." Chest **123**(2): 530-538.

Davis, S., T. H. Aldrich, et al. (1996). "Isolation of Angiopoietin-1, a Ligand for the TIE2 Receptor, by Secretion-Trap Expression Cloning." Cell **87**(7): 1161-1169.

Delia, D., M. Lampugnani, et al. (1993). "CD34 expression is regulated reciprocally with adhesion molecules in vascular endothelial cells in vitro." Blood **81**(4): 1001-1008.

Deng, H., S. NicholasMason, et al. (2000). "Lung Inflammation in Hyperoxia Can Be Prevented By Antichemokine Treatment in Newborn Rats." Am J Respir Crit Care Med **162**(6): 2316-2323.

Deschaseaux, F., Z. Selmani, et al. (2007). "Two types of circulating endothelial progenitor cells in patients receiving long term therapy by HMG-CoA reductase inhibitors." European Journal of Pharmacology **562**(1–2): 111-118.

Dombrowsky, H., T. Tschernig, et al. (2006). "Molecular and functional changes of pulmonary surfactant in response to hyperoxia." Pediatr Pulmonol **41**(11): 1025-1039.

Dumont, D. J., G. Gradwohl, et al. (1994). "Dominant-negative and targeted null mutations in the endothelial receptor tyrosine kinase, tek, reveal a critical role in vasculogenesis of the embryo." Genes & Development **8**(16): 1897-1909.

Elshal, M. F., S. S. Khan, et al. (2005). "CD146 (Mel-CAM), an adhesion marker of endothelial cells, is a novel marker of lymphocyte subset activation in normal peripheral blood." Blood **106**(8): 2923-2924.

Engelhardt, J. F. (2001). "Stem Cell Niches in the Mouse Airway." American Journal of Respiratory Cell and Molecular Biology **24**(6): 649-652.

Fehrenbach, H., R. Voswinckel, et al. (2008). "Neoalveolarisation contributes to compensatory lung growth following pneumonectomy in mice." Eur Respir J **31**(3): 515-522.

Firsova, A., T. Hyakumura, et al. (2010). Epithelial-mesenchymal interactions during lung development and their potential relevance to lung repair. Cell therapy for lung disease. J. Polak. London, UK, Imperial College Press**:** pp. 91-124.

Fu, J. H., X. D. Xue, et al. (2008). "[Expression of HoxB5 mRNA and their effect on lung development in premature rats with hyperoxia-induced chronic lung disease]." Zhonghua Er Ke Za Zhi **46**(7): 540-543.

Gang, E. J., D. Bosnakovski, et al. (2007). "SSEA-4 identifies mesenchymal stem cells from bone marrow." Blood **109**(4): 1743-1751.

Gehling, U. M., S. Ergün, et al. (2000). "In vitro differentiation of endothelial cells from AC133-positive progenitor cells." Blood **95**(10): 3106-3112.

Grove, J. E., C. Lutzko, et al. (2002). "Marrow-Derived Cells as Vehicles for Delivery of Gene Therapy to Pulmonary Epithelium." American Journal of Respiratory Cell and Molecular Biology **27**(6): 645-651.

Hanahan, D. (1997). "Signaling vascular morphogenesis and maintenance." Science **277**(5322): 48-50.

Harding, R. and S. B. Hooper (1996). "Regulation of lung expansion and lung growth before birth." J Appl Physiol **81**(1): 209-224.

Hitka, P., M. Cerny, et al. (2004). "Assessment of exhaled gases in ventilated preterm infants." Physiol Res **53**(5): 561-564.

Holmes, K., O. L. Roberts, et al. (2007). "Vascular endothelial growth factor receptor-2: Structure, function, intracellular signalling and therapeutic inhibition." Cellular Signalling **19**(10): 2003-2012.

Ingbar, D. H. (2000). "Mechanisms of repair and remodeling following acute lung injury." Clin Chest Med **21**(3): 589-616.

Ionescu, L. I., R. S. Alphonse, et al. (2012). "Airway delivery of soluble factors from plastic-adherent bone marrow cells prevents murine asthma." Am J Respir Cell Mol Biol **46**(2): 207-216.

Ishizawa, K., H. Kubo, et al. (2004). "Bone marrow-derived cells contribute to lung regeneration after elastase-induced pulmonary emphysema." FEBS letters **556**(1): 249-252.

Jaffe, E. A., L. W. Hoyer, et al. (1974). "Synthesis of von Willebrand Factor by Cultured Human Endothelial Cells." Proceedings of the National Academy of Sciences **71**(5): 1906-1909.

Jobe, A. H. and E. Bancalari (2001). "Bronchopulmonary dysplasia." Am J Respir Crit Care Med **163**(7): 1723-1729.

Johnston, C. J., G. W. Mango, et al. (1997). "Altered pulmonary response to hyperoxia in Clara cell secretory protein deficient mice." Am J Respir Cell Mol Biol **17**(2): 147-155.

Johnston, C. J., T. W. Wright, et al. (1997). "Comparison of adult and newborn pulmonary cytokine mRNA expression after hyperoxia." Exp Lung Res **23**(6): 537-552.

Kahler, C., J. Wechselberger, et al. (2007). "Peripheral infusion of rat bone marrow derived endothelial progenitor cells leads to homing in acute lung injury." Respiratory Research **8**(1): 50.

Kajstura, J., M. Rota, et al. (2011). "Evidence for human lung stem cells." N Engl J Med **364**(19): 1795-1806.

Kalka, C., H. Tehrani, et al. (2000). "VEGF gene transfer mobilizes endothelial progenitor cells in patients with inoperable coronary disease." The Annals of Thoracic Surgery **70**(3): 829-834.

Kang, Y., F. Wang, et al. (2006). "Knockdown of CD146 reduces the migration and proliferation of human endothelial cells." Cell Res **16**(3): 313-318.
Kasahara, Y., R. M. Tuder, et al. (2000). "Inhibition of VEGF receptors causes lung cell apoptosis and emphysema." The Journal of Clinical Investigation **106**(11): 1311-1319.
Kauffman, S. L., P. H. Burri, et al. (1974). "The postnatal growth of the rat lung. II. Autoradiography." Anat Rec **180**(1): 63-76.
Khakoo, A. Y. and T. Finkel (2004). "Endothelial Progenitor Cells*." Annual Review of Medicine **56**(1): 79-101.
Kim, T.-H., Y.-H. Chow, et al. (2012). "Effect of IGF Blockade on Hyperoxia-Induced Lung Injury." American Journal of Respiratory Cell and Molecular Biology.
Kotton, D. N., B. Y. Ma, et al. (2001). "Bone marrow-derived cells as progenitors of lung alveolar epithelium." Development **128**(24): 5181-5188.
Krause, D., T. Ito, et al. (1994). "Characterization of murine CD34, a marker for hematopoietic progenitor and stem cells." Blood **84**(3): 691-701.
Krause, D. S., N. D. Theise, et al. (2001). "Multi-Organ, Multi-Lineage Engraftment by a Single Bone Marrow-Derived Stem Cell." Cell **105**(3): 369-377.
Kumar, B. M., J. G. Yoo, et al. (2007). "In vitro differentiation of mesenchymal progenitor cells derived from porcine umbilical cord blood." Mol Cells **24**(3): 343-350.
Kunig, A. M., V. Balasubramaniam, et al. (2005). "Recombinant human VEGF treatment enhances alveolarization after hyperoxic lung injury in neonatal rats." Am J Physiol Lung Cell Mol Physiol **289**(4): L529-535.
Lackmann, M., R. J. Mann, et al. (1997). "Ligand for EPH-related Kinase (LERK) 7 Is the Preferred High Affinity Ligand for the HEK Receptor." Journal of Biological Chemistry **272**(26): 16521-16530.
Lackmann, M., A. C. Oates, et al. (1998). "Distinct Subdomains of the EphA3 Receptor Mediate Ligand Binding and Receptor Dimerization." Journal of Biological Chemistry **273**(32): 20228-20237.
Langford, D. J., A. L. Bailey, et al. (2010). "Coding of facial expressions of pain in the laboratory mouse." Nat Meth **7**(6): 447-449.
MacPherson, H., P. Keir, et al. (2005). "Bone marrow-derived SP cells can contribute to the respiratory tract of mice in vivo." Journal of Cell Science **118**(11): 2441-2450.
Maniscalco, W. M., R. H. Watkins, et al. (1995). "Vascular endothelial growth factor mRNA increases in alveolar epithelial cells during recovery from oxygen injury." Am J Respir Cell Mol Biol **13**(4): 377-386.
Masood, A., M. Yi, et al. (2009). "Therapeutic effects of hypercapnia on chronic lung injury and vascular remodeling in neonatal rats." American Journal of Physiology - Lung Cellular and Molecular Physiology **297**(5): L920-L930.
Massaro, G. D. and D. Massaro (1992). "Formation of alveoli in rats: postnatal effect of prenatal dexamethasone." Am J Physiol **263**(1 Pt 1): L37-41.
Massaro, G. D. and D. Massaro (1996). "Postnatal treatment with retinoic acid increases the number of pulmonary alveoli in rats." Am J Physiol **270**(2 Pt 1): L305-310.
Massaro, G. D. and D. Massaro (1997). "Retinoic acid treatment abrogates elastase-induced pulmonary emphysema in rats." Nat Med **3**(6): 675-677.
Mataloun, M. M., C. M. Rebello, et al. (2006). "Pulmonary responses to nutritional restriction and hyperoxia in premature rabbits." J Pediatr (Rio J) **82**(3): 179-185.
Mattsson, J., M. Jansson, et al. (2004). "Lung epithelial cells and type II pneumocytes of donor origin after allogeneic hematopoietic stem cell transplantation." Transplantation **78**(1): 154-157.
May, T., P. P. Mueller, et al. (2005). "Establishment of murine cell lines by constitutive and conditional immortalization." Journal of Biotechnology **120**(1): 99-110.
McGowan, S. E. (1992). "Extracellular matrix and the regulation of lung development and repair." FASEB J **6**(11): 2895-2904.

McGowan, S. E., Snyder, J.M. (2004). Development of alveoli. The Lung: Development, aging and environment. P. R. Harding, K.E., Plopper, C.G. London, Elsevier Academic Press**:** 55-73.
Medici, D., E. M. Shore, et al. (2010). "Conversion of vascular endothelial cells into multipotent stem-like cells." Nat Med **16**(12): 1400-1406.
Miraglia, S., W. Godfrey, et al. (1997). "A Novel Five-Transmembrane Hematopoietic Stem Cell Antigen: Isolation, Characterization, and Molecular Cloning." Blood **90**(12): 5013-5021.
Mizrak, D., M. Brittan, et al. (2008). "CD133: molecule of the moment." The Journal of Pathology **214**(1): 3-9.
Nachman, R., R. Levine, et al. (1977). "Synthesis of Factor VIII Antigen by Cultured Guinea Pig Megakaryocytes." The Journal of Clinical Investigation **60**(4): 914-921.
Newman, P. J. (1997). "The biology of PECAM-1." J Clin Invest **100**(11 Suppl): S25-29.
Ng, Y. S., R. Rohan, et al. (2001). "Differential expression of VEGF isoforms in mouse during development and in the adult." Developmental Dynamics **220**(2): 112-121.
Noer, A., A. Boquest, et al. (2007). "Dynamics of adipogenic promoter DNA methylation during clonal culture of human adipose stem cells to senescence." BMC Cell Biology **8**(1): 18.
Oates, A. C., M. Lackmann, et al. (1999). "An early developmental role for eph-ephrin interaction during vertebrate gastrulation." Mech Dev **83**(1-2): 77-94.
Olsson, F., M. Denham, et al. (2007). "Deriving respiratory cell types from stem cells." Curr Stem Cell Res Ther **2**(3): 197-208.
Orkin, S. H. (2000). "Diversification of haematopoietic stem cells to specific lineages." Nat Rev Genet **1**(1): 57-64.
Ortiz, L. A., F. Gambelli, et al. (2003). "Mesenchymal stem cell engraftment in lung is enhanced in response to bleomycin exposure and ameliorates its fibrotic effects." Proceedings of the National Academy of Sciences **100**(14): 8407-8411.
Ozer, E. A., A. Kumral, et al. (2005). "Effects of erythropoietin on hyperoxic lung injury in neonatal rats." Pediatr Res **58**(1): 38-41.
Panos, R. J., P. M. Bak, et al. (1995). "Intratracheal instillation of keratinocyte growth factor decreases hyperoxia-induced mortality in rats." The Journal of Clinical Investigation **96**(4): 2026-2033.
Patan, S. (1998). "TIE1 and TIE2 receptor tyrosine kinases inversely regulate embryonic angiogenesis by the mechanism of intussusceptive microvascular growth." Microvasc Res **56**(1): 1-21.
Patel, A., B. Fine, et al. (2006). "Elastin biosynthesis: The missing link in tissue-engineered blood vessels." Cardiovasc Res **71**(1): 40-49.
Quirici, N., D. Soligo, et al. (2001). "Differentiation and expansion of endothelial cells from human bone marrow CD133+ cells." British Journal of Haematology **115**(1): 186-194.
Reimann, I. and S. B. Christensen (1977). "A histological demonstration of nerves in subchondral bone." Acta Orthop Scand **48**(4): 345-352.
Rochefort, G. Y., P. Vaudin, et al. (2005). "Influence of hypoxia on the domiciliation of Mesenchymal Stem Cells after infusion into rats: possibilities of targeting pulmonary artery remodeling via cells therapies?" Respiratory Research **6**(1): 125.
Rogers, I. and R. F. Casper (2004). "Umbilical cord blood stem cells." Best Pract Res Clin Obstet Gynaecol **18**(6): 893-908.
Rojas, M., J. Xu, et al. (2005). "Bone marrow-derived mesenchymal stem cells in repair of the injured lung." Am J Respir Cell Mol Biol **33**(2): 145-152.
Sadler, J. E. (1998). "BIOCHEMISTRY AND GENETICS OF VON WILLEBRAND FACTOR." Annual Review of Biochemistry **67**(1): 395-424.
Sato, A., A. Iwama, et al. (1998). "Characterization of TEK receptor tyrosine kinase and its ligands, Angiopoietins, in human hematopoietic progenitor cells." International Immunology **10**(8): 1217-1227.

Sato, T. N., Y. Qin, et al. (1993). "Tie-1 and tie-2 define another class of putative receptor tyrosine kinase genes expressed in early embryonic vascular system." Proceedings of the National Academy of Sciences **90**(20): 9355-9358.

Schniedermann, J., M. Rennecke, et al. (2010). "Mouse lung contains endothelial progenitors with high capacity to form blood and lymphatic vessels." BMC Cell Biology **11**(1): 50.

Schwarz, M., M. Lee, et al. (1999). "EMAP II: a modulator of neovascularization in the developing lung." Am J Physiol **276**(2 Pt 1): L365-375.

Sekiguchi, H., M. Ii, et al. (2011). "Improved Culture-Based Isolation of Differentiating Endothelial Progenitor Cells from Mouse Bone Marrow Mononuclear Cells." PLoS ONE **6**(12): e28639.

Shalaby, F., J. Rossant, et al. (1995). "Failure of blood-island formation and vasculogenesis in Flk-1-deficient mice." Nature **376**(6535): 62-66.

Shibuya, M. (2006). "Differential roles of vascular endothelial growth factor receptor-1 and receptor-2 in angiogenesis." J Biochem Mol Biol **39**(5): 469-478.

Silva, G. V., S. Litovsky, et al. (2005). "Mesenchymal Stem Cells Differentiate into an Endothelial Phenotype, Enhance Vascular Density, and Improve Heart Function in a Canine Chronic Ischemia Model." Circulation **111**(2): 150-156.

Spees, J. L., M. J. Whitney, et al. (2008). "Bone marrow progenitor cells contribute to repair and remodeling of the lung and heart in a rat model of progressive pulmonary hypertension." FASEB J **22**(4): 1226-1236.

Spooner, B. S. and N. K. Wessells (1970). "Mammalian lung development: interactions in primordium formation and bronchial morphogenesis." J Exp Zool **175**(4): 445-454.

Stephen, L. J., A. L. Fawkes, et al. (2007). "A critical role for the EphA3 receptor tyrosine kinase in heart development." Developmental Biology **302**(1): 66-79.

Suratt, B. T., C. D. Cool, et al. (2003). "Human Pulmonary Chimerism after Hematopoietic Stem Cell Transplantation." Am J Respir Crit Care Med **168**(3): 318-322.

Thebaud, B. and S. H. Abman (2007). "Bronchopulmonary dysplasia: where have all the vessels gone? Roles of angiogenic growth factors in chronic lung disease." Am J Respir Crit Care Med **175**(10): 978-985.

Tomashefski, J. F., Jr. (2000). "Pulmonary pathology of acute respiratory distress syndrome." Clin Chest Med **21**(3): 435-466.

Tropea, K. A., E. Leder, et al. (2012). "Bronchioalveolar stem cells increase after mesenchymal stromal cell treatment in a mouse model of bronchopulmonary dysplasia." American Journal of Physiology - Lung Cellular and Molecular Physiology **302**(9): L829-L837.

Tse, W. and M. J. Laughlin (2005). "Umbilical cord blood transplantation: a new alternative option." Hematology Am Soc Hematol Educ Program: 377-383.

Vadivel, A., T. van Haaften, et al. (2012). "Critical role of the axonal guidance cue EphrinB2 in lung growth, angiogenesis, and repair." Am J Respir Crit Care Med **185**(5): 564-574.

Vail, M., A. Tan, et al. (2012). "Targeting EphA3 in the tumour microenvironment inhibits tumour growth by disrupting stromal and vascular architecture." J. Clin. Investigation, prepared for resubmission (reference 64453-RG-1).

van Haaften, T., R. Byrne, et al. (2009). "Airway delivery of mesenchymal stem cells prevents arrested alveolar growth in neonatal lung injury in rats." Am J Respir Crit Care Med **180**(11): 1131-1142.

Vearing, C., F. T. Lee, et al. (2005). "Concurrent binding of anti-EphA3 antibody and ephrin-A5 amplifies EphA3 signaling and downstream responses: potential as EphA3-specific tumor-targeting reagents." Cancer Res **65**(15): 6745-6754.

Visner, G. A., E. D. Staples, et al. (1994). "Isolation and maintenance of human pulmonary artery endothelial cells in culture isolated from transplant donors." American Journal of Physiology - Lung Cellular and Molecular Physiology **267**(4): L406-L413.

Voswinckel, R., T. Ziegelhoeffer, et al. (2003). "Circulating Vascular Progenitor Cells Do Not Contribute to Compensatory Lung Growth." Circulation Research **93**(4): 372-379.

Wang, G., B. A. Bunnell, et al. (2005). "Adult stem cells from bone marrow stroma differentiate into airway epithelial cells: Potential therapy for cystic fibrosis." Proceedings of the National Academy of Sciences of the United States of America **102**(1): 186-191.

Warburton, D., J. Gauldie, et al. (2006). "Lung development and susceptibility to chronic obstructive pulmonary disease." Proc Am Thorac Soc **3**(8): 668-672.

Warburton, D. and M. K. Lee (1999). "Current concepts on lung development." Curr Opin Pediatr **11**(3): 188-192.

Warburton, D., L. Perin, et al. (2008). "Stem/progenitor cells in lung development, injury repair, and regeneration." Proc Am Thorac Soc **5**(6): 703-706.

Watkins, R. H., C. T. D'Angio, et al. (1999). "Differential expression of VEGF mRNA splice variants in newborn and adult hyperoxic lung injury." Am J Physiol **276**(5 Pt 1): L858-867.

Wessells, N. K. (1970). "Mammalian lung development: interactions in formation and morphogenesis of tracheal buds." J Exp Zool **175**(4): 455-466.

Wilkins, B. S. (1992). "Histology of normal haemopoiesis: bone marrow histology. I." J Clin Pathol **45**(8): 645-649.

Wu, X., M. W. Lensch, et al. (2007). "Hemogenic endothelial progenitor cells isolated from human umbilical cord blood." Stem Cells **25**(11): 2770-2776.

Yamada, M., H. Kubo, et al. (2004). "Bone Marrow-Derived Progenitor Cells Are Important for Lung Repair after Lipopolysaccharide-Induced Lung Injury." The Journal of Immunology **172**(2): 1266-1272.

Yamamoto, H., E. J. Yun, et al. (2007). "Epithelial-vascular cross talk mediated by VEGF-A and HGF signaling directs primary septae formation during distal lung morphogenesis." Dev Biol **308**(1): 44-53.

Yang, J., M. Ii, et al. (2011). "CD34⁺ Cells Represent Highly Functional Endothelial Progenitor Cells in Murine Bone Marrow." PLoS ONE **6**(5): e20219.

Yen, C. C., S. H. Yang, et al. (2006). "Stem cells in the lung parenchyma and prospects for lung injury therapy." Eur J Clin Invest **36**(5): 310-319.

Yin, A. H., S. Miraglia, et al. (1997). "AC133, a Novel Marker for Human Hematopoietic Stem and Progenitor Cells." Blood **90**(12): 5002-5012.

Yoder, M. C., L. E. Mead, et al. (2007). "Redefining endothelial progenitor cells via clonal analysis and hematopoietic stem/progenitor cell principals." Blood **109**(5): 1801-1809.

Yoon, C. H., J. Hur, et al. (2005). "Synergistic neovascularization by mixed transplantation of early endothelial progenitor cells and late outgrowth endothelial cells: the role of angiogenic cytokines and matrix metalloproteinases." Circulation **112**(11): 1618-1627.

Zander, D. S., M. A. Baz, et al. (2005). "Bone marrow-derived stem-cell repopulation contributes minimally to the Type II pneumocyte pool in transplanted human lungs." Transplantation **80**(2): 206-212.

Zheng, C., Y. Qiu, et al. (2009). "Endothelial CD146 is required for in vitro tumor-induced angiogenesis: The role of a disulfide bond in signaling and dimerization." The International Journal of Biochemistry & Cell Biology **41**(11): 2163-2172.

Ziegelhoeffer, T., B. Fernandez, et al. (2004). "Bone Marrow-Derived Cells Do Not Incorporate Into the Adult Growing Vasculature." Circulation Research **94**(2): 230-238.

Zimova-Herknerova, M., J. Myslivecek, et al. (2008). "Retinoic acid attenuates the mild hyperoxic lung injury in newborn mice." Physiol Res **57**(1): 33-40.

Appendices

Section I. Multiple group comparison using Student Newman-Keuls posthoc

The data presented in the tables indicate statistical subgroups with average values for each group. Each subgroup is presented in one column, indicating that there is no significant difference (P value is shown at the bottom of each subset) between the groups within one subgroup. There is a significant difference (P<0.05, n=4-5) between groups, allocated into different subgroups, and presented in different columns.

Alveolar size (μm) at D28

Group		N	Subset 1	2	3	4
Student-Newman-Keuls[a,b,c]	Normoxia PBS	2921	26.68922			
	Normoxia PAC	1604	26.98351			
	Normoxia Kdr	2358	28.39344	28.39344		
	Normoxia EphA3 P12	1524		29.52917	29.52917	
	Hyperoxia Kdr	2940			29.84725	
	Normoxia EphA3 P8	1616			30.61717	30.61717
	Hyperoxia EphA3 P8	1608			30.63144	30.63144
	Hyperoxia PAC	2017			31.06047	31.06047
	Hyperoxia EphA3 P12	1625				32.25391
	Hyperoxia PBS	2510				32.0139
	Sig.		.064	.085	.121	.051

Means for groups in homogeneous subsets are displayed. Based on observed means. The error term is Mean Square(Error) = 4013.294.

a. Uses Harmonic Mean Sample Size = 2053.515.

b. The group sizes are unequal. The harmonic mean of the group sizes is used. Type I error levels are not guaranteed.

c. Alpha = 0.05.

Alveolar size (µm) at D56

Group		N	Subset 1	Subset 2
Student-Newman-Keuls[a,b,c]	Hyperoxia Kdr	2020	30.09602	
	Normoxia PBS	2413	30.43542	
	Normoxia PAC	2410	30.94568	30.94568
	Normoxia EphA3 P12	1619	31.30832	31.30832
	Normoxia Kdr	2013		32.57051
	Hyperoxia PBS	2021		32.77614
	Hyperoxia PAC	1208		32.81674
	Hyperoxia EphA3 P12	1612		32.95401
	Sig.		.361	.072

Means for groups in homogeneous subsets are displayed.
Based on observed means.
The error term is Mean Square(Error) = 4376.421.
a. Uses Harmonic Mean Sample Size = 1825.729.

b. The group sizes are unequal. The harmonic mean of the group sizes is used. Type I error levels are not guaranteed.
c. Alpha = 0.05.

Number of alveoli per 3.63 mm at D28

Group		N	Subset 1	Subset 2
Student-Newman-Keuls[a,b,c]	Hyperoxia Kdr	30	71.97	
	Hyperoxia PBS	25	72.16	
	Hyperoxia EphA3 P12	20	72.50	
	Hyperoxia PAC	25	72.76	
	Normoxia EphA3 P12	20	73.95	73.95
	Hyperoxia EphA3 P8	20	75.60	75.60
	Normoxia EphA3 P8	20	76.35	76.35
	Normoxia PAC	20	76.95	76.95
	Normoxia Kdr	25		78.20
	Normoxia PBS	25		78.84
	Sig.		.106	.057

Means for groups in homogeneous subsets are displayed.
Based on observed means.
The error term is Mean Square(Error) = 43.360.
a. Uses Harmonic Mean Sample Size = 23.443.

b. The group sizes are unequal. The harmonic mean of the group sizes is used. Type I error levels are not guaranteed.
Student-Newman-Keuls

c. Alpha = 0.05.

Number of alveoli per 3.63 mm at D56

Group		N	Subset 1
Student-Newman-Keuls[a,b,c]	Hyperoxia PAC	15	67.87
	Hyperoxia EphA3 P12	20	68.50
	Hyperoxia PBS	25	71.04
	Normoxia Kdr	25	71.52
	Normoxia PAC	35	72.63
	Hyperoxia Kdr	25	73.56
	Normoxia PBS	25	74.08
	Normoxia EphA3 P12	20	74.25
	Sig.		.106

Means for groups in homogeneous subsets are displayed.
Based on observed means.
The error term is Mean Square(Error) = 59.100.
a. Uses Harmonic Mean Sample Size = 22.520.

b. The group sizes are unequal. The harmonic mean of the group sizes is used. Type I error levels are not guaranteed.
c. Alpha = 0.05.

Lung tissue area at D28 (mm)

Group		N	Subset 1	2	3
Student-Newman-Keuls[a,b,c]	Hyperoxia EphA3 P12	20	0.180549		
	Normoxia EphA3 P12	20	0.183129		
	Normoxia EphA3 P8	20	0.186147	0.186147	
	Hyperoxia Kdr	30	0.187429	0.187429	
	Hyperoxia PBS	30	0.192466	0.192466	
	Normoxia PBS	25	0.194659	0.194659	0.194659
	Normoxia PAC	20		0.201134	0.201134
	Hyperoxia EphA3 P8	25		0.202621	0.202621
	Normoxia Kdr	20		0.203216	0.203216
	Hyperoxia PAC	25			0.208552
	Sig.		.109	.053	.075

Means for groups in homogeneous subsets are displayed. Based on observed means. The error term is Mean Square(Error) = 1874415263.341.
a. Uses Harmonic Mean Sample Size = 23.105.

b. The group sizes are unequal. The harmonic mean of the group sizes is used. Type I error levels are not guaranteed.
c. Alpha = 0.05.

Lung tissue area at D56 (mm)

Group		N	Subset 1
Student-Newman-Keuls[a,b,c]	Hyperoxia PAC	15	0.173921
	Normoxia Kdr	25	0.174150
	Hyperoxia EphA3 P12	20	0.174744
	Hyperoxia PBS	25	0.175344
	Normoxia EphA3 P12	20	0.176906
	Normoxia PAC	35	0.178079
	Hyperoxia Kdr	25	0.180360
	Normoxia PBS	25	0.184224
	Sig.		.402

Means for groups in homogeneous subsets are displayed.
Based on observed means. The error term is Mean Square(Error) = 1294393006.212.
a. Uses Harmonic Mean Sample Size = 22.415.

b. The group sizes are unequal. The harmonic mean of the group sizes is used. Type I error levels are not guaranteed.
c. Alpha = 0.05.

Number of secondary septa per 1mm^2 of lung tissue area at D28

Group		N	Subset 1	2	3	4
Student-Newman-Keuls[a,b,c]	Normoxia PAC	20	231.1847			
	Hyperoxia EphA3 P8	25	231.9755			
	Normoxia PBS	25	253.2593			
	Hyperoxia PAC	25	265.2240			
	Normoxia Kdr	20	278.0833			
	Normoxia EphA3 P8	20	280.4296			
	Hyperoxia Kdr	30	305.5002	305.5002		
	Normoxia EphA3 P12	20		344.8140	344.8140	
	Hyperoxia PBS	30			365.3160	
	Hyperoxia EphA3 P12	20				443.5047
	Sig.		.054	.120	.417	1.000

Means for groups in homogeneous subsets are displayed. Based on observed means. The error term is Mean Square(Error) = 14.767.
a. Uses Harmonic Mean Sample Size = 23.105.

b. The group sizes are unequal. The harmonic mean of the group sizes is used. Type I error levels are not guaranteed.
c. Alpha = 0.05.

Number of secondary septa per 1mm^2 of lung tissue area (mm) at D56

Group		N	Subset 1	Subset 2
Student-Newman-Keuls[a,b,c]	Normoxia PBS	25	282.5492	
	Normoxia PAC	35	300.3888	
	Hyperoxia Kdr	25	311.4265	
	Hyperoxia PBS	25	314.3857	
	Hyperoxia PAC	15	339.8015	
	Normoxia EphA3 P12	20	351.4927	
	Normoxia Kdr	25	363.0489	
	Hyperoxia EphA3 P12	20		430.6951
	Sig.		.153	1.000

Means for groups in homogeneous subsets are displayed.Based on observed means. The error term is Mean Square(Error) = 23.612.
a. Uses Harmonic Mean Sample Size = 22.415.

b. The group sizes are unequal. The harmonic mean of the group sizes is used. Type I error levels are not guaranteed.
c. Alpha = 0.05.

Number of blood vessels per 0.564 mm^2 at D28

Group		N	Subset 1	Subset 2	Subset 3	Subset 4
Student-Newman-Keuls[a,b,c]	Normoxia EphA3 P12	20	16.40			
	Hyperoxia EphA3 P12	20	19.15	19.15		
	Normoxia PBS	25	19.38	19.38		
	Hyperoxia Kdr	30		20.25		
	Normoxia Kdr	20		20.50		
	Hyperoxia PBS	30		21.53	21.53	
	Hyperoxia EphA3 P8	25		21.76	21.76	
	Normoxia EphA3 P8	20		21.90	21.90	
	Normoxia PAC	20			24.60	24.60
	Hyperoxia PAC	25				25.24
	Sig.		.057	.337	.084	.620

Means for groups in homogeneous subsets are displayed.
Based on observed means.
The error term is Mean Square(Error) = 19.783.
a. Uses Harmonic Mean Sample Size = 23.105.

b. The group sizes are unequal. The harmonic mean of the group sizes is used. Type I error levels are not guaranteed.
c. Alpha = 0.05.

Number of blood vessels per 0.564 mm^2 at D56

Group		N	Subset 1	Subset 2
Student-Newman-Keuls[a,b,c]	Hyperoxia PBS	25	17.84	
	Normoxia PAC	35	19.06	19.06
	Hyperoxia PAC	15	19.07	19.07
	Normoxia EphA3 P12	20	19.40	19.40
	Hyperoxia EphA3 P12	20	19.75	19.75
	Hyperoxia Kdr	25	20.00	20.00
	Normoxia Kdr	25	20.29	20.29
	Normoxia PBS	25		22.24
	Sig.		.514	.203

Means for groups in homogeneous subsets are displayed.
Based on observed means.
The error term is Mean Square(Error) = 19.586.
a. Uses Harmonic Mean Sample Size = 22.415.
b. The group sizes are unequal. The harmonic mean of the group sizes is used. Type I error levels are not guaranteed.
c. Alpha = 0.05.

Section II. Company addresses

Below are the addresses and company names where reagents for this project were ordered.

Company name	Address and phone number	Web or email details
Abcam	Sapphire Bioscience Pty Ltd 126 Cope Street Waterloo – NSW 2017 Australia +61 2 9698 2022	sales@sapphirebioscience.com www.sapphirebioscience.com
Axygen	Pacific Laboratory Products Level 1, 15-33 Alfred Street Blackburn, Victoria 3130 P: 03 9845 0300	info@pacificlab.com.au www.pacificlab.com.au
BD Falcon	4 Research Park Drive Macquarie University Research Park North Ryde, NSW, 2113 AUSTRALIA + 61 2 8875 7000	bd_anz@bd.com www.bd.com/anz/
BDH Laboratory	Unit 1/31 Archimedes Place, Murarrie, QLD 4172, Australia +61 7 3009 4100	csaus@au.vwr.com
BioRad	Level 5, 446 Victoria Road Gladesville, NSW 2111 +61 2 9914-2800	Sales.Australia@bio-rad.com www.bio-rad.com
Cascade Biologics, Gibco, Life Technologies, Invitrogen	Life Technologies Australia Pty Ltd. 30-32 Compark Circuit, Mulgrave Victoria 3170 Australia 1800 636 327	mail.anz@lifetech.com www.invitrogen.com
Coregas	66 Loftus Road Yennora, NSW 2161 Australia +61 2 9794 2223	www.coregas.com/
DAKO	8 The Crossway Campbellfield VIC 3061 +61 3 9357 0892	CustomerCare.AU@dako.com www.dako.com.au
eBiosciences	Jomar Bioscience 15 Maesbury Street Kensington SA 5068 South Australia +61 8 8431 2041	jomar@adelaide.on.net www.jomar.on.net www.eBioscience.com
Fisons Pharmaceuticals	160 Wecker Rd, Mount Gravatt, QLD 4122 +61 2 9894 3500	Discontinued
Fujifilm	41 Jesica Road CAMPBELLFIELD VIC 3061, Australia 61 3 9221 4200	melbourne@fujifilm.com.au www.fujifilm.com.au
GE Healthcare	Bldg 4B, Parklands Estate 21 South Street RYDALMERE NSW 2116 Australia + 61 2 9846 4964	sales.au@ge.com www.gelifesciences.com
IBM	Level 13, IBM Centre, 601 Pacific Highway, St Leonards NSW 2065 Australia +61 2 9354 4000	askibm@au1.ibm.com www.ibm.com
ID Labs	100 Collip Circle, Unit 117 London ON, Canada N6G 4X8 +1 519 434-5057	idinfo@idlabs.com www.idlabs.com

Company name	Address and phone number	Web or email details
Media Cybernetics	401 N. Washington Street, Suite 350 Rockville, MD 20850 USA + 1 301-495-3305	www.mediacy.com
Millipore	207 Colchester Road Kilsyth VIC 3137 +61 3 9728 7600	orders.aus@merckgroup.com www.millipore.com
Miltenyi	Unit 16A 2 Eden Park Drive North Ryde NSW 2113 +61 2 8877 7400	macs@miltenyibiotec.com.au www.miltenyibiotec.com
Olympus	Ground Floor, 82 Waterloo Rd, Macquarie Park, NSW 2113, Australia +61 2 9888 7538	www.olympusaustralia.com.au
Perkin Elmer	Lvl 2, Bldg 5, Brandon Office Park 530-540 Springvale Road Glen Waverley Melbourne VIC 3150 Australia +61 3 9212 8500	ausales@perkinelmer.com www.perkinelmer.com.au
Santa Cruz	Millennium Science Pty Ltd 2, 390 Canterbury Road Surrey Hills VIC 3127 Australia +61 3 9830 7922	sales@mscience.com.au www.mscience.com.au
Servomex	Valley Point 491B River Valley Road Singapore 248373 +86 216 489 7570	asia_sales@servomex.com www.servomex.com
Sigma (Sigma Aldrich), Costar	Sigma-Aldrich Pty. Ltd. Sydney, Australia 61 2 9841 0555	anzcs@sial.com www.sigmaaldrich.com/australia.html
Techniplast	8, rue de Léry 27400 Louviers France 02 32 25 26 47	techniplast@techniplast.com www.techniplast.com
Thermo Scientific	P.O Box 9092 Scoresby, Victoria 3179 Australia +61 3 9757 4300	www.thermoscientific.com

Section III. Buffer recipes

PBS 10x

NaCl – 80 g
KCl – 2 g
Na_2HPO_4 – 14.4 g
KH_2PO_4 – 2.4 g
Distilled water – 800 ml
Ph adjusted to 7.4
Distilled water – up to 1 L

EDTA 0.5M

NaOH – 20 g
Distilled water – 400ml
EDTA – 93 g
pH adjusted to 8
Distilled water - up to 500 ml

PBS-EDTA

PBS 10x – 100 ml
Distilled water – 896 ml
EDTA 0.5M – 4 ml

Protein Sample Buffer 2x

1M Tris (pH = 6.8) – 1.25 ml
SDS (10%) - 4 ml
Glycerol - 2 ml
Bromophenol Blue (4%) – 125 µl
B-Mercaptoethanol (Sigma) – 200 µl
Distilled water – up to 10 ml

Resolving Gel Buffer (Western blots)

Tris – 48 g
Distilled water – 100 ml
pH adjusted to 8.8
Distilled water – up to 200 ml

Stacking Gel Buffer (Western blots)

Tris – 12.1 g
Distilled water – 100 ml
pH adjusted to 6.5
Distilled water – up to 200 ml

Running Buffer 10x (Western blots)

Tris – 30 g
Glycine – 148 g
SDS – 10 g
Distilled water – 1 L

Transfer Buffer 10x (Western blots)

Tris – 30 g
Glycine – 148 g
Distilled water – 1 L

Transfer Buffer 1x (Western blots)

Transfer Buffer 10x – 100 ml
Distilled water – 700 ml
Methanol – 200 ml

SSC 2x

NaCl – 17.5 g
$Na_3C_6H_5O_7$ – 8.8 g
pH adjusted to 7.0
Distilled water – up to 1 L

List of abbreviations

Abbreviation	Description
AEC	Alveolar epithelial cells
Ang	Angiotensin
ANOVA	Analysis of variance
ANPEP	alanyl-aminopeptidase
Aqp	Aquaporin
BM	Bone marrow
BPD	Bronchopulmonary dysplasia
C57Bl/6J	C57 black 6J
Cd34	Cd34 molecule, cluster of differentiation 34
D	Day
DAB	3,3' Diaminobenzidine
DMEM	Dulbecco's Modified Eagle Medium
DNA	Deoxyribonucleic acid
DPX	Di-n-butyl-Phthalate in Xylene
EBM	Basal Medium
EDCM	Endothelial differentiation cell medium
EGF	Epidermal growth factor
EGM	Endothelial Cell Growth Medium
Eng	Endoglin
eNOS	Endothelial nitric oxide synthase
EPCs	Endothelial progenitor cells
EphA3	Ephrin type-A receptor 3

EPO-R	Erythropoietin receptor
FACS	Fluorescence-activated cell sorting
FAK	PTK2 protein tyrosine kinase 2
Fgf	Fibroblast growth factor
FISH	Fluorescence in situ hybridisation
Flt1	fms-like tyrosine kinase 1
GFP	Green fluorescent protein
GFP	Green fluorescent protein
Hgf	Hepatocyte growth factor
Hoxb	Homeobox B cluster
HRP	Horse radish peroxidase
HSCs	Hemopoietic stem cells
IFs	Interstitial fibroblasts
Ig	Immunoglobulin
IGF	Insulin-like growth factor
IKK	Inhibitor of kappaB kinase
IL	Interleukin
IMDM	Iscove's Modified Dulbecco's Medium
ITS	Insulin, transferrin, selenite
Kdr	Kinase insert domain protein receptor
Kit	v-kit Hardy-Zuckerman 4 feline sarcoma viral oncogene homolog
LDL	Low-density lipoprotein
LPS	Lipopolysaccharide
MACS	Magnetic-activated cell sorting
MAP kinase	Mitogen-activated protein kinase

MARP	Monash Animal Research Platform
Mcam	Melanoma cell adhesion molecule
mRNA	Messenger ribonucleic acid
MSCs	Mesenchymal/marrow stromal cells
Nck	Non-catalytic region of tyrosine kinase adaptor protein
NFκB	Nuclear factor of kappa light polypeptide gene enhancer in B-cells
NHMRC	National Health and Medical Research Council
OCT	Optimal Cutting Temperature
P	Passage
PAS	Periodic acid and Schiff's reagent
PBS	Phosphate buffer saline
PBST	Phosphate buffer saline with Tween-20
PCR	Polymerase chain reaction
Pecam	Platelet endothelial cell adhesion molecule
PFA	Paraformaldehyde
PI3K	Phosphatidylinositol-4,5-bisphosphate 3-kinase
PK	Proteinkinase
PLC	Phospholipase C
Prom	Prominin
Ptpr	Protein tyrosine phosphatase receptor
RA	Retinoic acid
RIPA	Radio-immunoprecipitation assay
SCF	Kit ligand, stem cell factor
SCGF	Stem cell growth factor, C-type lectin domain family 11, member a
SD	Standard deviation

SDS	Sodium dodecyl sulphate
SEM	Standard error of mean
Sftp	Surfactant protein
Shb	Src homology 2 domain-containing transforming protein B
SPF	Specific pathogen free
Src	Rous sarcoma oncogene
SSEA	Stage-specific embryonic antigen
Tek	TEK tyrosine kinase, endothelial
UCB	Umbilical cord blood
VEGF	Vascular endothelial growth factor
VRAP	SH2 domain protein 2A
vWF	von Willebrandt Factor